

THE UNIVERSITY
of ADELAIDE

Targeted Unmixing of Particles in Suspension

Mei C. Cheong

School of Mechanical Engineering
The University of Adelaide
South Australia 5005
Australia

A thesis submitted in fulfillment of
the requirements for the degree of
PhD in Engineering

PhD Thesis

October 2021

School of Mechanical Engineering
The University of Adelaide
South Australia 5005
Australia

Typeset by the author using LaTeX.
Printed in Australia.

Copyright © 2021, The University of Adelaide, South Australia.
All right reserved. No part of this report may be used or reproduced in any form or by any means, or stored in a database or retrieval system without prior written permission of the university except in the case of brief quotations embodied in critical articles and reviews.

To who I was, to who I am, and to who I will be.

Contents

Summary **v**

Declarations **vii**

Acknowledgements **ix**

List of Figures **xi**

List of Tables **xvii**

Nomenclature **xxi**

1 Introduction **1**
1.1 Aims 4
1.2 Thesis Outline 5

2 Literature Review **7**
2.1 Particle-Laden Fluids 7
2.2 Governing Parameters 9
2.2.1 Particle Mass Loading 9
2.2.2 Particle Volume Loading 10
2.2.3 Particle Reynolds Number 12
2.2.4 Particle Stokes Number 14
2.2.5 Particle-Fluid Surface Interaction Influences . . . 19
2.3 The Preferential Concentration Phenomenon 23
2.4 Consolidation of Literature and Research Objectives . . . 33

3 Measurement Techniques **37**
3.1 Velocity Measurements 37
3.2 Flow Visualisation 39

3.3 Concentration Measurements 41
3.3.1 Laser Attenuation Correction 43
3.4 Summary 61

4 Experimental Apparatus **63**
4.1 Zero-Net Mass Flux Jets 63
4.1.1 Acoustic Excitation 64
4.1.2 Cavitation Bubbles 64
4.1.3 Diaphragm Systems 66
4.1.4 Piston Systems 68
4.1.5 Evaluation of ZNMF Systems 69
4.2 Development of a Vortex Generator 71
4.2.1 Vortex Generator Outlet 71
4.2.2 Nozzle Exit Geometry 73
4.2.3 Driving Mechanism 74
4.3 Experimental Arrangement 78
4.3.1 Tank 78
4.3.2 Solid Phase 79
4.3.3 Experimental Layout 82
4.4 Summary 83

5 Preferential Concentration **85**
5.1 Particle Tracking Experiments 85
5.1.1 Experiment-Specific Details 86
5.1.2 Results and Discussion 87
5.1.3 Conclusions of the Particle Tracking Experiments 96
5.2 Preferential Concentration Experiments 97
5.2.1 Experiment-Specific Details 97
5.2.2 Results and Discussion 98
5.2.3 Conclusions of the Preferential Concentration Experiments 125
5.3 Summary 127

6 Particle-Fluid Surface Interactions **129**
6.1 Validation Experiments 129
6.1.1 Experiment Specific Details 130
6.1.2 Results and Discussion 132
6.1.3 Conclusion of Validation Experiments 139
6.2 Focused Experiments 139

6.2.1 Experiment-Specific Details 140
6.2.2 Results and Discussion 140
6.2.3 Conclusion of Focused Experiments 149
6.3 Summary 150

7 Fluid Excitation Frequency **151**
7.1 Fluid Excitation Frequency Experiments 151
7.1.1 Experiment-Specific Details 152
7.1.2 Results and Discussion 152
7.1.3 Conclusions of Fluid Excitation Frequency Experiments 160
7.2 Additional Experiments 161
7.2.1 Experiment-Specific Details 161
7.2.2 Dye Visualisation Results 162
7.2.3 Conclusions of the Additional Experiments 164
7.3 Summary 164

8 Conclusions and Future Work **169**
8.1 Conclusions 169
8.2 Suggested Future Work 173

References **175**

Summary

Solid-liquid separation in residential and industrial effluents generally describes the separation and removal of specific particulates from the effluents. This process is often difficult to achieve when dealing with toxic or valuable particulates that must be extracted from the working liquid. Despite the availability of numerous separation methods, situations exist where particles are too fine to settle at an appreciable rate or to be extracted economically using existing separation techniques.

The work presented in this thesis involves the examination of a novel approach to particle separation using fluid turbulence to induce directed motion in particles to accumulate in specific regions of the fluid flow field; a mechanism known as preferential concentration. Hence, an extended objective of the presented research is to determine the feasibility of using the preferential concentration mechanism for the purpose of selective particle un-mixing.

Experiments investigated the capabilities of the preferential concentration mechanism at causing directed motion in non-inertial particles within a fluid suspension. By tracking non-inertial particles within a vortex ring flow field, the influences of particle inertia were effectively suppressed to allow the examination of other factors that may influence the preferential concentration mechanism; factors such as particle-fluid surface interaction. Particles within the vicinity of vortex structures were observed to move in a directed manner; a behaviour that cannot be fully explained using existing preferential concentration theories based solely on particle mass and inertia.

Further investigations examined the possibility that particle-fluid surface interactions contribute to directed motion in particles and/or influence the preferential concentration mechanism. The results obtained supported previous indications that particle-fluid surface interactions are able to influence particle and fluid behaviour, which in turn contributed to directed particle motion. However, the relationship between these interactions and the preferential concentration mechanism could not be validated within the experimental work undertaken. Consideration was therefore given to the possibility that the observed directed motion, although associated with particle-fluid surface interactions, may not be due to the preferential concentration mechanism.

Collectively, the outcomes of the current research established that particle-fluid surface interactions are able to influence particle and fluid behaviour, thus contributing to directed particle motion. However, the occurrence of the preferential concentration mechanism could not be confirmed and as such the influence of particle-fluid surface interactions on the mechanism itself could not be substantiated experimentally. The current work supports the conclusion that experiments involving particle-laden fluids are highly dynamic and complex, and particle and fluid behaviour can be influenced by numerous factors to varying degrees. Further understanding of particle-laden fluids as well as the preferential concentration mechanism will require a means of examining individual factors contributing to particle and fluid behaviour either in isolation or with minimal effects from other factors. It is anticipated that through future work that integrates experiments with computational methods, a further understanding of directed particle motion and the preferential concentration will lead to the development of a successful preferential-concentration-based selective particle un-mixing technique suitable for industrial applications.

Declarations

I certify that this work contains no material which has been accepted for the award of any other degree or diploma in my name, in any university or other tertiary institution and, to the best of my knowledge and belief, contains no material previously published or written by another person, except where due reference has been made in the text. In addition, I certify that no part of this work will, in the future, be used in a submission in my name, for any other degree or diploma in any university or other tertiary institution without the prior approval of the University of Adelaide and where applicable, any partner institution responsible for the joint-award of this degree.

I acknowledge that copyright of published works contained within this thesis resides with the copyright holder(s) of those works.

I give permission for the digital version of my thesis to be made available on the web, via the Universitys digital research repository, the Library Search and also through web search engines, unless permission has been granted by the University to restrict access for a period of time.

I acknowledge the support I have received for my research through the provision of an Australian Government Research Training Program Scholarship.

Mei C. Cheong

Acknowledgements

The thesis journey has been a life changing experience, one that truly tested my self-confidence, my perseverance and my resilience. It was a journey that I hope to this end, helped further myself professionally and personally, and a journey to remind myself in times of self-doubt that I am capable of more.

The biggest challenge was that it was always difficult to know what was achievable within a timeframe. Every task undertaken often consumed more time than expected. Unavoidable delays, frequent failures, and time pressures were all part of an all-consuming vicious cycle that was the thesis. There was also the expectation of being able to manage and master the various skills required to get a thesis completed: the preparations and techniques in the lab, the dealings with workshops and manufacturing, the analysis and processing of data into useful outcomes, the write-ups that led to never ending mammoth scale revisions, restructures and rework - all these in hope of acquiring this mythical creature called a thesis at the end of the journey. Juggling these matters simultaneously proved mentally, physically and emotionally exhausting and strenuous. Whenever one of these balls were unintentionally dropped, self-doubt crept in, which stretched the journey through even darker paths and longer detours.

Overcoming these challenges then became a major part of the thesis journey. I learned to gauge what was achievable in terms of research objectives, I learned to face one challenge at a time and take days one step at a time, and I learned to seek academic and technical advice and support whenever needed. At the end of this journey, the skills, knowledge and experience I have gained would need a multitude of these thesis write-ups to do it justice. All I can offer in return is that

everything I have learned from this journey, I will take on board as I embark on the next chapter in my life.

The research documented in this thesis would not have been possible without the invaluable support of a number of individuals. To all of you I express my sincere gratitude.

Thank you to Richard Kelso for your encouragement, your invaluable advice and feedback to get my work up to scratch, and for keeping a sense of humour when I had lost mine. This journey has been one that has demanded extraordinary patience and dedication on both of our parts. I thank you for staying true. Thank you to Zhao Tian for your review and feedback. The updates implemented have certainly improved the quality of my work. I truly appreciate your assistance.

Thank you to all my friends and colleagues who have supported me throughout my research endeavours. In particular, my sincere thanks to Alison-Jane Hunter and Brad Gibson for selflessly volunteering to read my thesis just because, Zebb Prime for all things Matlab and LaTex, Eyad Hassan for all things PIV, and Dorothy Missingham for all your good intentions.

To all the workshop staff at the School of Mechanical Engineering, thank you for all your help, patience, support, guidance and jokes. You have all been a source of knowledge and friendliness, making my thesis journey a little more fun and bearable when I truly needed it.

Thank you to my parents and my siblings. No words can fully express my appreciation in knowing that you were all by my side on this journey.

Finally, thank you to my selfless and dedicated better half, John Codrington. You kept me going on this journey by steadily being by my side, through the frustration, the anger, the confusion, the self doubt and the despair. You believed in me even when I did not. Your stubborn determination that I had it in me to complete this thesis might have been just the thing that helped me finish this journey. This thesis is as much yours as it is mine. Thank you for all that you are and all that you do.

List of Figures

2.1 Conceptual model of the effect of Stokes numbers on directed particle motion postulated by Crowe *et al.* (1988, 1995). 18

2.2 Schematic representation of the flow curve of a suspension (adapted from Barnes *et al.*, 1989). 20

2.3 Particle dispersion patterns for a plane mixing layer (a) Unforced condition (b) Forced near dominate instability frequency (Wen *et al.*, 1992). 24

2.4 Particle dispersion pattern for a plane wake (a) Experimental result (b) Simulated result (Tang *et al.*, 1992). 25

2.5 Particle dispersion patterns in the wake of a bluff body (a) Particles with small Stokes numbers ($St << 1$) (b) Particles with intermediate Stokes numbers ($St \approx 1$) (Crowe *et al.*, 1995). 25

2.6 (a) Single-phase and particle-laden flow forced at low frequencies (Longmire & Eaton (1992) (b) Phase-locked images of droplet-laden jet (non-reacting flow) (Wark *et al.*, 2000) (c) Postulation by Longmire and Eaton (1992) that particles are pulled out of the streaming region inside the vortex rings and pushed into the regions downstream of the vortex cores where particle clusters appear. 26

2.7 Sketch for illustrative purposes only: (a) inertial bias influence of particles interacting with flow vortical structures (b) preferential sweeping mechanism for a heavy particle interacting with local flow vortical structures under its inertia and body force (c) particle clusters that are formed continues to settle, entraining other particles which in turn increases its settling velocity. Settling velocities for particles in (c) were found to be larger than (b) (Aliseda *et al.*, 2002). Illustration adapted from Wang & Maxey (1993). 27

2.8 The stretching and folding mechanism proposed by Wen *et al.* (1992) (a) Stretching of particle streak-lines near boundaries of vortices (b) Folding of particle streak-lines during vortex pairing (Tang *et al.*, 1992). 28

3.1 Imaged plane in the region of interest (dy and dz are in-plane resolution while dx relates to the laser sheet thickness). 49

3.2 Attenuation of light intensity propagating through the imaged plane of interest (I_o and I_{end} are the light intensities entering and exiting a plane of M voxels, while I_m is the light intensity exiting voxel m). 49

3.3 Schematic diagram of experimental setup. 52

3.4 Schematic diagram of the experimental chambers: (a) single-chamber configuration; (b) two-chamber configuration. 53

3.5 Averaged signal intensities against the laser path (background noise removed but uncorrected for attenuation) - single-chamber configuration. 55

3.6 Particle concentration as a function of laser propagation path (corrected for laser attenuation) for the single-chamber configuration. 56

3.7 Particle concentration against laser path for the two-chamber configuration: corrected for attenuation and the acrylic sheet. 57

3.8 Percentage relative error as a function of particle loading cases for the single-chamber configuration. 59

4.1 Large-scale vortices in the upstream region of a lifted flame (a) Planar images of lifted a flame - (i) unexcited, (ii) excited at 670Hz, (iii) excited at 1200Hz (Chao & Jeng, 1992) (b) Typical jet flow visualisation of the entrainment process (Chao *et al.*, 2002). 65

4.2 A ZNMF jet from an ultrasonic transducer (a) Dye is entrained radially from an injection port near the edge of the diaphragm; (b) Jet formation mechanism: (i) flow about a cavitation bubble (ii) momentary jet due to the collapse of a cavitation bubble (James *et al.*, 1996). . . . 65

4.3 A ZNMF jet from a sealed cavity (a) Schematic diagram of the setup (b) Schelieren image of the jet at 1140Hz excitation (Smith & Glezer, 1998). 67

4.4 Piston-cylinder generated vortex ring (a) Schematic diagram (b) Visualisation using fluorescent dye (Allen & Auvity, 2002). 67

4.5 (a) Schematic diagram of the ultrasonic transducer setup (b) Cavitation damage on the disk used. 70

4.6 The diaphragm and orifice plate approach (a) Schematic diagram (b) Experimental setup. 70

4.7 Cylindrical outlets of piston-cylinder vortex ring generators. 72

4.8 Basic parameters of a nozzle for the piston-cylinder setup. 73

4.9 (a) Critical dimensions of the nozzle and piston-cylinder rig with the crankshaft setup (b) The piston-cylinder system with the crankshaft setup. 77

4.10 The experimental rig layout of the nozzle and the Bellofram. 77

4.11 Schematic diagram of the experimental equipment and setup. 80

4.12 The layout of the experimental rig - crankshaft setup. . . 80

5.1 Single-pulses used for current experiments, with pulse duration varying from 0.4s to 1.4s, at intervals of 0.2s. . 86

5.2 Trajectory tracking of two large agglomerated particles (highlighted blue) and two small agglomerated particles (highlighted red) within a vortex laden with particles, generated using a pulse duration of 0.8s, with $Re_f = 830$. 89

5.3 Trajectory tracking of agglomerated particle structures and particle concentration measurements of a particle-laden vortex ring, generated using a pulse duration of 1s, with $Re_f = 1040$. 91

5.4 Trajectory tracking of agglomerated particles in a particle-laden vortex, generated using a pulse duration of 0.4s, with $Re_f = 415$ - part A. 92

5.5 Trajectory tracking of agglomerated particles in a particle-laden vortex, generated using a pulse duration of 0.4s,with $Re_f = 415$ - part B. 93

5.6 Ensemble-averaged velocity measurements of a vortex generated using a pulse duration of 0.4s with $Re_f = 415$, propagating into a working fluid for different particle loading cases - part A. 100

5.7 Ensemble-averaged velocity measurements of a vortex generated using a pulse duration of 0.4s with $Re_f = 415$, propagating into a working fluid for different particle loading cases - part B. 101

5.8 Ensemble-averaged velocity measurements of a vortex generated using a pulse duration of 0.4s with $Re_f = 415$, propagating into a working fluid for different particle loading cases - part C. 102

5.9 Ensemble-averaged velocity profiles at the nozzle exit for a vortex generated using a pulse duration of 0.4s, with $Re_f = 415$. 103

5.10 Ensemble-averaged velocity profiles through vortex cores for a vortex generated using a pulse duration of 0.4s, with $Re_f = 415$. 105

5.11 Ensemble-averaged vorticity plots of a vortex generated using a pulse duration of 0.4s, propagating into a working fluid for different particle loading cases: (i) Case A - particles in ambient fluid, (ii) Case B - particles in a vortex ring, and (iii) Case C - particles in a vortex ring and ambient fluid - part A. 112

5.12 Ensemble-averaged vorticity plots of a vortex generated using a pulse duration of 0.4s, propagating into a working fluid for different particle loading cases: (i) Case A - particles in ambient fluid, (ii) Case B - particles in a vortex ring, and (iii) Case C - particles in a vortex ring and ambient fluid - part B. 113
5.13 Vorticity plots of a vortex generated using a pulse duration of 0.4s, at $t = 0.9s$ for Case B: a) with low constant-vorticity levels suppression b) without suppression. . . . 114
5.14 Vorticity plots of a vortex generated using a pulse duration of 0.4s, at $t = 0.9s$ for Case B: a) ensemble-averaged b) instantaneous. 115
5.15 Vortex generated using a pulse duration of 0.4s, at $t = 1.7s$ for Case A: a) vorticity plot c) region of integration used to determine the path of integration for the circulation calculations. 120
5.16 Ensemble-averaged vortex ring circulation of vortices generated using a pulse duration of 0.4s, propagating into a working fluid for different particle loading cases: (i) Case A - particles in ambient fluid, (ii) Case B - particles in vortex ring, and (iii) Case C - particles in vortex ring and ambient fluid. 121
5.17 Ensemble-averaged and instantaneous vortex ring circulation of vortices generated using a pulse duration of 0.4s, for Case B - particles seeded in the vortex ring. Coloured lines indicate instantaneous vortex ring circulation values. 122

6.1 Continuous pulses used for current experiments, with pulse duration, P, varying from 0.4s to 1.4s, at intervals of 0.2s and a time delay of 1.0s between pulses. 130
6.2 Flow visualisation of the evolution and interaction of a vortex ring with a previous vortex ring, generated using pulse duration of 0.4s with a time delay of 1.0s between successive vortex structures, with $Re_f = 415$. 131
6.3 (a) Acoustically excited particle-laden jet (Wark *et al.*, 2000), (b) Flow visualisation of a vortex ring at $t = 1.5s$, generated using pulse duration of 1.0s, with 1.0s time delay between pulses, and $Re_f = 1040$. 134

6.4 (a) Flow visualisation of a vortex ring at $t = 1.5s$, generated using a pulse duration of 1.0s, with $Re_f = 1040$ (b) Illustrated concept of the particle-fluid interaction proposed by Longmire and Eaton (1992) superimposed on image (a). 134
6.5 Normalised particle concentration measurements in vortex structures, generated using pulse duration of 0.4s, with a time delay of 1.0s between successive pulses, and with $Re_f = 415$. 136
6.6 Phase-locked PIV images of vortex structures, generated using pulse duration of 0.4s, with a time delay of 1.0s between successive vortex structures, and with $Re_f = 415$. 137
6.7 Close-up of the velocity vectors of particles in braid regions of Figure 6.6e. 138
6.8 Instantaneous particle concentration measurements normalised to maximum recorded concentration values of single pulsed particle-laden vortex rings, generated using a pulse duration of 0.4s for flow case $Re_f = 415$: (a)-(c) Typical set of images, (d)-(f) Vortex ring displaying unusual behaviour. 142
6.9 PIV image of the trail of particles featured in Figure 6.8a-c: a) velocity vectors b) velocity contours. 143
6.10 Normalised particle concentration of single pulsed particle-laden vortex rings interacting with a trail of particles in its propagation front, generated using a pulse duration of 0.4s for flow case $Re_f = 415$. 145
6.11 Instantaneous velocity profiles through vortex cores featured in: (a) Figure 6.10(c), (b) Figure 6.10(f). The red profiles represent cores with a counter-clockwise rotation; the green profiles represent cores with a clock-wise rotation. 147

7.1 Particle settlement patterns after interacting with vortex structures generated at different fluid excitation frequencies for a period of 15 minute intervals. The views show the floor of the water tank, viewed from above. The nozzle head can be seen at the centre of the floor. . . . 153
7.2 Particle settlement at $f = 10$Hz (a) Without a false ceiling (b) With a false ceiling. 159

7.3 (a) Cylindrical tank setup (b) Particle settlement at $f =$ 10Hz. 159
7.4 The movement of dye, outlined in red, initially placed along a 0^o plane. 163
7.5 Movement of dye when dye is initially laid at the edge of the tank. 166
7.6 The movement of dye, laid initially at the edge of the tank, directed towards the 0^o planes. 167
7.7 Dye movement indicates that ambient fluid recirculates within the tank quadrant. 168

List of Tables

3.1 Particle concentration in each chamber in different cases. The laser sheet propagates in the direction of Chamber 1 *en route* to Chamber 2. 54
3.2 Signal attenuation analysis for 10 ppm particles at various tank displacements from the camera. 60

5.1 Average vortex diameter of ensemble-averaged velocity profiles through vortex cores for a vortex generated using a pulse duration of 0.4s, with $Re_f = 415$. 104
5.2 Propagation velocity of ensemble-averaged velocity profiles through vortex cores for vortex generated using a pulse duration of 0.4s, with $Re_f = 415$. 106
5.3 Physical characteristics of the vortex rings generated using a pulse duration of 0.4s for the different particle loading cases. 126

7.1 The particle Stokes number at different fluid excitation frequencies. 154

Nomenclature

Variables

Greek

α	Constant of path length and extinction coefficient of particles [-]
β	Particle mass loading [-]
γ	Euler's constant [-]
Γ	Circulation[$m^2\ s^{-1}$]
δ	Radius of the cross section of the vortex core [m]
ϵ	Dissipation rate of turbulent kinetic energy per unit mass [$m^2\ s^{-3}$]
η	Effective/apparent viscosity of suspension [kg $m^{-1}\ s^{-1}$]
η_o	Viscosity of the pure fluid phase [kg $m^{-1}\ s^{-1}$]
θ	Nozzle edge angle [^{o}]
ι	Spectral transmissivities [-]
λ	Wavelength [m]
μ	Dynamic viscosity [kg $m^{-1}\ s^{-1}$]
ν	Kinematic viscosity [$m^2\ s^{-1}$]
ρ	Density [kg m^{-3}]
σ	Particle scattering cross section [m^2]
τ	Response time (time-scale) [s]

Variables

Greek (continued)

$\boldsymbol{\upsilon}$	Velocity vector [m s^{-1}]
ϕ	Particle volume fraction (particle volume loading) [-]
Φ	Energy flux incident on the photo-detector [W]
χ	Particle packing fraction [-]
ψ	Scatter function [-]
ω	Solid angles of divergence [sr]
$\boldsymbol{\omega}$	Vorticity vector [s^{-1}]

Roman

A	Cross-sectional area [m^2]
B	Constant [-]
C	Local particle concentration [ppm]
C_o	Pertaining to an arbitrary closed path [-]
C_C	Stokes-Cunningham factor [-]
C_D	Drag coefficient [-]
d	Pertaining to an interval [-]
d	Diameter [m]
D	Nozzle diameter [m]
E	Constant [-]
f	Fluid excitation frequency [Hz]
$\mathbf{f}$	body force per unit volume [N m^{-3}]
I	Local light intensity (radiant flux) [W]

Variables

Roman (continued)

K	Constant for particle characteristics, experimental setup, equipment efficiency [-]
L	Length-scale or Piston stroke length [m]
m	Mass [kg]
$\mathbf{n}$	unit vector [-]
N	Number of particles (Particle number density) [-]
p	Pressure [Pa]
P	Pulse duration [s]
Re	Reynolds number [-]
r	Radius [m]
S	Minimum distance between the front face of the piston and the cylinder exit [m]
S_o	Pertaining to an arbitrary surface [-]
St	Particle Stokes number [-]
V	Volume [m^3]
u	Mean velocity [m s^{-1}]
U	Propagation velocity [m s^{-1}]
x	x-direction [m]
y	y-direction [m]
z	z-direction [m]

Subscripts

Roman

av	Pertaining to average values
c	Pertaining to critical values
cv	Pertaining to a control volume
end	Pertaining to light exiting a region of interest
f	Pertaining to fluids
i	Pertaining to the location corresponding to pixel i
in	Pertaining to light entering a voxel
inc	Pertaining to incident light beams
int	Pertaining to the integral time-scale
k	Pertaining to the Kolmogorov time-scale
M	Pertaining to the maximum number M
m	Pertaining to the number m
o	Pertaining to the initial light entering a region of interest
out	Pertaining to light exiting a voxel
p	Pertaining to particles
sc	Pertaining to scattered light beams
T	Pertaining to translational components
v	Pertaining to coherent vortices (vortex structures)
vel	Pertaining to velocity
vor	Pertaining to vorticity

Subscripts

Mathematical

1 Pertaining to the media between a light source and a control volume

2 Pertaining to the media between a control volume and a photo-detector

Acronyms

CCD	Charged Couple Device
DC	Direct Current
IVM	Integral Value Method
LDA	Laser Doppler Anemometry
LDV	Laser Doppler Velocimetry
MN	Marker Nephelometry
PDA	Phase Doppler Anemometry
PDI	Phaser Doppler Interferometry
PIV	Particle Image Velocimetry
PN	Planar Nephelometry
PTV	Particle Tracking Velocimetry
SLIPI	Structured Laser Illumination Planar Imaging
ZNMF	Zero-Net Mass Flux

1 Introduction

Solid-liquid separation is a vital process in mining and chemical industries where there is a need to separate and remove specific particulates from effluents (Concha, 2014; Wakeman & Tarleton, 2005). Situations where the separation and extraction of suspended particles from a working fluid occur include, but are not limited to: removal of fine solids from industrial and municipal waste streams, removal of fine particles from turbid water, and recovery of valuable metals from ores and waste rocks. Particle separation processing of industrial effluents containing substantial quantities of toxic or valuable components is of significant environmental and economic interest. Adverse ecological impacts are minimised through the removal of suspended solid particulates (especially heavy metals) from waste water before it is returned to the environment. The recovery of valuable minerals from industrial effluent ensures the effective use of raw materials with minimal wastage. Although numerous separation techniques are currently available, situations exist where solid-liquid separation is required with particles that are too fine to settle at an appreciable rate or to be extracted out economically using conventional methods (Limbach *et al.*, 2008; Rezakazemi *et al.* 2018). The implementation of more stringent environmental legislation and rising costs of raw materials consequently further drive the demand for more effective particle separation methods.

Current physical solid-liquid separation technologies are based on two principal methods: filtration and sedimentation (Rushton *et al.*, 1996). Filtration involves passing the solid-liquid mixture through a filter medium, allowing the liquid phase through but retaining the solid phase either on the surface or within the filter medium. Despite the advancement of membrane filters allowing filtration to extend to

particulates in the nano-scale, this method is inadequate due to the physical limitation of the filter medium itself, which still has difficulty separating hazardous colloids frequently encountered in sewage wastes (Bowen & Jenner, 1995; Chang & Lee, 1998; Myers, 1999; Rezakazemi *et al.* 2018; Song, 1998). The fine particulate colloids tend to clog the filter medium (a phenomenon known as fouling), which eventually results in system blockage (Anlauf, 2007; Bouhabila *et al.*, 2001; Iritani & Katagiri, 2016; Labanda & Llorens, 2008; Pronk *et al.*, 2019; Rezakazemi *et al.* 2018). Such limitations in filtration techniques significantly impact on the effectiveness of their separation capabilities as well as operational costs.

Sedimentation utilises the difference in densities between solid and liquid phases within a force field to separate the phases. Consequently, the effectiveness of sedimentation when dealing with colloidal systems is limited due the small density differences between the solid and liquid phases. Sedimentation, in particular the gravity-based variants, also requires a substantial operating space, an issue when dealing with large fluid volumes typical of industrial effluents. Sedimentation is effective only if particles are sufficiently large and dense to ensure that particles settle at an appreciable rate (Murugananthan *et al.*, 2004; Stumm, 1977; Tarleton & Wakeman, 2016; Yokomizo, 1994). Floatation, utilises gas bubbles that attach themselves to particles and float them to the surface of the working fluid (Rubio *et al.*, 2002). Although floatation is effective when dealing with finer particles, this method is difficult to apply to the separation of ultra-fine particulates. Bubbles generated must be comparable to the size of the particles to be floated, a task that is highly complex and ineffective when dealing with effluents containing high concentrations of solid particulates (Rubio *et al.*, 2002; Merkus, 2016; Moses & Petersen, 2000). Sedimentation and floatation techniques are therefore restricted in terms of their applications since these methods are very time consuming and physically large.

Chemical solid-liquid separation techniques commonly implemented on residential and industrial waste streams include chemical leaching and coagulation-flocculation. The basic principle of chemical leaching is the removal of specific substances from the working fluid by the action of extremely corrosive aqueous solutions which are generally acidic. The use of these acidic solutions and the toxic residual effluents produced as

a by-product of these processes, presents a significant environmental hazard that is of great concern for the health and safety of workers at these processing plants (Chmielewski *et al.*, 1997; Geoffroy & Cardarelli, 2005; Pant *et al.*, 2012). In addition, chemical leaching requires low operating temperatures which result in the processes being time consuming and relatively ineffective at times (Moses & Petersen, 2000). This separation technique also incurs high capital and operational costs when implemented for commercial mining purposes (Bosecker, 1997). The application of chemical leaching is therefore implemented with caution due to the various environmental and health hazards this method generates.

Coagulation-flocculation utilises chemical reagents to induce particle aggregation for the purposes of solid-liquid separation (Lopez-Maldonado *et al.*, 2014; Pearse, 2003). This method of separation is limited in its application since large amounts of chemical reagents are required to process large volume waste streams, resulting in high capital and operating costs, and large spaces being required (Labanda & Llorens, 2008; Lapsirikul *et al.*, 1994; Zouboulis & Katsoyiannis, 2002). A certain level of particle concentration is also required to provide sufficient contact opportunities between coagulants and particulates to enable coagulation to be accomplished at reasonable detention times (Lopez-Maldonado *et al.*, 2014; Stumm, 1977). Effluents being treated are also inevitably contaminated with coagulate chemicals which reduce the quality of the filtrate and can at times produce toxic sludge which requires further treatment to enable safe disposal (Chmielewski *et al.*, 1997; Murugananthan *et al.*, 2004; Stumm, 1977; Zouboulis & Katsoyiannis, 2002). This method is therefore restrictive due to its high operational costs which must account for pre-treatment work to ensure that effluents respond well to coagulation techniques, as well as post-treatment processes on the toxic sludge by-products.

Biological solid-liquid separation methods such as activated sludge and anaerobic digestion are commonly employed to treat residential and industrial waste streams (Ehlers & Turner, 2011; Van Dierdonck *et al.*, 2012). Bacteria and micro-organisms are used to flocculate (bio-flocculate) and aggregate suspended particulates in effluents in order to generate larger and denser solid particles which have shorter

settling times. Despite being environmentally friendly, this method suffers from poor reproducibility and consistency because the growth of the microbes is difficult to control and the continual changes in environmental conditions tends to destabilise the microbe conditions (Logan & Hunt, 1988; Urbain *et al.*, 1993). When the environment for the microbes destabilises, the settling characteristics of the aggregates deteriorate drastically, causing deflocculation, which increases effluent turbidity and decreases filterability (Forster, 1976; Logan & Hunt, 1988; Sanin & Vesilind, 2000; Urbain *et al.*, 1993). This method also requires large, expensive digesters and extensive mechanical aeration areas which incur significant operational costs (Lapsirikul *et al.* 1994). Bioflocculation remains an inconsistent and unreliable method since it is dependent on the stochastic processes of microbe growth, flocculation, and aggregation, thereby limiting its industrial applications.

Solid-liquid separation techniques are important processes that are used extensively for treating residential and industrial effluents. Conventional particle separation methods present significant limitations, namely: being slow, spatially demanding, having high operational costs, requiring chemical reagents which introduce significant health hazards, and being highly inconsistent and unreliable. These limitations introduce a need for the advancement of existing separation techniques or the development of new techniques capable of addressing current market demands in solid-liquid separation technologies. The motivation for this research is to explore a new approach to solid-liquid separation and to determine the feasibility of using this approach to generate a new particle separation technique that addresses the limitations of existing techniques.

1.1 Aims

The aim of this research is to examine a novel approach to particle separation using fluid turbulence to induce directed motion in particles, causing them to accumulate in specific regions of the fluid flow field; a mechanism known as preferential concentration. The idea of using fluid turbulence as a means of un-mixing particles in a fluid suspension has never been examined before, and the complex nature of particle-fluid

dynamics and interactions has led to numerous open-ended questions in studies pertaining to particle-laden fluids. Consequently, the research presented in this thesis focuses on contributing to the limited literature available on particle-fluid interactions and the driving mechanisms behind preferential concentration, as well as to further the fundamental knowledge pertaining to particle-laden fluids. The present research is limited in that investigations are focused on the effects of particle-fluid interactions on the particle phase, with the aim of determining the feasibility of using this research to uncover a new method of particle separation.

1.2 Thesis Outline

A review of the existing literature in particle-laden fluid studies is detailed and discussed in Chapter 2, from which the objectives of the present research were formulated.

Measurement techniques that were used in the experiments undertaken for this research are presented in Chapter 3. Since one of the laser diagnostic techniques used introduces errors into the measurements, Chapter 3 also details the development of a correction algorithm implemented specifically on that technique for the purposes of this research.

Chapter 4 presents the experimental apparatus and equipment used in this research. In addition, a brief review of Zero-Net-Mass-Flux Jets is provided, which is used as a basis for the design and development of the experimental rig.

Experimental investigations aimed at substantiating existing theories on the preferential concentration mechanism are discussed in Chapter 5. The outcomes of this chapter indicate the possibility of other factors contributing to the directed motion in particles, which may or may not be associated with the preferential concentration mechanism.

Bench-marking studies to determine the feasibility of particle-fluid surface interactions driving the preferential concentration mechanism are discussed in Chapter 6. Experiments established that particle-fluid

surface interactions contribute to particles moving in a directed manner; however, the link to the preferential concentration mechanism remains unsubstantiated.

The effect of fluid excitation frequency on directed particle motion is discussed in Chapter 7. The outcomes of these investigations provide further evidence to indicate that particle-fluid surface interactions influence the directed motion in particles observed in the current research. However, these findings are unlikely to be due to the preferential concentration mechanism.

The final chapter, Chapter 8, presents the conclusions of this present research and recommends future work related to this study.

2 Literature Review

A review of existing particle-laden fluid studies is presented in this chapter. The review includes a discussion of important governing parameters that affect particle-fluid interactions and how these interactions cause directed motion in particles. Particular attention is given to the identification of mechanisms through which this directed particle motion can be controlled so as to enable the formulation of feasible selective particle separation strategies. The chapter concludes with a summary of the research objectives of this thesis and the identified experimental strategies to investigate directed particle motion in fluids for the purposes of selective particle concentration and exclusion.

2.1 Particle-Laden Fluids

The current research proposes the use of fluid turbulence to obtain solid-liquid separation in particle-laden fluids, an idea that relies on the potential of fluid turbulence structures (eddies or vortices) to induce directed motion in particles. However, the understanding of particle-laden flows remains incomplete due to the complexities of flow dynamics following the presence of a broad spectrum of turbulence time scales and length scales associated with both small- and large-scale fluid structures. Berlemont *et al.* (1990), Crowe *et al.* (1988), and Maxey (1987) established that particle behaviour in fluids is determined by particle characteristics and their coupling interaction with the fluid phase. The mechanics of particle-laden flows is further complicated by the different types of coupling interactions that can occur.

Di Giacinto *et al.* (1982) identified two coupling regimes, namely one-way and two-way coupling. One-way coupling is considered when the fluid flow field is not affected by the presence of the particles (Di Giacinto *et al.*, 1982; Kulick *et al.*, 1994). This interaction is dominant when particle concentrations are sufficiently low such that the rate of momentum transfer from particle to fluid is insignificant and fluid turbulence is not affected by particles (Elghobashi, 1991, 1994; Geiss *et al.*, 2004). Conversely, when the presence of particles is capable of modifying the fluid flow field significantly, two-way coupling is considered (Alletto & Breuer, 2012; Di Giacinto *et al.*, 1982). This situation is prevalent when particles carry a significant fraction of the flow's mass, so as to cause significant modifications to turbulence structures due to solid-liquid momentum exchange (Elghobashi, 1991, 1994; Kulick *et al.*, 1994; Vreman *et al.*, 2009). Elghobashi (1991, 1994) identified conditions for which particle-particle collisions are significant in addition to the two-way coupling interactions, a regime termed as four-way coupling. Four-way coupling is considered when inelastic particle-particle collisions are dynamically significant and contribute considerably to the behaviour of the particle ensemble (Alletto & Breuer, 2012; Geiss *et al.*, 2004; Vreman *et al.*, 2009).

Although full physical understanding of particle-laden flows has yet to be achieved, the type of coupling interactions applied to/sustained by the particle-fluid system impacts the behaviour of both the particles and the fluid. Alletto and Breuer (2012) established that simulations using two-way coupling and four-way coupling resulted in significant difference in flow behaviour in their study of bluff-body particle-laden flow. Salehi *et al.* (2019) found that the difference between one-way and two-way coupling was more significant for smaller particles owing to the stronger effect of the carrier phase on the smaller particles (i.e. lower Stokes number). Since the type of phase coupling sustained by the particle-fluid system is a function of a number of governing parameters, appropriate manipulation of these parameters would allow control over fluid turbulence to obtain the desired motion in particles for the purpose of selective solid-liquid separation.

2.2 Governing Parameters

2.2.1 Particle Mass Loading

A parameter termed particle mass loading, introduced by Di Giacinto *et al.* (1982), determines the influence of particle mass on the coupling interaction sustained between both particle and fluid phases. Particle mass loading is expressed as a ratio of particle mass, m_p, to fluid mass, m_f:

$$\beta = \frac{m_p}{m_f} \tag{2.1}$$

Di Giacinto *et al.* (1982) determined that varying β induces different types of particle-fluid coupling, thereby affecting the characteristics of particle-laden flows. These authors indicated that for very small β, the continuous phase is independent of particle influences, while for large β (for instance $\beta > 0.1$), the effect of particles on fluid flow is significant and two-way coupling is considered. Geiss *et al.* (2004) established that two-way coupling interactions are evident when $\beta > 0.05$ while Lain *et al.* (2002) noted that when modelling particle-laden fluid systems, different coupling considerations affected the system differently. For instance, Lain *et al.* (2002) reported that turbulent kinetic energy is reduced with increasing β under two-way coupling considerations, whilst a slight enhancement in turbulence was observed when four-way coupling was considered.

Crowe (2000) found that increasing mass loading results in a two-way coupling situation when the momentum exchange between particles and fluid results in a significant modulation of the base flow. Similarly, Boree *et al.* (2001) found that at moderate to high mass loadings, the presence of particles induced a large modification of the fluid turbulence. Two-way coupling was required to account for the partly responsive particles in their prediction of turbulence attenuation by the particles in bluff-body flows. Such an outcome is an indication that the nature of turbulence modulation due to the presence of particles is also highly dependent on the type of phase coupling considered and the balance between particle-induced turbulence production and dissipation.

Studies examining the influence of β on the characteristics of particle-laden flows have also determined that particles may adhere to a pattern of selective turbulence energy redistribution when attenuating or augmenting the turbulence levels in the fluid phase. Elghobashi and Truesdell (1993) established that particles tend to extract energy from a preferred range of flow scales which in turn affects the energy cascade across the entire turbulence scale. Kulick *et al.* (1994) suggest that at low β, dissipation due to particles acts on the same scales as viscous dissipation, while at higher β, particles affect larger scale structures since heavy particles are less responsive to small-scale fluctuations. Both Di Giancinto *et al.* (1982) and Squires and Eaton (1990) determined that increasing β increases the turbulence kinetic energy in small-scale structures, thereby increasing viscous dissipation which attenuates fluid turbulence. The generalisation of these ideas is cautioned since analyses were limited to a variation of β through a change in particle number density, and that variation of β through the change of particle density was neither accounted for nor considered for comparative purposes.

These studies confirm that the type of phase coupling interactions sustained by a system of particle-laden fluid is a function of β, and the variation of β is capable of modulating the fluid turbulence levels in the system. In addition, although these studies indicate that β can be used to classify the different phase-coupling interactions, a study to establish coupling classification based on β has yet to be undertaken. Consequently, further studies addressing these issues are necessary and warranted.

2.2.2 Particle Volume Loading

When considering mass and momentum conservation equations, Di Giacinto *et al.* (1982) determined that if coupling interactions are accounted for, particle volume fraction is a significant constraint (Berlemont *et al.*, 1990). Particle volume loading can be expressed as a ratio of particle volume to fluid volume:

$$\phi = \frac{V_p}{V_f} \tag{2.2}$$

where V_p is the volume occupied by particles and V_f is the volume occupied by the fluid phase. Berlemont *et al.* (1990) verified that numerical modelling particle-laden flows using ϕ is valid since results obtained are comparable with experimental results, an outcome also confirmed by Durst *et al.* (1984). Reviews by Elghobashi (1991, 1994) utilised ϕ as a means of classifying phase coupling interactions whereby, for very low values, $\phi \leq 10^{-6}$, one-way coupling is assumed, two-way coupling is considered when $10^{-6} < \phi \leq 10^{-3}$ and for very large values, $\phi > 10^{-3}$, four-way coupling is considered. Although these classifications have been used as a guide for simulations and computational modelling work, they have yet to be substantiated experimentally. Nonetheless, the characteristics of particle-laden fluids have been established to be affected by ϕ in that a variation in ϕ (controlled through the variation of particle diameters) is capable of modulating the turbulence level in a fluid phase.

Various studies have established that when ϕ is small (achieved by using small particles), the particles have a tendency to attenuate fluid turbulence (Elghobashi & Truesdell, 1993; Gore & Crowe, 1989; Kulick *et al.*, 1994; Sheen *et al.*, 1994). Elghobashi and Truesdell (1993) explain that these particles impart their energy directly to the small eddy scales, thereby increasing dissipation and leading to an energy cascade from the large- to the small-scale structures, resulting in an overall turbulence attenuation within the system. Kulick *et al.* (1994), in agreement with this idea, determined that turbulence attenuation displayed a range of preferred scales where attenuation was strongest. Particles were observed to absorb energy non-uniformly from large-scale turbulence to augment small-scale turbulence. Gore and Crowe (1989) postulate that fluid turbulence is attenuated because particles follow and extract energy from eddies while Sheen *et al.* (1994) propose that the particles attenuate fluid turbulence because they are unable to respond completely to eddy motions.

When ϕ is large (achieved by using large particles), some studies determined that turbulence levels in the fluid phase are enhanced (Gore & Crowe, 1989; Sheen *et al.*, 1994) while other studies established, in contrast, that fluid turbulence levels are attenuated (Kulick *et al.*, 1994; Squires & Eaton, 1991; Wang & Maxey, 1993). Gore and Crowe (1989) and Sheen *et al.* (1994) suggest that turbulence created in the wake of

particles increases the overall turbulence intensity of the fluid phase. It has also been suggested that particles attenuate fluid turbulence because they are relatively unresponsive to small-scale turbulence fluctuations, thereby damping out these energetic turbulent eddies (Crowe, 2000; Fan *et al.*, 1996; Kulick *et al.*, 1994; Squires & Eaton, 1991; Wang & Maxey, 1993). There is also a possibility that when ϕ is large, both turbulence attenuation and augmentation can occur simultaneously. For instance, particles incur drag forces that attenuate turbulence but wake generation and streamline distortion augment fluid turbulence. This notion in turn suggests that there exist flow conditions whereby one effect (either turbulence attenuation or augmentation) is dominant over the other, an issue yet to be fully investigated.

The studies discussed above have collectively established that the variation of ϕ through particle size is capable of affecting the characteristics of particle-laden flows. However, the consequences of varying ϕ through the change in particle number density have yet to be fully determined, leading to a lack in the literature pertaining to this field of research. It should be noted that the variation of particle number density also impacts on the particle mass loading parameter. Consequently, examination of the effects of particle number density on particle-laden flows involves two inter-dependent parameters. Although studies of this nature are necessary and justified, this field of investigation is yet to be addressed to date due to the high level of complexity associated with the investigations required.

2.2.3 Particle Reynolds Number

Examination of particle-fluid interactions in particle-laden fluids requires the consideration of particle Reynolds numbers (Kulick *et al.*, 1994; Lun, 2000). The flow Reynolds number, Re_f, is conventionally defined as the ratio of inertial forces to viscous forces. However, particle Reynolds numbers are defined in terms of particle inertia and the forces acting on particles since these factors play a vital role in particle dynamics (Best, 1998; Elghobashi *et al.*, 1984; Hetsroni, 1989):

$$Re_p = \frac{2r_p(u_f - u_p)(\rho_p - \rho_f)}{\mu_f} \tag{2.3}$$

where u_f is the mean fluid velocity and u_p is the mean particle velocity (whereby the magnitude of the difference between these two parameters gives the total relative mean velocity or slip velocity between the two phases), r_p is the particle radius, ρ_p is the particle density while ρ_f is the fluid density and μ_f is the fluid dynamic viscosity.

Particle-laden-fluid characteristics have been determined to be affected by Re_p as this parameter can indicate the enhancement or suppression of the fluid turbulence levels due to the presence of particles. Hetsroni (1989) determined that particles with low Re_p attenuate fluid turbulence but indicated that when $Re_p > 400$, particles are able to augment fluid turbulence due to the occurrence of vortex shedding in the wakes of the particles (Achenbach, 1974). Best (1998) and Hadinoto *et al.* (2005) argued that although wake instability and vortex shedding explain fluid turbulence enhancement for $Re_p > 400$, the criterion presented by Hetsroni (1989) is insufficient to explain their findings and may not be applicable for $Re_p < 400$. Best (1998) instead proposed that particle rotation, which influences the fluid flow pattern around particles, causes the enhancement of fluid turbulence and this notion in turn indicates that particles in a flow can cause turbulence enhancement to occur at a much lower Re_p than previously proposed by Hetsroni (1989). It has also been suggested that the nature of turbulence modulation due to particles is dependent on the critical particle Reynolds number, Re_c, which indicates the onset of flow separation around the particles. Lun (2000), using $Re_c \approx 300$ (for the initiation of vortex shedding in particles to occur) established that when the $Re_p < Re_c$, the turbulence field is always attenuated. In situations where $Re_p \approx Re_c$, a combination of turbulence suppression and enhancement can occur in the flow field, and when $Re_p > Re_c$, then turbulence enhancement is prevalent.

Studies have also been undertaken to determine whether particle behaviour in particle-laden fluids are affected by Re_f, a parameter generally used to define flow conditions. Collins and Keswani (2004), Fiabane *et al.* (2012) and Obligado *et al.* (2011) found that particle behaviour leading to the occurrence of particle clustering is Re_f dependent and that particle clustering increased with Re_f. Investigations by Obligado *et al.* (2014) established the range of Re_f

whereby high levels of particle clustering were observed. In contrast, Hogan and Cuzzi (2001) determined that particle clustering is insensitive to Re_f.

Particle-fluid interactions are highly complex and when considered together with fluid turbulence, the interactions are more complicated when compared with simple isolated particles in flows. It should be noted that the nature of particle-laden-fluid studies is such that the influences of individual parameters are very difficult to study in isolation therefore other parameters are generally taken into account concurrently. Re_f and/or Re_p alone will be insufficient at predicting and explaining particle-fluid interactions. The challenge is therefore to determine which parameters should be investigated parametrically and which can be fixed/constrained.

2.2.4 Particle Stokes Number

The particle Stokes number relates both particle and fluid properties in terms of particle inertia and the strength of fluid turbulence. This is an important parameter in particle-laden flows since it can be used to classify how particles respond to the flow, which in turn indicates the dominant type of phase coupling sustained in the system. The particle Stokes number is defined as the ratio of the particle response time, τ_p, to an appropriate turbulence time scale, τ_f:

$$St = \frac{\tau_p}{\tau_f} \tag{2.4}$$

For particles within the Stokes regime ($Re_p << O(1)$), particle inertia, which defines τ_p, may be quantified by calculating the particle time constant (Eaton & Fessler, 1994; Squires & Eaton, 1990):

$$\tau_p = \frac{(2\rho_p + \rho_f)d_p^2}{36\mu_f} \tag{2.5}$$

where ρ_p is the particle density, ρ_f is the fluid density, μ_f is the fluid dynamic viscosity and d_p is the particle diameter. When particles are much denser than the fluid phase, this equation reduces to:

$$\tau_p = \frac{\rho_p d_p^2}{18\mu_f} \tag{2.6}$$

These expressions for time constants are still accurate for $Re_p \to O(1)$ despite the fact that the assumptions of Stokes' analysis may be violated under some of these situations (Eaton & Fessler, 1994). However, in situations where Re_p is too large for the Stokes law approximation to hold, i.e. $Re_p > O(1)$, particle time constants are estimated using simplistic drag laws such as the one reported by Friedlander (1977, p. 105):

$$C_D = \frac{24}{Re_p}(1 + 0.158Re_p^{2/3}) \tag{2.7}$$

This expression had previously been verified to agree well with experimental results for $Re_p \to 1000$ (Serafini, 1954). In numerical simulations by Wang *et al.* (2016), Equation 2.7 was applied in the calculation of τ_p for when $Re_p < 1000$, resulting in the following:

$$\tau_p = \frac{\rho_p d_p^2 C_c}{18\mu_f(1 + 0.15Re_p^{0.687})} \tag{2.8}$$

where C_c is the Stokes-Cunningham factor.

The strength of local fluid turbulence, τ_f, can be determined using either micro or macro fluid time scales, unlike τ_p. As a consequence, the definition of τ_f is highly dependent on the nature of the investigation undertaken. One typical value is determined through consideration of the Kolmogorov time scale. The Kolmogorov time scale represents the turnover time of eddies at the smallest scales of turbulence, and is given by:

$$\tau_k = (\frac{\nu_f}{\epsilon})^{\frac{1}{2}} \tag{2.9}$$

where ν_f is the fluid kinematic viscosity and ϵ is the dissipation rate of the turbulent kinetic energy in the flow per unit mass.

Wang and Maxey (1993) determined that fluid turbulence at the Kolmogorov scale induces localised particle accumulation in the system,

an indication that small-scale dissipation plays an important role in particle-laden fluid dynamics. Fessler *et al.* (1994) established that when flow conditions are such that $St \approx O(1)$ using the Kolmogorov time scale, particle motion is significantly affected by fluid turbulence. However, particles were also observed to be affected by fluid turbulence at length scales significantly larger than the Kolmogorov scale, indicating that each particle is most affected by fluid structures corresponding to $St \approx O(1)$ (Fessler *et al.*, 1994). Consequently particle-laden fluid characteristics are affected by, but not limited to, the influence of fluid turbulence on the Kolmogorov scale and such an outcome indicates that Kolmogorov scaling is limited to studies where small-scale turbulent structures are investigated (Aliseda *et al.*, 2002; Squires & Eaton, 1991; Wang & Maxey, 1993).

Alternatively, the integral fluid time scales which are associated with large-scale eddies in the fluid flow can also be used in the determination of the St parameter. In free shear flows, this time scale is often based on the length scale of the vortex structures, L, and the propagation velocity of coherent vortices, U_v, formed due to Kelvin-Helmholtz instabilities (Anderson & Longmire, 1995):

$$\tau_{int} = \frac{L}{U_v} \tag{2.10}$$

This definition by Anderson and Longmire (1995) is justified since a study by Crow and Champagne (1971), investigating large-scale structures in jet turbulence, established that large-scale vortex rings roll up quasi-periodically downstream of the jet nozzle exit as a result of the Kelvin-Helmholtz instability. Crow and Champagne (1971) also established that these large-scale vortex rings dominate the structures of single-phase jets up to four nozzle diameters downstream. However, Petersen and Samet (1988) determined that organised helical structures are still important beyond this axial location and Dahm and Dimotakis (1987) established that large-scale structures have a strong influence on fluid mixing and entrainment in the far field of turbulent jets. Extending these outcomes to studies involving particle-laden fluids, this definition of τ_{int} to determine the St parameter has also been used when large-scale fluid structures are dominant in the system (Crowe *et al.*, 1988, 1995). Various studies have established that when $St \approx O(1)$

using the integral time scale, particle motion is significantly influenced by large-scale turbulence structures (Hishida *et al.*, 1992; Longmire & Eaton, 1992; Tang *et al.*, 1992; Wark *et al.*, 2000; Wen *et al.*, 1992). These studies have indicated that particles in this Stokes range are unable to respond to small-scale vortices in the flow but are influenced by large-scale vortices which possess fluid time scales approximately equivalent to the particle response time. This notion is supported by results from Anderson and Longmire (1995) and Yang *et al.* (2000). These outcomes therefore indicate that the integral time scale is also applicable when determining the Stokes number and that particle-laden flow characteristics are also influenced by large-scale turbulence structures.

Collectively, these studies indicate that both Kolmogorov and integral time scales are applicable when determining the Stokes number and that the fluid time scale used should be based entirely on the scale of fluid turbulence involved in a particular study. Scott *et al.* (2009) established that inertial particles interact with a broad range of fluid scales or eddy sizes, and so concluded that both integral-size and Kolmogorov-size eddies have significant contributions to the preferential concentration mechanism. Experimental results by Sumbekova *et al.* (2016) indicate that clustering of inertial particles occurs at all scales of turbulence and this observation is in agreement with Wood *et al.* (2005) who found that preferential concentration occurs over a wide range of scales, with the peak shifting towards the larger length scales at higher St and Re_p. These studies therefore indicate that the preferential concentration is a multi-scale phenomenon, with particles responding to fluid turbulence scales that correspond to $St \approx O(1)$ (Coleman & Vassilicos, 2009; Scott *et al.*, 2009; Wood *et al.*, 2005).

Ordered particle dispersion patterns are observed to be evident when $St \cong O(1)$ in studies using either τ_k or τ_p in the determination of the Stokes number since the particle time scale is selected based on the fluid scale investigated (Aliseda *et al.*, 2002; Crowe *et al.*, 1995; Eaton & Fessler, 1994; Longmire & Eaton, 1992; Monchaux *et al.*, 2012; Wen *et al.*, 1992; Yang *et al.*, 2000). When $St < O(1)$, particles act as flow tracers, following all fluid motions and maintaining velocities similar to those of fluid elements (Crowe *et al.*, 1988, 1995), as illustrated in Figure 2.1. Conversely, when $St > O(1)$, particles are unresponsive to

fluid motions and turbulence structures have insufficient time to influence particle motion (Crowe *et al.*, 1988, 1995) (Figure 2.1). When $St \cong O(1)$, particles are partially responsive to fluctuations in the flow velocity, in that their paths are influenced by fluid motion, although they do not follow the trajectories of fluid elements precisely (Longmire & Eaton, 1992). As a result, these particles tend to move in a directed manner to accumulate in specific regions within the fluid flow field, resulting in the occurrence of preferential concentration (Crowe *et al.*, 1988, 1995; Scott *et al.*, 2009; Tang *et al.*, 1992). Figure 2.1 depicts one model explaining the preferential concentration mechanism attributed to a vortical centrifuging effect (Anderson & Longmire, 1995; Crowe *et al.*, 1988, 1995; Eaton & Fessler, 1994; Longmire & Eaton, 1992; Tang *et al.*, 1992; Wen *et al.*, 1992; Wood *et al.*, 2005).

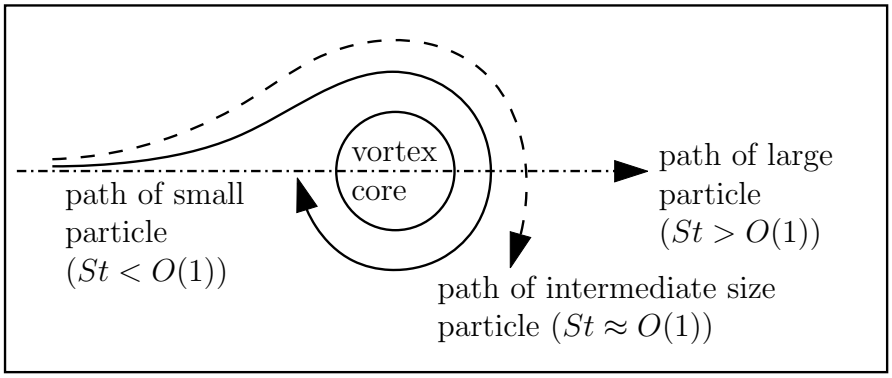


Figure 2.1: Conceptual model of the effect of Stokes numbers on directed particle motion postulated by Crowe *et al.* (1988, 1995).

In contrast, although Han *et al.* (2020) found that maximum preferential concentration occurred when $St \cong O(1)$, this study still observed preferential concentration occurring at $St > O(1)$. For $St < O(1)$, it was found that preferential concentration was hardly present (Han *et al.*, 2020). Obligado *et al.* (2014) similarly found that particles were clustering for $St \geq O(1)$ in their study of inertial particles in homogenous isotropic turbulence while Wittemeier and Shrimpton (2018) reported that depending on the average particle number density and gravity, the maximum preferential concentration does not necessarily occur at $St \cong O(1)$. Coleman and Vassilicos (2009) and Goto and Vassilicos (2006) previously found that the centrifuging

effect is unable to explain the multi-scale clustering of particles with high Stokes number and proposed an alternative mechanism whereby the clustering of inertial particles reflects the clustering of acceleration stagnation points. This mechanism termed 'sweep-stick' has since been used to explain particle concentration in specific points of a carrier flow, particularly for conditions whereby $St > O(1)$ (Obligado *et al.*, 2014; Sumbekova *et al.*, 2016). The physical mechanisms mentioned here that are based on the centrifuging effect and the sweep-stick mechanism will be discussed further later in this chapter.

2.2.5 Particle-Fluid Surface Interaction Influences

Figure 2.2 shows a schematic representation of viscosity (sometimes referred to as 'apparent viscosity' or shear-dependent viscosity in literature) versus shear rate (or velocity gradient) curve for all suspensions (Barnes *et al.*, 1989). The curve indicates that in the limit of very low shear rates the viscosity is constant and in the limit of high shear rates the viscosity is again constant but at a lower level. These two regions of constant viscosities are known as the lower and upper Newtonian regions (the lower and upper refer to the shear rate not viscosities) and are used to describe the two regions where the viscosity reaches constant values. Between these two Newtonian regions is a region where viscosity is found to decrease with increasing shear rate, giving rise to a behaviour called 'shear-thinning' in various materials. At some point and under the appropriate conditions (beyond the second Newtonian region), there are cases where the viscosity increases with shear rate, a behaviour generally called 'shear-thickening'.

Factors controlling the details of the general flow curve of suspensions are highly dependent on hydrodynamic forces which act on the surface of particles or the aggregate of particles in the working fluid (Barnes *et al.*, 1989), which in turn requires consideration of the particle-fluid surface (interfacial) interactions. Since these forces are generally independent of particle density, it follows that ϕ is considered the dominant parameter over β (despite the inter-dependency of these parameters) in studies concerned with particle-fluid surface interactions. Hydrodynamic forces acting on particles suspended in a

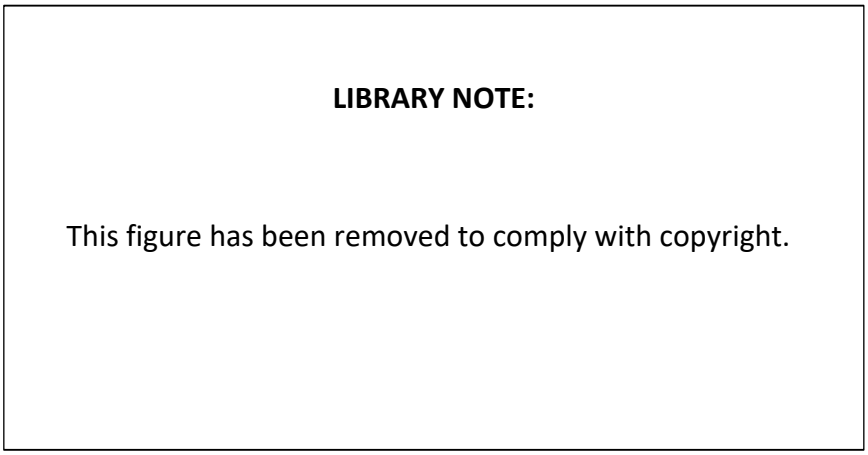


Figure 2.2: Schematic representation of the flow curve of a suspension (adapted from Barnes *et al.*, 1989).

liquid include (Barnes *et al.*, 1989):

- **colloidal forces** arising from the interactions between particles that are controlled by fluid properties (such as polarisability but not by viscosity), resulting in an overall attraction or repulsion between particles;
- **Brownian randomising forces** that are strongly dependent on particle size (these forces are negligible for particle sizes above 1μm);
- **viscous forces** acting on particles.

Particular attention is given to the viscous forces acting on particles since flow conditions in the experiments undertaken, with ϕ within the two-way coupling regime and particle sizes being much greater than 1μm, effectively make viscous forces the dominant particle-fluid-surface interaction.

The viscous forces are proportional to the local velocity difference between particles and the ambient fluid. Consequently, the viscosity of

the continuous phase, which scales all particle-fluid surface interactions, affects the suspension viscosity. The suspension viscosity can therefore be considered as the viscosity relative to that of the continuous phase (Barnes *et al.*, 1989). Induced particle motion due to fluid structures (such as the preferential concentration mechanism) observed macroscopically would, in turn, be highly dependent on microstructural considerations of this nature. The direction of the present discussion therefore explores the link between particle motion due to the preferential concentration mechanism and suspension rheology by considering the contribution of individual particles towards the overall suspension viscosity.

Consider an isolated particle within a fluid flow field. The presence of the particle would cause deviations in the fluid streamlines, which would increase the 'flow resistance' (i.e. viscosity). In fluid flow fields with a high particle concentration, particles have to move out of each other's way and the continuous phase has to flow around more particles, causing the fluid flow between particles to experience more resistance, resulting in a further increase in suspension viscosity. In situations involving particles that agglomerate or flocculate, which effectively increases the apparent phase volume, even more resistance is encountered between particulate structures, which gives rise to a higher than expected viscosity (based on the nominal volume loading). This line of reasoning has been examined extensively in studies concerned with the rheology of suspension since Einstein (1906, 1911), as cited in Barnes *et al.* (1989) and Mueller *et al.* (2010), who theorised that particles are capable of increasing the viscosity of a liquid as a function of their particle volume loading:

$$\eta = \eta_o(1 + 2.5\phi) \tag{2.11}$$

where η is the effective/apparent viscosity of the suspension, η_o is the viscosity of the pure fluid phase, and ϕ is the particle volume fraction in the suspension. This theory neglects the effects of other particles since the consideration of particle-particle interaction is accounted for by higher order terms in ϕ. In situations whereby interactions between particles are significant, Batchelor (1977) gives:

$$\eta = \eta_o(1 + 2.5\phi + 6.2\phi^2) \tag{2.12}$$

Therefore, the mathematical expression presented by Einstein (1906, 1911) (Equation 2.11) is restricted to predicting the viscosity of a Newtonian fluid containing a dilute suspension of particles ($\phi \leq 10\%$). Non-Newtonian behaviour is generally observed when $\phi > 40\%$ (Stickel & Powell, 2005), and such fluids are beyond the scope of the current research. In situations for concentrated suspensions, the Krieger-Dougherty microstructure viscosity equation (Krieger, 1972) is often used (Luckham & Ukeje, 1999; Mueller *et al.*, 2010; Nicodemo *et al.*, 1974; Stickel & Powell, 2005; Wildemuth & Williams, 1984):

$$\eta = \eta_o \left(1 - \frac{\phi}{\chi}\right)^{-[\eta]\chi} \tag{2.13}$$

where χ refers to the packing fraction of the particles and $[\eta]$ refers to the intrinsic viscosity of the suspending medium, and is 2.5 for spheres. The $[\eta]$ parameter is dimensionless and is defined as (Krieger, 1972):

$$[\eta] = lim_{\phi \to 0} \left(\frac{\eta}{\eta_o} - 1\right) / \phi \tag{2.14}$$

Equation 2.13 reduces to Einstein's equation (2.11) when ϕ is small. These correlations indicate that viscosity increases with increasing volume fraction, whereby the sensitivity of the viscosity to that of the continuous phase is multiplicative instead of additive. Consequently, particle volume fraction affects the nature of the relationship between the shear rate and viscosity for the working system. Since hydrodynamic forces acting on particle surfaces are a principal influence over flow characteristics of particle suspensions, particle-fluid surface interactions should also be considered when investigating particle-laden flows (Barnes *et al.*, 1989; Mueller *et al.*, 2010; Stickel & Powell, 2005).

2.3 The Preferential Concentration Phenomenon

When particle-laden fluids are subjected to certain flow conditions, the fluid turbulence is capable of inducing directed motion in particles, resulting in strong inhomogeneities in the particle concentration field. The occurrence of this non-random accumulation of particles within the fluid has been described in the literature as the preferential concentration phenomenon. Governing parameters (discussed in the previous section) influencing particle-laden fluid characteristics have been used as a means of identifying the flow conditions necessary for this phenomenon to occur.

According to a review by Monchaux *et al.* (2012), the preferential concentration phenomenon can be decomposed into three distinct aspects. The first aspect is clustering, which is the accumulation and segregation of particles, which in turn generates both very high and low particle concentration regions within the fluid. The second aspect is clusters, which refers to the groups of particles that remain close to one another on time scales comparable to some turbulence time scale. The third aspect is preferential concentration, which is the preferential movement of particles towards specific regions in the flow which are associated with some particular strain rate distributions or fluid acceleration within the flow. As a consequence of these definitions, clustering is considered a concentration issue, clusters are considered to be time-dependent entities with possible collective effects, and preferential concentration refers to the mechanism responsible for both clustering and cluster evolution (Monchaux *et al.*, 2012). The authors of this review consider that preferential concentration still holds for individual inclusions or in diluted conditions, even when particle accumulation is not visually identifiable.

Various studies with different experimental conditions, have been undertaken to investigate preferential concentrations. For instance, in the examination of particles in a mixing layer, Brown and Roshko (1974) established that heavy particles interact in a very specific manner with large-scale turbulence structures, but the authors were

unable to ascertain any specific conclusions regarding the nature of these interactions. Experiments by Wen *et al.* (1992) examining the role of organised spanwise vortex structures in directed particle dispersion, established that heavy particles disperse significantly faster than the fluid. These authors proposed that the vortices act as mobile centrifuges, displacing particles radially from their centres to the outer edges of the vortices as they convect downstream (Figure 2.3). The dispersion of particles, effectively migrating away from the centre of the mixing layer, indicates that individual particle motions are connected to large-scale organised vortex dynamics and are strongly dependent on the time-scale ratios of the particles.

LIBRARY NOTE:

This figure has been removed to comply with copyright.

Figure 2.3: Particle dispersion patterns for a plane mixing layer (a) Unforced condition (b) Forced near dominate instability frequency (Wen *et al.*, 1992).

In contrast with mixing layers, large-scale vortices in a wake do not pair and merge but instead move downstream in a separate but organised pattern (Crowe *et al.*, 1995). Despite these differences, experiments by Tang *et al.* (1992) investigating directed particle dispersion in the wake of a thick plate, observed results that were comparable with Wen *et al.* (1992) (Figure 2.4).

Large-scale vortex structures were also found to dominate the organised particle dispersion in a plane wake, and the numerical results presented are in agreement with actual instantaneous velocity fields (Tang *et al.*, 1992). Similar behaviours were also reported by Crowe *et al.* (1995) in photographic results for a bluff body wake flow containing heavy particles with very small and intermediate Stokes numbers (Figure 2.5). The photographs demonstrated a high degree of inhomogeneity, whereby intermediate size particles appear to concentrate near the

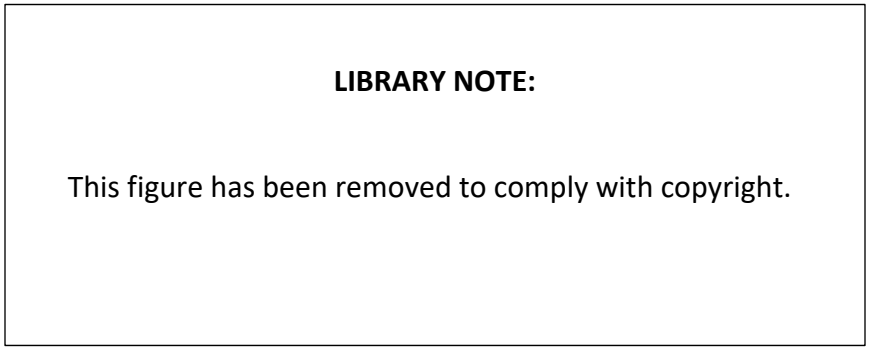


Figure 2.4: Particle dispersion pattern for a plane wake (a) Experimental result (b) Simulated result (Tang *et al.*, 1992).

edges of the vortices while particles with smaller Stokes numbers followed the fluid path lines and distributed themselves throughout the vortex structures. These results indicate that intermediate-size particles accumulated in thin regions on the outer edges of the large vortex structures, thus indicating that particle dispersion rates are also strongly dependent on particle Stokes numbers.

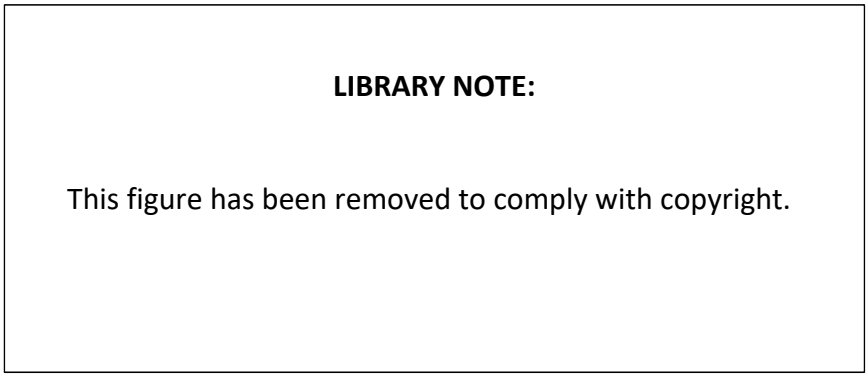


Figure 2.5: Particle dispersion patterns in the wake of a bluff body (a) Particles with small Stokes numbers ($St << 1$) (b) Particles with intermediate Stokes numbers ($St \approx 1$) (Crowe *et al.*, 1995).

Longmire and Eaton (1992) and Wark *et al.* (2000) investigated the effects of acoustically-excited particle-laden jets to generate consecutive vortex ring structures (Figure 2.6). The acoustic forcing provided a means of controlling the vortex structures, which in turn controlled the location of particle dispersion and accumulation. These authors

observed that particles with $St \approx O(1)$ were accumulating in the saddle regions between vortices and being entrained at the periphery of the vortices while leaving the vortex cores devoid of particles. These results indicate that particles strongly concentrate in high strain-rate regions between vortex structures rather than high vorticity regions in vortex cores.

LIBRARY NOTE:

This figure has been removed to comply with copyright.

Figure 2.6: (a) Single-phase and particle-laden flow forced at low frequencies (Longmire & Eaton (1992) (b) Phase-locked images of droplet-laden jet (non-reacting flow) (Wark *et al.*, 2000) (c) Postulation by Longmire and Eaton (1992) that particles are pulled out of the streaming region inside the vortex rings and pushed into the regions downstream of the vortex cores where particle clusters appear.

The influence of gravity on inertial particles as they interact with fluid turbulence was also found to have a significant impact on the preferential concentration mechanism (Aliseda *et al.*, 2002; Dejoan & Monchaux, 2013; Wang & Maxey, 1993). Numerical work by Wang & Maxey (1993) discussed the influences of preferential sweeping, where gravity causes these particles to have a downward trajectory with respect to the surrounding fluid and these particles interact with different vortices along their trajectories (Figure 2.7b). Experiments by Aliseda *et al.* (2002) established that particle settling velocity is enhanced by turbulence and that large inhomogeneities are generated within a particle concentration field, observations similarly established by Dejoan and Monchaux (2013). This study supported all qualitative features of the numerical results by Wang & Maxey (1993), however, the quantitative differences observed were attributed to the contributions of preferential sweeping and the preferential concentration of particles in turbulence structures. Aliseda *et al.* (2002) considered that as particles come close enough and cluster, they start to interact

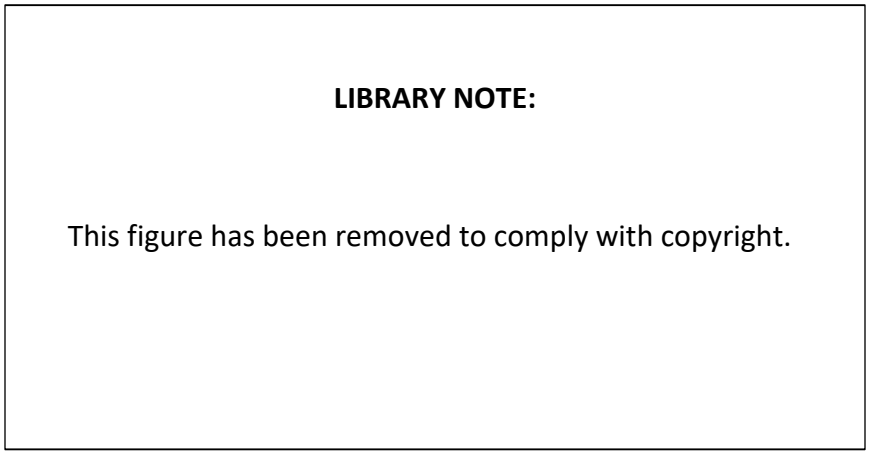


Figure 2.7: Sketch for illustrative purposes only: (a) inertial bias influence of particles interacting with flow vortical structures (b) preferential sweeping mechanism for a heavy particle interacting with local flow vortical structures under its inertia and body force (c) particle clusters that are formed continues to settle, entraining other particles which in turn increases its settling velocity. Settling velocities for particles in (c) were found to be larger than (b) (Aliseda *et al.*, 2002). Illustration adapted from Wang & Maxey (1993).

with the surrounding fluid collectively, behaving as large pseudo particles and as such no longer react to turbulence independently. These clusters continue to settle and due to their increased relative density, experiences an increase in settling velocity while still entraining other particles into the clusters (Figure 2.7c). Preferential concentration of particles is then observed when particle clusters are entrained by turbulence structures and redistributed (or accumulated) in a non-random manner.

Although the physics and fundamental understanding of the preferential concentration mechanism itself is yet to be established, various theories have been discussed in the literature in an attempt to explain this phenomenon. Wen *et al.* (1992) attributed the preferential concentration phenomenon to a particle dispersion process that is

separated into a stretching sequence and a folding sequence (Figure 2.8). The stretching sequence is associated with regions of high velocity gradient on the boundaries of adjacent vortex structures (such as vortex sheet regions connecting the large-scale vortices). Squires and Eaton (1990) used a pseudo-spectral technique to simulate forced isotropic turbulence and found that particles tend to concentrate in areas of high shear. This observation supports the stretching hypothesis presented by Wen *et al.* (1992).

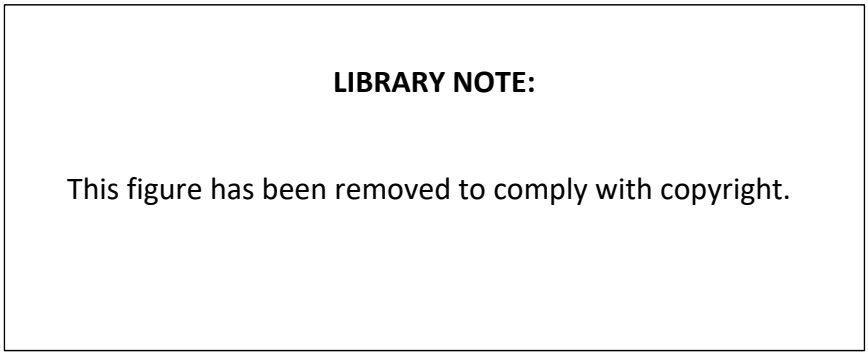


Figure 2.8: The stretching and folding mechanism proposed by Wen *et al.* (1992) (a) Stretching of particle streak-lines near boundaries of vortices (b) Folding of particle streak-lines during vortex pairing (Tang *et al.*, 1992).

According to Crowe *et al.* (1995), the rotational nature of large vortex structures tends to separate neighbouring particles rapidly in these high shear regions. Sheets of particles therefore either ride on the upstream side of the large-scale vortices, or they are centrifuged into the high-speed stream as a direct result of this stretching mechanism. The second stage of the dispersion process, the folding sequence, is associated with the pairing interactions of adjacent large-scale vortices. As vortex structures pair and merge with each other, the particle sheets tend to fold on each other towards the low speed side of the mixing layer. This folding sequence could explain the thin regions of particle accumulation on the outer edges of vortex structures in plane mixing layers observed by Wen *et al.* (1992) and would seem to be associated with the vortex pairing phenomena intrinsic to mixing layers. However, this theory does not explain the occurrence of particle accumulation in the absence of vortex pairing interactions, for instance the particle dispersion process in a wake flow where vortex pairing interactions are

rarely observed (Tang *et al.*, 1992). In this study by Tang *et al.* (1992), the authors observed a highly-organised accumulation of intermediate size particles ($St = 1$) along the boundaries of the large-scale vortex structures while larger or smaller size particles ($St = 10$ and $St = 0.01$ respectively) produced considerably less-organised dispersion patterns.

Alternatively, the speculation by Crowe *et al.* (1988) on the potential role of large eddies causing a systematic dispersion of particles (observed qualitatively in experiments) led Eaton and Fessler (1994) to attribute the preferential concentration mechanism primarily to coherent vortical structures. Eaton and Fessler (1994) established that a dense particle in the vicinity of a vortex structure does not follow fluid streamlines close to the vortex core (Figure 2.1). As this particle moves towards the outer boundary of the vortex structure, the curvature of the local flow eventually decreases such that the particle will then follow local fluid path lines which circulate around the vortex. An alternative view of this theory is that the dense particle in a vortical structure is centrifuged from the vortex core and viscous dissipation causes the particle motion to be damped (Longmire & Eaton, 1992). This leads to the forming particle clusters in the braid regions between vortices (areas of high strain rates and low vorticity).

Similar observations were noted in various numerical simulation investigations concerned with the interaction between particles and large eddies in cellular flows (Maxey & Corrsin, 1986), discrete vortices (Chein & Chung, 2004; Chung & Troutt, 1988) and Stuart vortices (Crowe *et al.*, 1985). These investigations show that significant local accumulations of particles do occur due to the effects of particle inertia. Kinematic simulations by Maxey (1987) provided evidence that the divergence of particle velocity is negative in regions of high strain rate and low vorticity, indicating that these regions are where particle accumulation occurs. Investigations by other researchers have since verified Maxey's theory, confirming that inertial particles influenced by fluid turbulence do indeed preferentially concentrate at these regions (Anderson & Longmire, 1995; Eaton & Fessler, 1994; Longmire & Eaton, 1992; Scott *et al.*, 2009; Squires & Eaton, 1990, 1991; Wang & Maxey, 1993; Wood *et al.*, 2005). It should be noted that this theory has only considered systems with inertial particles having densities that are significantly larger than the density of the fluid phase.

Bec *et al.* (2006) determined that inertial particles with small St ($\tau_p << \tau_k$) within a flow, behaving like flow tracers, may be trapped in vortices for rather long times, and the relative numbers of particles with $St \rightarrow O(1)$ tend to decrease over time. The authors found that such inertial particles concentrate in regions of low vorticity, and hence concluded that preferential concentration is very effective on inertial particles with small St. Such observations further support the work of Eaton and Fessler (1994) regarding the preferential concentration mechanism. However, Bec *et al.* (2006) found that the response time of inertial particles with large St is too large to maintain the correlation between particle trajectories and the local flow pattern, and hence speculated that the role of preferential concentration becomes less important for $St > O(1)$. The centrifuging theory proposed by Eaton and Fessler (1994) is therefore unable to explain clustering at moderately high particle Stokes numbers. Similarly, Coleman and Vassilicos (2009) determined that the centrifuging theory is likely to prevail for particles with $St < O(1)$, while 'sweep-stick' (discussed in further detail below) is expected to dominate for $St > O(1)$. Such results indicate the possibility that there are other physical processes contributing to the occurrence of the preferential concentration phenomenon. Further investigation to determine if such mechanisms occur concurrently or perhaps transition between the different mechanisms under specific conditions would help understanding of the different outcomes of the various work.

Goto and Vassilicos (2006) suggested that the claim that particles tend to move away from vortical regions and accumulate in high strain rate regions cannot be generalised since previous numerical and experimental work supporting this theory were completed for a very limited range of particle Reynolds numbers. According to Goto and Vassilicos (2006), particle clustering in fluid turbulence requires consideration of the entire range of fluid scales involved through a sequence of processes termed sweeping and stickiness. The sweeping process considers that large eddies (sweeping both small eddies and particles with them) cause particles to stay within eddies long enough to be centrifuged out of them. Goto and Vassilicos (2006) also indicated that "the sweeping of the acceleration field by the velocity field" causes the inertial particles to cluster in a way that closely mimics the

zero-acceleration points cluster. These authors asserted that clustering of inertial particles in high Reynolds number turbulence would not occur without this sweeping of turbulence and particles and this claim is supported by results using 2D simulations, establishing that clustering of inertial particles occurs at zero-acceleration points instead of high strain rate regions. The stickiness process relies on the fact that the movement of zero-acceleration points, together with nearby inertial particles within the local velocity fields, is induced by larger eddies. The sweeping and stickiness concepts have been extended to 3D turbulence on a more quantitative level and were introduced collectively as the sweep-stick theory by Chen *et al.* (2006) to explain particle clustering (Chen *et al.*, 2006; Coleman & Vassilicos, 2009; Goto & Vassilicos, 2006). Goto and Vassilicos (2006) claim that this mechanism confirms that the clustering of inertial particles occurs over many length scales and that this mechanism is valid over the entire Stokes number range.

Building on the work of Goto and Vassilicos (2006), Sumbekova *et al.* (2016) have since indicated that preferential concentration is a multi-scale clustering process triggered by mechanisms such as the sweeping and stickiness process, a finding in agreement with Obligado *et al.* (2014). Sumbekova *et al.* (2016) indicates that the Reynolds number has a more dominant role compared to the Stokes number, hence explaining observations where particle clustering occurs when Stokes number exceeds unity. Falkinhoff *et. al* (2020) utilised the sweep-stick mechanism argument for heavy particles with gravity which aligned with the work of Sumbekova *et al.* (2016). However, the findings of Falkinhoff *et. al* (2020) established the dependence of particle accumulation on Stokes number and the settling velocity of particles. Uhlmann and Chouippe (2017) noted that the precise mechanism by which particles are attracted to the specific vicinities in the flow (locations termed 'sticky' points) remains unknown and therefore it remains unclear how effective the sweep-stick mechanism is at parameter points other than those with detailed data. In addition, while this study was able to find evidence of the sticking part of the sweep-stick mechanism, the sweeping part remains an unknown. With many questions remaining unanswered relating to the sweep-stick mechanism, caution should be taken against generalising that centrifuging effects be used to explain particle concentration occurring

at low-vorticity points and sweep-stick be used for particles concentrating at low-acceleration points. Collectively, these studies reaffirm that various inter-dependent parameters do affect the preferential concentration of particles. Noting that the separation and/or isolation of these various parameters is an extremely difficult task, further studies to extend quantitative understanding of preferential concentration to a broader range of parameter values is therefore warranted.

Although a significant number of studies have been undertaken to investigate the preferential concentration phenomenon to date, these studies have only examined dense, inertial particles within a fluid system. Consequently, the theories and postulations presented are principally based on the momentum exchanged between the particle and fluid phases since only inertial particles (i.e. particle density is significantly larger than fluid density) are considered. Although the sweep-stick mechanism has been used on occasions to compensate for the shortfalls of the centrifugal theory, many questions regarding the relevance of the sweep-stick mechanism for finite-size particles still remain. The effects of particle-fluid interfacial influences on the preferential concentration phenomenon therefore remains an unanswered question and the applicability of existing theories explaining the preferential concentration mechanism, when applied to non-inertial particles, is yet to be explored. Further research examining these issues is therefore necessary and warranted.

2.4 Consolidation of Literature and Research Objectives

The field of particle-fluid un-mixing has grown due to the preferential concentration mechanism that is capable of inducing non-random, directed motion in particles for the purposes of particle exclusion and/or selective particle extraction. The preferential concentration mechanism is influenced by the coupling interaction between the particle and fluid phases, leading to particle-laden-fluid systems having highly complex flow dynamics. In addition, studies concerning preferential concentration are restricted by the limitations of existing experimental techniques, leading to a prevalence in computational and numerical simulations over the past 30 years (Monchaux *et al.*, 2012). Despite all these studies, the understanding of particle-laden fluids and the preferential concentration mechanism are still limited, and this is reflected by the inadequacy of current computational models to provide an accurate representation of this type of working system. There is therefore a need for more experimentally-based investigations into particle-laden flows to demonstrate the existence of preferential concentration, to provide a means to understand this mechanism, and to establish a method to relate its features to specific characteristics of the continuous phase.

Existing experimental studies involving particle-laden flows have been dominated by jet flows and no studies within these constraints have been extended to particles in a fluid suspension. In addition, these studies have only examined dense, inertial particles. Consequently, system characteristics have only been explained using mass and momentum exchanges brought on by the presence of inertial particles in jets. Neither accountability nor consideration has been given to the influence of interfacial interactions between the surfaces of the particle and the fluid phases, resulting in a paucity of knowledge in regards to this issue relating to particle-laden fluid characteristics. Therefore, it remains unclear if the system characteristics would change with the use of non-inertial particles as the solid phase and should a change exist, how it would affect the capabilities of the preferential concentration mechanism as a means of particle exclusion and/or concentration.

Existing theories presented to explain the preferential concentration mechanism, based on mass and momentum exchanges, are thus restricted in their applicability to dense, inertia particles in fluids. Such an unintentional gap in research activities to date has contributed to the existing deficiency in both the fundamental understanding of particle-laden flows and the experimental substantiation of the underlying physics governing the preferential concentration mechanism.

A number of flow parameters governing particle-laden flow characteristics can be used as the means of identifying the conditions necessary for preferential concentration to occur. Studies involving particle-laden fluids have indicated that the Stokes number, St, is a major predictor of the occurrence of preferential concentration and the determination of the St parameter relies on the fluid length scale being investigated. Conversely, due to the nature and the definition of the particle Reynolds number, Re_p, studies involving non-inertial particles render Re_p irrelevant as a preferential concentration indicator. Analyses and comparisons of the influences of particle volume loading, ϕ, and particle mass loading, β, on the preferential concentration mechanism are highly complicated due to the inconsistent use of these parameters in the literature. Consequently, the effects of ϕ and β on the preferential concentration mechanism remain an open question which requires further investigation to facilitate a deeper understanding of particle-laden flows.

The preferential concentration mechanism presents the potential of solid-liquid separation (separating all solids from the liquid phase) as well as selective particle un-mixing (separating specific solids from a range of solids within the liquid phase) in industrial applications involving colloids and/or effluents in large tonnages. To date, there are no experimental data relating preferential concentration to the un-mixing of particles in a fluid suspension, and no available data on the velocity profile and particle distribution undergoing preferential concentration in a fluid suspension. Therefore, although evidence suggests the feasibility of this mechanism as a novel approach to selective particle un-mixing in fluid suspensions, this proposition has yet to be validated experimentally.

Based on the review of the theory and literature pertaining to particle-laden fluids and the preferential concentration mechanism, the objectives of this research are defined as follows:

- to design, manufacture and develop a suitable vortex generator setup capable of providing the flow conditions that would enable particle velocity and concentration measurements to be acquired simultaneously;
- to measure velocity profiles and concentration distributions of particles within the vicinity of vortex structures;
- to develop a laser attenuation correction algorithm to improve the accuracy of particle concentration measurements acquired through the Planar Nephelometry technique;
- to substantiate existing theories on the preferential concentration mechanism experimentally;
- to establish whether preferential concentration is able to cause non-inertial particles to move in a directed manner experimentally;
- to establish the relationship between regions of particle accumulation in relation to specific features of the continuous phase;
- to examine alternative factors, besides particle mass and inertia, contributing to the directed motion in particles;
- to determine the influences of particle-fluid surface interactions on the directed motion of particles;
- to determine the influences of fluid excitation frequency on the directed motion of particles;
- to determine the relationship between particle-fluid surface interactions and the preferential concentration mechanism;
- to determine the feasibility of using the preferential concentration mechanism for the purposes of un-mixing particles within a fluid suspension.

The research objectives discussed here were conceived so as to contribute to the fundamental knowledge of particle-laden flows. For this reason the research is formulated to focus on the control of the preferential concentration mechanism to be applied to particles in a fluid suspension. Through further understanding of particle-laden flows, the eventual expectation of this work is that it will lead to improvements in the effectiveness of existing solid-liquid separation processes, and the development of a novel selective particle un-mixing and separation technique. Not only has such research not been performed before, it would also provide the most fundamental point of reference for studies involving preferential concentration and selective particle separation technologies. Consequently, for these reasons, investigations into the preferential concentration mechanism on particles in a fluid suspension is warranted and justified.

3 Measurement Techniques

Simultaneous measurements of both the velocity field and the concentration distribution of particles were required to address the aims and objectives of the research. This chapter discusses the measurement techniques selected and their implementation. This discussion also explores the methods developed to mitigate sources of error in the experimental data.

3.1 Velocity Measurements

The particle-laden flow studies discussed in the literature have predominantly adopted Laser Doppler Velocimetry (LDV) to measure particle velocities (Fan *et al.*, 1996; Hishida *et al.*, 1992; Kulick *et al.*, 1994; Longmire & Eaton, 1992; Modarress *et al.*, 1984; Popper *et al.*, 1974). This technique, also referred to as Laser Doppler Anemometry (LDA), utilises two collimated coherent laser beams intersecting at a point in the flow, generating an optical probe volume. At the point of intersection, the beams interfere to produce a set of straight fringes and as particles pass through the fringes, they scatter light which is recorded by photo-detectors as a series of pulsed signals. The frequency of these pulses is then used to infer particle velocities (Durst *et al.*, 1976). When LDV/LDA is applied to particle-laden flows, issues associated with cross talk (the ability to discriminate between the signals from smaller particles representing the continuous phase and signals from larger particles representing the discrete phase) require customised data processing algorithms capable of signal discrimination (Modarress *et al.*, 1984). Although capable of providing good temporal data, this technique is restricted to single-point measurements and,

when applied to particle-laden flows presents difficulties associated with the interpretation of data into meaningful physical mechanisms which control the dynamics between phases (Bastiaans, 2000).

Particle Image Velocimetry (PIV), is a laser diagnostic technique capable of measuring a very large number of instantaneous velocity vectors simultaneously, in either a two-dimensional or a three-dimensional construct. This technique requires the projection of a laser sheet into a flow field at successive time intervals, with Charge Couple Devices (CCDs) recording the light scattered by particles in the flow (flow tracers or otherwise) at time intervals in-phase with the laser pulses. Images recorded by the CCDs detail the positions of the particles and when successive image pairs are used, particle displacement over a time period can be determined, from which average particle velocities over that time period are inferred. Results of this type of analysis enable the reconstruction of the particle velocity fields at various instances in time.

The PIV technique has been useful in studies involving particle-laden flows due to the fact that the experimental setup can be implemented relatively quickly (Bastiaans, 2000; Kiger & Pan, 2000; Miyazaki *et al.*, 1999). A limitation with PIV, however, is that the dynamic velocity range (defined as the maximum velocity measurable divided by the minimum velocity measurable) of the technique has to be sufficiently large for the method to be of value. Although dynamic ranges have increased to somewhere between 100 and 200, large enough to permit accurate velocity measurements, this is only true provided the PIV system is optimised (Adrian, 1997, 2005).

Particle Tracking Velocimetry (PTV), like PIV, is also a laser diagnostic technique that involves a similar procedure of recording the images of particles in a flow field. The difference is that in PTV, the coordinates of individual particles are recorded instead of the average displacements. Consequently, localised velocity measurements of individual particles are obtained through this technique. In PTV, successive images of the experiment are recorded and the coordinates of individual particles are linked to each other between the recorded images. Therefore, intensive effort is required for this technique since

the measurements of a large number of particles in many images must be identified and matched (Maas *et al.*, 1993). The digitising of image photogrammetry to enable PTV to be computed automatically has improved the computational time of this technique, but it is in turn limited by the imaging rate of the recording sensors which affect the temporal resolution of the technique. Algorithms to construct the matching of individual particles between successive images are generally not straightforward and not well defined (Bastiaans, 2000). Therefore, automated PTV is susceptible to ambiguities in particle identification, which cannot always be resolved when applied to flows with high particle densities, thereby limiting the spatial resolution of this technique (Gharib & Daribi, 2000; Maas *et al.*, 1993; Ohmi & Li, 2000). Despite these disadvantages, PTV can be a powerful flow visualisation and velocity measurement tool when individual particles can be identified in images. Therefore, although not used to obtain velocity measurements of particles, this technique has been applied in specific instances in the current research (when particle concentrations are low enough) to acquire trajectories of individual particles for their qualitative value.

3.2 Flow Visualisation

Hydrogen bubble visualisation is a technique involving the introduction of very small hydrogen bubbles from a fine wire cathode, generated by a process of electrolysis in a water flow. The bubble probe, which is often positioned normal to the fluid flow, ensures that bubbles are swept off to follow the fluid flow. When properly illuminated, these bubbles provide detailed visualisations of the fluid flow field, as has been demonstrated in various studies (Haidari & Smith, 1994; Kelso & Smits, 1995; Kline *et al.*, 1967; Lu & Smith 1985; Xue *et al.* , 2011; Zhang *et al.*, 1995). This technique is simple, cost effective and highly versatile as the bubble probe can be located anywhere in a flow field, and in any orientation (Smith *et al.*, 2000). In addition, this technique does not contaminate the working fluid and therefore does not need to be changed regularly. Although there may be negligible or limited bubble probe interference with the local flow, the wake of the probe can be significant enough to disturb the motion of bubbles downstream.

Bubble buoyancy also limits the speed range over which the bubbles can be used. Smaller bubbles rise less rapidly and scatter light more effectively, but tend to coagulate immediately after their formation (Merzkirch, 1987). Hydrogen bubbles tend to dissolve within a moderate distance downstream of the bubble probe, thereby limiting the time period and flow regions that can be visualised effectively using this method. Since dispersion of the bubbles increases with the Reynolds number and is very rapid in turbulent flows, this technique is limited to low speed flows (Merzkirch, 1987; Smith *et al.*, 2000).

Dye visualisation is used to study fluid motion since it is capable of offering significant insights into the driving mechanisms of complex fluid flows (Kelso *et al.*, 1996; Lim & Nickels, 1992; Lim, 1997; Lim *et al.*, 2001). Food dye and laundry brighteners are generally used as the dye medium, making this technique inexpensive, relatively easy to implement and safe (Lim, 2000). However, when the specific gravity of the dye used is greater than 1, pre-treatment to make the dye neutrally buoyant before use is required so as to ensure that the dye follows the fluid flow field accurately. Dye is generally introduced into the flow using a probe, allowing this technique to be highly versatile since the probe can be relocated easily within a flow. However, the use of a probe may introduce disturbances in the flow field and the useful running time of this technique is often limited due to the dye contamination of the operating fluid. This technique also requires a degree of trial and error and personal judgement in terms of dye dilution and dye delivery into the system. The concentration of the dye depends on the application; with too high a concentration obscuring salient flow features while too low a concentration provides poor contrast in the flow images (Lim, 2000). In addition, the dye delivery velocity is also dependent on the local flow velocity - if too low a velocity, the dye forms unwanted wake structures while too high a velocity causes the behaviour of the flow field investigated to be significantly altered (Merzkirch, 1987). Despite the uncertainties associated with this technique, this visualisation method has been used in the current research due to the large amount of qualitative information that can be obtained with relative simplicity.

3.3 Concentration Measurements

Sensor probes such as optical fibre probes have been used to measure particle concentrations in particle-laden fluids (Herbet *et al.*, 1994; Lischer & Louge, 1992; Rundqvist *et al.*, 2003). Optical fibre probes deduce particle concentrations using the signal cross-correlation between the light emitted and the light received by the fibres, based on the principle that the amount of light reflected by particles is proportional to the surface area of the particles, thus giving their volumetric concentration. The major problem with optical fibre probes is that it is difficult to generate a reference suspension of particles with a given uniform concentration in order to establish a valid and reproducible calibration procedure (Herbet *et al.*, 1994; Lischer & Louge, 1992; Rundqvist *et al.*, 2003). Therefore, although sensor probes are highly versatile, they are highly intrusive and they introduce probe interferences into the flow field as well as disadvantages associated with single-point measurements.

Phase Doppler Interferometry (PDI), also known as Phase Doppler Anemometry (PDA), has been used to measure particle concentration at discrete points within particle-laden fluids (Grehan *et al.*, 1994; Liu & Montaser, 1994; McDonell *et al.*, 1995; Sommerfeld & Qiu, 1995; Wark *et al.*, 2000). For this technique, a laser beam is typically divided into two or four beams which are then refocused on a very small measurement volume. Particles moving through this measurement volume scatter light at various frequencies from which particle concentration can be determined. This technique is essentially an extension of the LDV technique used for measuring fluid velocity, with the exception that scattered light is observed at large angles using two or more photo-detectors (Liu & Montaser, 1994). Consequently, this technique, like LDV, is inherently a single-point technique and is unsuitable for resolving large-scale structures within particle suspensions. Moreover, it is highly time consuming when entire planes within the particle suspension have to be mapped out so as to determine particle concentration distributions (McDonell *et al.*, 1995).

Planar measurements of particle number density can be obtained using images of particles illuminated by a pulsed laser sheet (Fessler *et al.* 1994; Lazaro & Lasheras, 1992; Longmire & Eaton, 1992). Each image

is then converted into a binary matrix, from which particles are identified computationally and individually counted. While absolute planar particle number density measurements are obtained through this method, this highly laborious technique is limited to low particle loadings where particles are individually identifiable. Also, particle sizes used must be significantly larger than pixel sizes so as to facilitate particle counting.

Marker Nephelometry (MN) was a technique developed by Rosensweig *et al.* (1961) to detect concentration fluctuations that accompanied turbulent mixing in colloidal dispersions. This technique detects particle concentration by means of optical detection based on light scattering principles in order to enable *in situ* characterisation of particle concentration fields. Despite being an excellent technique for characterising turbulent concentration fluctuations in convection regions of the turbulence spectrum, MN suffers from the limitations associated with single-point measurement techniques. Extending the theory of MN (single-point measurement), the Planar Nephelometry (PN) technique is derived, giving rise to planar particle concentration measurements.

The PN technique is a non-intrusive laser diagnostic technique capable of determining planar particle concentration measurements without the need to identify individual particles. In this technique, the flow field is illuminated by a laser sheet and the intensity of light scattered by the particles is recorded by a CCD camera. Particle concentration is deduced from the recorded particle-scattered light intensity since it is a function of particle number density within the flow field. Although not commonly practised, this technique has been used successfully to measure particle concentration in jet flows (Birzer, 2009, 2011, 2012) with results providing a high degree of fidelity. The advantage of PN is that single images are processed to obtain concentration measurements, thus enabling instantaneous planar distributions of particles to be determined. Also, prior knowledge of the particle distribution is not required in order to use this technique.

The flexibility of the Planar Nephelometry technique makes it appropriate to provide planar particle concentration measurements for the research outlined in this thesis. The main limitation with this technique is that, since particle concentration is inferred from

particle-scattered-light intensity, the attenuation of the laser sheet intensity by the investigated medium introduces significant errors to the concentration measurements. To ensure adequate accuracy is obtained when using PN in the present research, special considerations were made to account for measurement errors due to laser attenuation.

3.3.1 Laser Attenuation Correction

Laser attenuation corrections can be done by relying on flow symmetry to obtain planar information regarding the level of attenuation sustained in the system. This method has been used in several particle-laden fluid studies (Abu-Gharbieh *et al.*, 2000; Koh *et al.*, 2003; Sick & Stojkovic, 2001; Talley *et al.*, 1996). In these studies, counter-propagating light sheets are used to negate the effects of laser attenuation, and by having both forward- and backward-scattered light recorded simultaneously, the different attenuation histories experienced by each laser sheet in the same medium are obtained (Koh *et al.*, 2003; Sick & Stojkovic, 2001; Talley *et al.*, 1996; Versluis *et al.*, 1997). The planar data are used to calculate local light extinction coefficients, used to reconstruct the corrected laser intensity distribution profile. The limitation with this technique is that it is not applicable in complex flows since it relies on the flow symmetry to verify the accuracy of the corrections. In addition, under conditions whereby high laser extinction values or high noise levels are encountered, low signal-to-noise ratios are generated due to the increased non-linearity of the sensitivity of this technique to noise (Verbiezen *et al.*, 2006).

Instead of measuring the absolute levels of attenuation, scaling factors have also been used to correct and compensate for errors associated with laser attenuation (Brugman *et al.*, 1997; Kalt *et al.*, 2007). A scaling factor which accounts for optical setup and particle scattering properties, obtained empirically and applied to detected signals directly, can be used to relate detected signals to particle number density (Kalt *et al.*, 2007). Alternatively, a scaling factor based on the full dynamic range of the imaging system can also be used but this approach is limited in its application because it assumes that the distribution of scattering particles within the imaged area is homogeneous (Brugman

et al., 1997). The major issue associated with using scaling factors is that they introduce uncertainties and degrade the quality of the corrected data obtained. Scaling factors themselves have tolerances which must be added to the overall errors associated with the measurements, which in turn increases the uncertainties of the data. Statistical methods of attenuation correction estimate the distribution of the laser intensity as a function of depth by forming a scaling factor which amplifies the recorded signals. However, the scaling factor used also amplifies the noise associated with the recorded signals. Consequently, the corrected data suffers from degradation of signal-to-noise ratios (Brugman *et al.*, 1997).

In addition to laser attenuation, it is noted that multiple scattering may also introduce errors into the concentration measurements acquired through the PN technique. Multiple scattering occurs when a photon from the light source is scattered by multiple particles before being recorded by a sensor. This phenomena is an issue since the single scattering assumption used by laser diagnostic techniques no longer applies. A correction technique called Structured Laser Illumination Planar Imaging (SLIPI) has been used successfully to correct for the effects of multiple scattering in laser sheet imaging techniques (Berrocal *et al.*, 2008; Kristensson *et al.*, 2008, 2011; Wellander *et al.*, 2011). However, the need for multiple imaging to resolve the effects of multiple scattering limits the application of this technique for highly turbulent flows requiring instantaneous planar information.

When the effects of multiple scattering are significant (particularly in optically dense media), the system becomes very complex (van de Hulst, 1957) causing correction algorithms for laser extinction and signal attenuation to become unreliable (Wellander *et al.*, 2011). Therefore, most correction techniques assume that the signals detected do not suffer from multiple scattering and few publications address multiple scattering corrections in particle-laden fluids. According to van de Hulst (1957), the scattering signals of particles will be independent of each other if they have a mutual distance of over three times the particle radius, which correspond to a volume fraction of particles of about 30% (Becker, 1977). Subsequent experiments conducted to verify this claim found that scattering independence is only true for volume

fractions below 25% (Blevin & Brown, 1961) whilst Churchill *et al.* (1960) presented a more conservative estimate of a 15% volume fraction threshold. Since all experimental conditions considered in this research are below the most conservative volume-fraction threshold of 15% for scattering independence, the laser attenuation correction method explored in this research does not require multiple scattering correction considerations.

Present laser attenuation correction methods are yet to be well established and are inadequate for the requirements of the present research. Consequently, an alternative laser attenuation correction method was developed specifically for the PN technique and its intended application in the current work. The proposed laser attenuation correction extends from the ray-based extinction model described by Kalt *et al.* (2007). Through additional mathematical considerations and a reflective strip placed down-beam from the flow region of interest, the level of attenuation sustained is corrected for shot-to-shot variations in laser light intensity. Since instantaneous images are processed for the corrections, the proposed correction method is suitable for highly-turbulent flows with no flow symmetry. Also, applying these corrections to PN measurements will significantly improve the accuracy of the concentration measurements obtained and provide accurate instantaneous planar particle concentration measurements.

Theoretical Considerations

The general outcome of the theory behind the MN technique is presented here in brief for the benefit for the reader. The reader is directed to Becker *et al.* (1967) and Becker (1977) for a more detailed discussion of the theoretical derivations of the MN technique.

Consider the light scattered by particles in the path of an incident light beam that is being recorded by a photo-detector placed perpendicular to that light beam. Normal conditions for the light scattering technique are where the wavelength are small and the scatter function, ψ, is given by the Mie equations (van de Hulst, 1957). Under these conditions, the energy flux scattered by N particles momentarily inside a control

volume, cv, is N times that scattered by one particle. The energy flux (from the cv) incident on a photo-detector over a wave interval $\mathrm{d}\lambda$ is given by:

$$\int_0^\infty \Phi_{cv}\mathrm{d}\lambda = \pi r_p^2 N \omega_{inc}\omega_{sc} \int_0^\infty \psi_{av}\iota_1\iota_2 I_o \mathrm{d}\lambda \tag{3.1}$$

where r_p is the particle radius, ψ_{av} is the average of the scatter function ψ taken over the solid angles of divergence of the incident and scattered beams, ω_{inc} and ω_{sc} respectively, ι_1 and ι_2 are the spectral transmissivities of all the media between the light source and the cv and between the cv and the photo-detector respectively, and I_o is the intensity of the radiant flux leaving the light source (in the direction of projection per unit of arc or filament surface per steradian).

Equation 3.1 considers that particle-scattered light intensity is dependent on the particle surface area being exposed to some form of illumination. Since particle surface area is a function of particle number density, it follows that particle-scattered light intensity (captured by a photo-detector positioned perpendicular to the light source) can be expressed as a function of particle concentration. This equation therefore assumes that particle-scattered light is effectively an independent scatter by mono-disperse spheres.

The PN technique extends the theory of MN by using a light sheet to illuminate a plane of particles and recording particle-scattered light onto a CCD, giving rise to planar concentration measurements. Where MN uses a single voltage to determine particle concentrations in a cv, PN uses the intensity value of each pixel in the CCD array to determine particle concentration in a plane. Consequently, additional considerations must be taken into account to enable a valid extension of the theory of MN technique onto the PN technique.

The nature of the derivation of Equation 3.1 assumes that the intensity of the light illuminating all N particles is constant. However, a particle in a light sheet will cast a shadow which diminishes the intensity of light illuminating other particles down-beam of this initial particle. In MN, due to the convergence of the light beam onto a small cv, the effect of the shadows also converges and becomes negligible. Whereas,

the light sheet used in PN typically diverges and the effect of particle shadows cannot be neglected. Therefore, valid implementation of PN for planar concentration measurements requires quantification of the attenuation caused by particle shadows and subsequent corrections for the occurrence of attenuation of the light sheet used.

When a suspension of particles is illuminated with a laser sheet (as is in the PN technique) with wavelengths smaller than or comparable with the particle size, Mie scattering dominates the light-particle interaction (Brugman *et al.*, 1997). In this situation, particles scatter light elastically based on the generalized Lorenz-Mie theory (Gouesbet, 1994). Taking these prerequisites into account, the scattered signals (as recorded by CCD cameras) provide a measure of the laser intensity distribution in the imaged area. Consequently, according to Brugman *et al.* (1997), Kalt *et al.* (2007) and Sick and Stojkovic (2001), the intensity of the scattered signal recorded for any point, Φ, in the imaged area can be expressed as:

$$\Phi_i = N_i I_i \sigma K \tag{3.2}$$

where subscript i refers to the location corresponding to pixel i, I is the local intensity of the laser sheet, N refers to the particle number density, σ denotes the particle scattering cross section and K is a constant that accounts for particle characteristics, experimental setup and equipment efficiency. The parameter σ relates to the considerations in Mie scattering theory whereby the light-particle interaction occurs over a cross-sectional area that is larger than the geometrical cross section of the particles. Since Mie scattering theory relates the particle scattered light to the particle surface area, particle number density can be determined from the intensity levels of the scattered light. This is the basis whereby PN infers the concentration of particles within a medium from particle scattered light (provided that the initial light intensity is known, particle diameters are constant and all particles behave similarly).

Since the scattered signals are recorded as a two-dimensional array of pixels, the pixel count (or pixel value) may be considered as a discrete signal from a pixel volume (voxel) with cross-sectional area $A = \mathrm{d}x\mathrm{d}y$. This consideration allows voxels to represent the laser intensity at the

imaged area. Consequently, the region of interest in the media may be considered to be a series of voxels through which the laser light propagates, thus generating different signal intensity values recorded by a CCD (Figure 3.1). When imaging an optically-dense medium, the large numbers of particles present in each voxel cause the laser intensity to diminish significantly as it propagates through each voxel (Figure 3.2). As a consequence, signals from each subsequent voxel no longer reflect the true distribution of the local particle concentration which results in the errors associated with laser attenuation. These recorded signals must therefore be corrected for the influence of laser attenuation before any interpretation of the recorded data can be made.

Development of the Correction Algorithm

The proposed correction considers the use of the probability of unobstructed light propagating through voxels, previously presented in Cheong *et al.* (2012a,b). When a collimated laser sheet (i.e. parallel, uniform light sheet) is used, the light flux may be assumed to be constant throughout the region of investigation (Kalt *et al.*, 2007). As a consequence, the laser sheet intensity is proportional to the cross-sectional area of the voxels (i.e. $A = \mathrm{d}x\mathrm{d}y$). Brugman *et al.* (1997) established that the absorption and Mie scattering of particles are the dominant mechanism contributing to the occurrence of laser attenuation. As such, laser attenuation may be effectively accounted for by considering the amount of light blocked-off by particles appearing within the voxels and generating a shadow. The probability of a particle shadow appearing within a pixel cross-section is:

$$\mathcal{P}(\text{particle}) = \frac{\pi r^2}{\mathrm{d}x\mathrm{d}y} \tag{3.3}$$

The complementary event of (3.3) provides the probability of unobstructed light propagating through the pixel. When N particles are present within this pixel, the probability of light being unobstructed is:

$$\mathcal{P}(\text{light}) = \left(\frac{\pi r^2}{\mathrm{d}x\mathrm{d}y}\right)^N \tag{3.4}$$

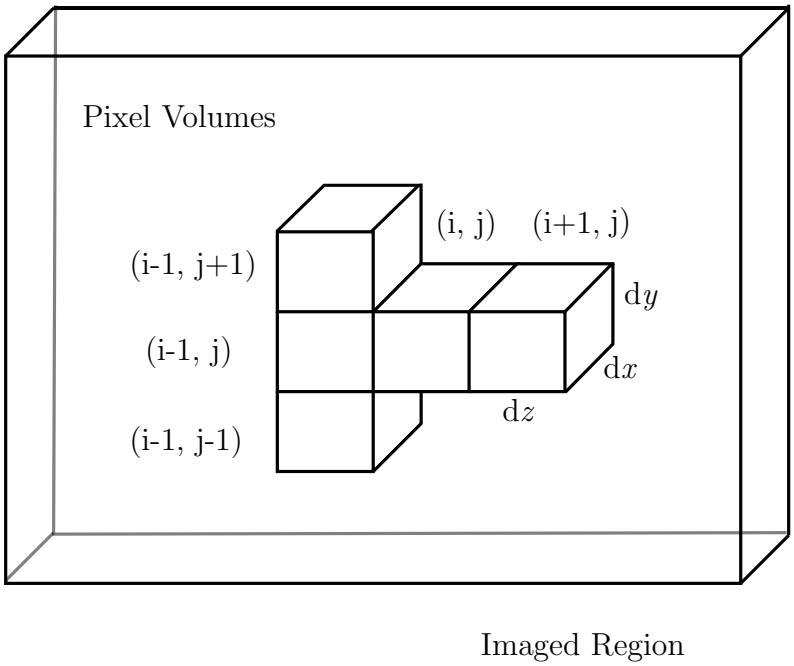


Figure 3.1: Imaged plane in the region of interest (dy and dz are in-plane resolution while dx relates to the laser sheet thickness).

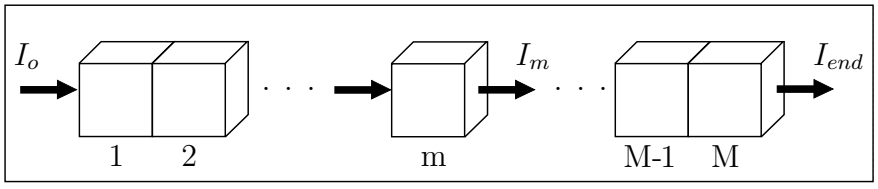


Figure 3.2: Attenuation of light intensity propagating through the imaged plane of interest (I_o and I_{end} are the light intensities entering and exiting a plane of M voxels, while I_m is the light intensity exiting voxel m).

Consequently, the intensity of light transmitted through a pixel volume is:

$$I_{out} = I_{in}\left(1 - \frac{\pi r^2}{\mathrm{d}x\mathrm{d}y}\right)^N \tag{3.5}$$

where I_{in} and I_{out} are the intensity of light entering and exiting the voxel respectively, and N is the number of particles with radius r within the voxel. When particles in the medium are of the same diameter, the bracketed terms of (3.5) are constant and can be expressed as B. Since the region of investigation will consist of numerous rows of voxels, the local laser intensity at any voxel, m, in the medium is:

$$I_m = \sum_{i=1}^{m} I_o B^{N_i} \tag{3.6}$$

Combining (3.2) with (3.6), and applying it over a single row with M voxels:

$$I_{end} = \sum_{i=1}^{M} I_o B^{E_i}, \qquad E_i = \frac{\Phi_i}{K\sigma I_i} \tag{3.7}$$

Equation (3.7) relates the initial laser intensity entering the region of interest, I_o to the intensity of light exiting that region, I_{end} (i.e. the signal from the attenuation strip) (Figure 3.2). Signals from the attenuation strip are used to establish variations in the intensity of the laser sheet exiting the media I_{end}.

For every voxel, I_m is determined either simultaneously or iteratively from (3.6), from which the distribution of the corrected laser intensities is reconstructed. Solving I_m simultaneously produces numerically exact solutions at the expense of higher computational requirements. In order to reduce processing costs, this study solves I_m iteratively and calculates approximated values of I_m. The corrected distribution of I_m propagating through the medium is substituted into (3.2) to obtain local particle number densities, using the following relationship:

$$C_i = \frac{N_i}{\mathrm{d}x\mathrm{d}y\mathrm{d}z} \tag{3.8}$$

where C refers to the local particle concentration and $\mathrm{d}x\mathrm{d}y\mathrm{d}z$ is the voxel volume. It is common in PN to assume that particle concentration is proportional to signal intensity, $C \propto I$ (since $I \propto N$ and $C \propto N$ through the consideration of (3.2) and (3.8)). It follows that subsequent calibration of the light intensity fields against a known concentration will enable the accurate particle concentration within the measured region to be determined. However, since it is very difficult to generate an accurate reference suspension of particles with a known concentration, errors associated with calibration issues should be considered. The proposed corrections also require the particle diameter and laser intensity (along a ray) to be constant and should conditions related to the experimental setup change, recalibration of the correction algorithm must be performed.

It should be noted that when (3.7) is expressed as a logarithmic ratio of the initial and final laser intensity (3.9), the mathematical expression obtained is a form of the Beer-Lambert Equation (3.10):

$$log\frac{I_{end}}{I_o} = \frac{logB}{K\sigma}\sum_{i=1}^{M}\frac{\Phi_i}{I_i} \tag{3.9}$$

$$log\frac{I_{end}}{I_o} = -\alpha N \tag{3.10}$$

where α is a constant depending on the path length and extinction coefficient of particles in the medium. This outcome indicates that the proposed corrections obtained from the development of (3.7) are in agreement with the Beer-Lambert Equation, and are therefore theoretically correct. The iterative application of (3.7) accordingly enables an instantaneous laser attenuation correction approach that accounts for fluctuations and variations in the laser intensity illuminating the particle suspension.

Experimental Validation

The experimental setup used in the validation work consisted of a laser system, a CCD camera and a transparent acrylic tank which was used to hold the medium under investigation (Figure 3.3). The laser system used was a pulsed Nd:YAG laser, emitting 532nm (second-harmonic output) light at a 10 Hz repetition rate. A collimated laser sheet of 2mm thickness and 25mm height was generated using this system to illuminate the investigated medium. A Redlake Megaplus II (10-bit dynamic range) CCD camera (2048 pixels $\times$ 2048 pixels) with a Nikon AF Nikkor 24mm-120mm f/3.5-5.6D lens was used to image an area of 500mm $\times$ 500mm. The medium investigated consisted of mono-disperse neutrally-buoyant spherical Polyamide Seeding Particles (PSP-20) with a mean particle diameter of 20μm $\pm$ 15μm suspended in water.

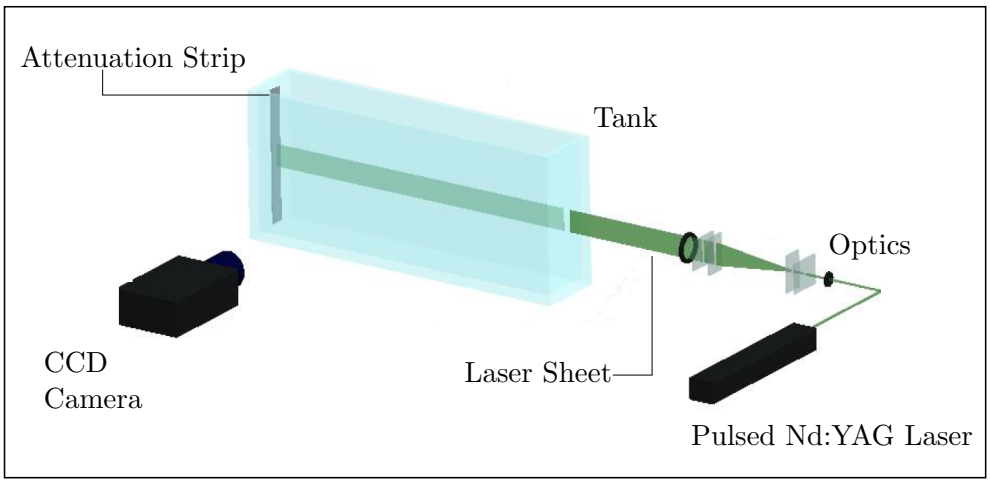


Figure 3.3: Schematic diagram of experimental setup.

Planar Nephelometry measurements were applied on known homogenous particle concentrations to validate the proposed attenuation correction method. The single-chamber configuration investigated one uniform particle concentration at a time. In this configuration, the particle suspension was placed in a 250mm $\times$ 200mm $\times$ 20mm chamber located in the middle of the acrylic tank (Figure 3.4a). Concentrations used for this configuration were 5, 10, 20,

30 and 40 ppm. Conversely, the two-chamber configuration allowed two particle concentrations to be investigated simultaneously. For this configuration, an additional acrylic sheet was placed in the middle of the existing chamber to obtain two adjacent chambers of equal size (Figure 3.4b). Particle concentrations investigated using the two-chamber configuration were 10, 20, 30, 40 and 50 ppm. For both experimental configurations, a highly-reflective polymer strip (an attenuation strip) was placed on the inside of the acrylic tank down-beam from the region of interest for both experimental configurations. The laser intensity from the polymer strip is recorded by the CCD camera and provides values for I_{end} (Equation (3.7), used in the laser attenuation correction algorithm.

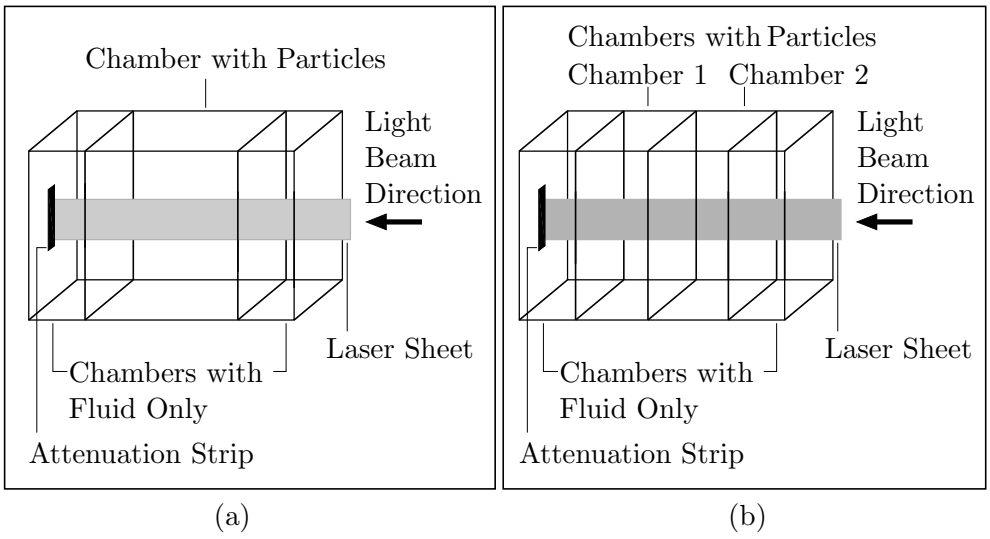


Figure 3.4: Schematic diagram of the experimental chambers: (a) single-chamber configuration; (b) two-chamber configuration.

The chamber(s) were placed away from both ends of the acrylic tank to minimise the effects on the recorded signals of any reflected or refracted light from the attenuation strip and the tank wall respectively. The suspensions were stirred intermittently before data were recorded to ensure that a homogenous distribution of particles was maintained in the chamber(s). Experiments which used two different particle concentrations simultaneously were investigated under a number of different conditions (Table 3.1).

The imaging of optically-dense media also introduces another form of error into the recorded signals; a problem known as signal trapping which is due to the attenuation of the scattered signals on their way to the detector. Since the proposed correction algorithm uses the relative variations in intensity of each pixel volume, signal trapping may be neglected if it is constant throughout the imaging region, assuming signal trapping is linear with the particle number density and laser light intensity (Kalt *et al.*, 2007). In addition, as the correction method uses instantaneous images of the entire tank, variations in the intensity of the laser sheet are inherently taken into account. Consequently, signals received from the attenuation strip provide accurate information on the laser intensity exiting the media.

Table 3.1: Particle concentration in each chamber in different cases. The laser sheet propagates in the direction of Chamber 1 *en route* to Chamber 2.

Case	Chamber 1	Chamber 2
Case 1	20 ppm	10 ppm
Case 2	30 ppm	20 ppm
Case 3	40 ppm	30 ppm
Case 4	50 ppm	40 ppm

Mie scattering signals for each experiment are determined from an ensemble of 429 images, spatially-averaged over the number of pixels corresponding to the height of the laser sheet (i.e. 25mm). The recorded signals are restricted to the dynamic range of the CCD camera in order to avoid signal saturation. This procedure is implemented so as to increase the statistical accuracy of the data. As a result, a single row of pixel values is generated to represent each investigated particle loading. An identical treatment is applied to the background noise, obtained when the laser is turned on and operating without particles present in the tank. Data used for the attenuation corrections are obtained by subtracting the background noise from the particle Mie scattering signals, as shown in Figure 3.5.

The increase in overall signal intensity as the particle concentration increases is expected since increasing the number of particles increases the total light scattered. The rate of decrease in signal intensity (over the laser path) increases with the particle concentration, thus indicating that laser attenuation becomes more significant at higher particle loadings. Since Planar Nephelometry generally assumes that the particle concentration is proportional to the signal intensity (i.e. $C \propto I$), a consistent decrease in signal intensities (Figure 3.5) is erroneously interpreted as a corresponding decrease in particle concentration. In order to overcome these inaccuracies, data from Figure 3.5 are processed using the proposed algorithm to obtain particle concentration measurements, correcting for the effects of laser attenuation.

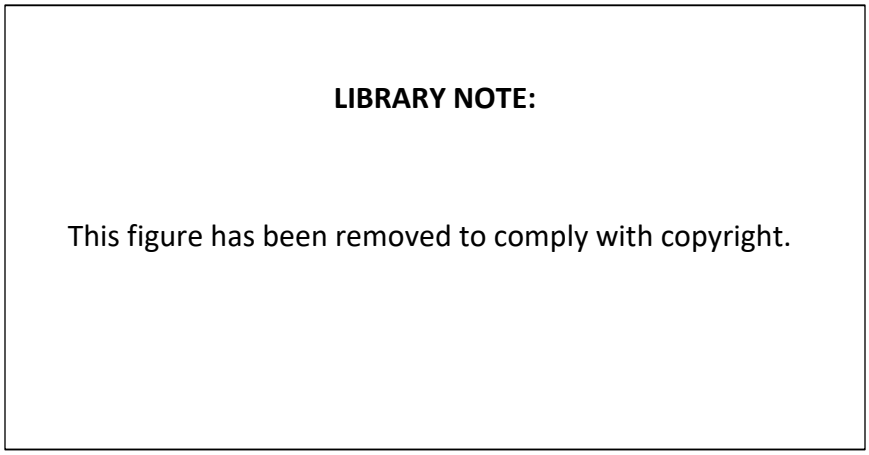


Figure 3.5: Averaged signal intensities against the laser path (background noise removed but uncorrected for attenuation) - single-chamber configuration.

For the single-chamber configuration, Figure 3.6 shows the corrected particle concentration measurements for a range of particle loadings. A small drop in concentration measurements is noted at a down-beam distance of 250mm onwards for the 10ppm, 20ppm and 30ppm cases.

Since this drop in concentration affects measurements further along the propagation path of the laser sheet, it is possible that some laser attenuation is still affecting the concentration measurements even after corrections are implemented. If this were the case, higher particle concentration measurements should be more susceptible to these inaccuracies. However, the concentration measurements for the 40ppm case were unaffected, thus making it unclear as to what is causing this anomaly, shown in Figure 3.6. Despite these inconsistencies, the mean concentration measurements obtained were in good agreement with the actual particle concentrations used in the experiments. When comparing the results in Figure 3.6 with Figure 3.5, significant improvements are observed in terms of correcting for the effects of laser attenuation. Such results indicate that the corrections successfully reconstructed the laser intensity distribution propagating through the medium, with the effects of laser attenuation addressed.

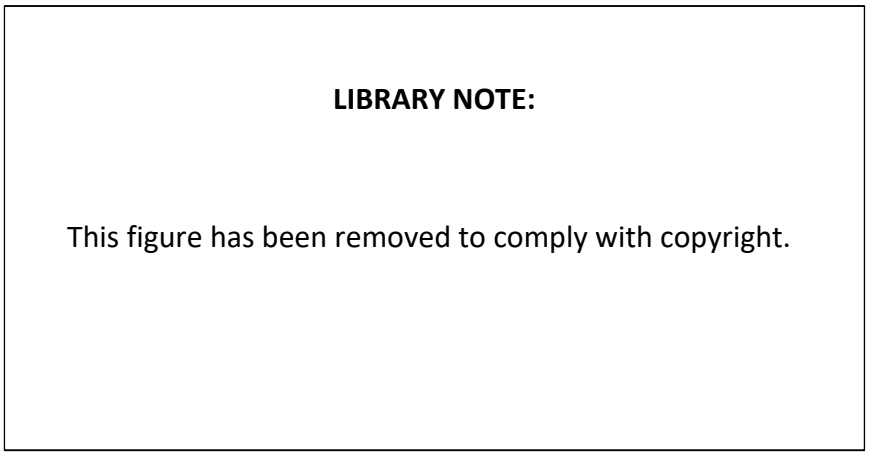


Figure 3.6: Particle concentration as a function of laser propagation path (corrected for laser attenuation) for the single-chamber configuration.

Corrected results for the two-chamber configuration are present in Figure 3.7. The large step-changes in signal intensity correspond to the location of the acrylic sheet placed between the chambers. Measurements generated in Chamber 1 are in agreement with the actual particle concentrations. However, observations in Chamber 2

show a prevailing discrepancy between actual and corrected particle concentrations, indicating a systematic error that is persistent and exclusive to Chamber 2.

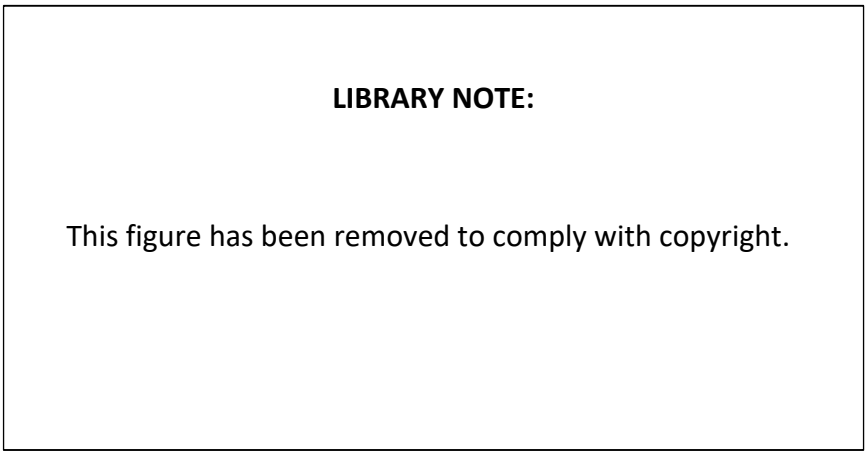


Figure 3.7: Particle concentration against laser path for the two-chamber configuration: corrected for attenuation and the acrylic sheet.

Additional two-chamber configuration experiments using identical particle concentrations for each chamber (20, 30 and 40 ppm) confirm that the presence of the acrylic sheet between the chambers contributed to a constant reduction in signal intensity. The laser sheet changes media as it passes through the acrylic sheet which results in the reduction of laser sheet intensity due to the properties (refractive index, reflection and absorption losses) of this additional medium. This explanation is in agreement with the theory presented by Becker (1977), whereby the energy flux incident on a photo-detector must account for all media spectral transmissivities in the imaging plane. An empirical determination of the transmission loss due to the acrylic sheet

is therefore engaged. The results, after incorporating both the laser attenuation and the acrylic sheet corrections, are presented in Figure 3.7.

Error Analysis

The level of noise associated with each particle loading was observed to increase with particle concentration. Subsequent calculations established that the variance of the signal distribution versus time for each particle loading also increased with particle concentration. This suggests that the source of noise is not entirely due to electrical noise, but rather due to the decreasing influence of independent particle scattering as the concentration increases. With increasing particle concentrations, inhomogeneities in particle dispersal will increase due to the increased likelihood of particle-particle interactions. Since the particles used are not charged, increased particle-particle interactions cause particles to agglomerate, resulting in the sporadic occurrence of non-independent particle scattering (van de Hulst, 1957). Although the concentrations used in this research are well below the threshold whereby the effects of multiple scattering are significant, further statistical analysis was conducted on the measurements to determine whether these inhomogeneities in particle dispersal affect the validity of the proposed corrections. The relative errors of each particle loading are determined by:

$$\text{Relative error}(\%) = \frac{\text{standard deviation}}{\text{mean concentration}} \times 100 \tag{3.11}$$

where the standard deviation and mean concentration of signal values are obtained over the laser propagation path. Considering the application of (3.11) on the data from the single-chamber configuration (Figure 3.6), the percentage relative error of each particle concentration investigated was determined (Figure 3.8) in order to establish the level of dispersion of data values used. A percentage relative error close to 0 indicates that the data points tend to be very close to the mean concentration. Relative errors of the order of 10% are comparable to the outcomes of studies by Herbet *et al.* (1994) and Sommerfeld and Qiu (1995), and can be attributed to the normal variation in

experimental measurements associated with particles in suspension. This outcome indicates the occurrence of non-independent particle scattering is not prevalent enough to cause any evident influence on the capabilities of the proposed corrections.

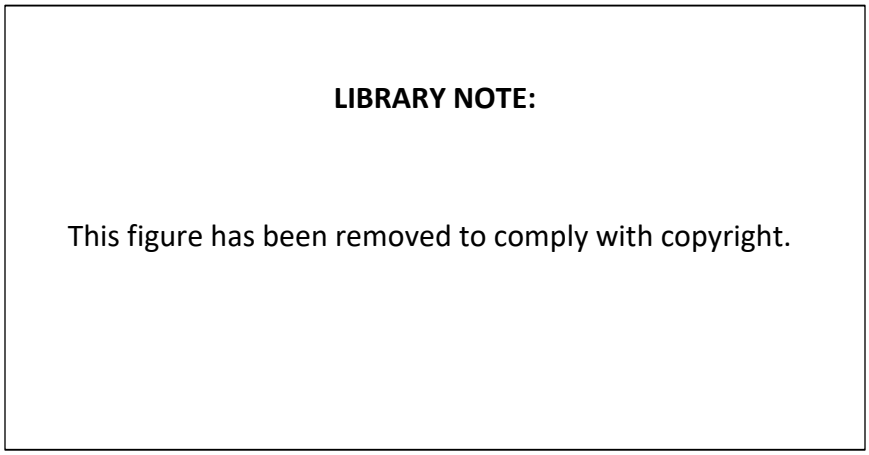


Figure 3.8: Percentage relative error as a function of particle loading cases for the single-chamber configuration.

Additional experiments to determine the effects of signal attenuation on the proposed corrections were also conducted. These experiments used the single-chamber configuration with a particle concentration of 10 ppm. The distance over which scattered light from the particles travels through the medium (i.e. the distance from the laser sheet to the tank wall as it propagates towards the CCD camera) was varied by displacing the entire acrylic tank from the CCD camera. Positive and negative displacements of 50 mm were applied to the original position of the tank (i.e. the position used for the previous experiments). The location of the laser sheet and camera were kept constant. A comparison between the signals recorded in these experiments demonstrated no dependence between the tank displacement and signal intensities, thus indicating no measurable influence of signal trapping (the attenuation of scattered signals on their way to the detector) on experimental results. Subsequent evaluation of individual experimental results indicates a minor disparity between the signal distribution and scatter (Table 3.2), with relative errors also in the order of 10%, that

are comparable with Figure 3.8. Such results further confirm the validity of the proposed corrections on the range of particle concentrations investigated.

Table 3.2: Signal attenuation analysis for 10 ppm particles at various tank displacements from the camera.

Data	-50mm	0mm	+50mm
Mean (ppm)	9.39	9.25	9.91
Standard Deviation (ppm)	0.664	0.732	0.695
Relative Error (%)	7.07	7.91	7.01

Conclusion of the Development of a Laser Attenuation Correction Method

The proposed correction method, using an attenuation strip placed down-beam from the flow region of interest, was validated experimentally using measurements from the PN technique. The Mie scattering, using a collimated laser sheet for various known homogenous particle concentrations in single and two chamber configurations, was recorded. The corrected concentration measurements are in agreement with the actual concentrations used, indicating that laser attenuation is effectively accounted for, and that accurate particle concentrations can be inferred from the Mie scattering signals. The proposed correction method, therefore, extends the accuracy and capability of the PN technique to enable effective particle concentration measurements for the current research.

3.4 Summary

In this chapter, the measurement techniques selected for the presented research were outlined. For quantitative and qualitative fluid velocimetry, Particle Image Velocimetry was used in conjunction with Particle Tracking Velocimetry and dye-based visualisation. The Planar Nephelometry technique was selected to measure particle concentrations. The use of Planar Nephelometry was contingent upon laser attenuation corrections, and a novel technique was devised and validated to facilitate the presented research, with benefits of accuracy and measurement efficiency. The application of these techniques to the experimental work is presented in the following chapters.

4 Experimental Apparatus

The experiments undertaken for the presented research require the examination of large-scale coherent structures with low Reynolds number turbulence generated at various fluid excitation frequencies. A suitable fluid excitation setup that allowed for the implementation and integration of the necessary measurement techniques (see Chapter 3) was therefore required. This chapter details the design and the development of the experimental rig used and discusses the conditions under which the experimental investigations were conducted.

4.1 Zero-Net Mass Flux Jets

Zero-Net Mass Flux (ZNMF) jets are generated using only the working fluid in which they operate, while conventional jets are produced by having a stream of fluid (generally from an alternate source) projected into the working fluid. As a consequence, ZNMF jets are able to impart momentum into the flow system without a net mass injection across the flow boundary (Glezer & Amitay, 2002). These jets can be generated using acoustic excitation, cavitation bubbles, or using diaphragms and pistons. The characteristics of the large-scale coherent structures generated by these ZNMF jets are controlled through the variation of flow conditions (outlet size and fluid slug length) and the frequencies of excitation, both of the suction and ejection phase.

The current research required a constant particle concentration within the fluid suspension, since measurements of the local particle concentration in the ambient fluid are used as a means of evaluating preferential concentration mechanisms. The use of ZNMF jets, whereby no net mass is added into the working system, renders them ideal for

the current research since large-scale vortex structures could be generated without changing the particle concentration of the investigated fluid suspension.

4.1.1 Acoustic Excitation

A ZNMF jet is generated acoustically when the pressure oscillations imposed by an acoustic field across an outlet large enough to generate vortex sheets are subsequently advected away from the source. Therefore, the acoustic source must be sufficiently strong to produce vortex sheets that are large enough to overcome suctions forces, both real and virtual (vortex images generated at the outlet) (Glezer & Amitay, 2002). Vortex generation using acoustic excitation has primarily been implemented in gaseous systems. For instance, Longmire and Eaton (1992) and Wark *et al.* (2000) used an audio speaker to pulse particle-laden jets from a plenum in order to study particle interactions with large-scale vortices (Figure 2.6). Other studies, such as Hwang and Cho (2003) used, sound waves to excite a main jet and a shear layer to determine the effects of acoustic excitation on the flow and heat transfer characteristics of an impinging jet, while Lawn *et al.* (2005) investigated the response of a turbulent flame front to an incident acoustic wave and modelled the thermo-acoustic excitation of flames. In the field of combustion, Chao and Jeng (1992) used large-scale vortical structures generated by audio speakers on lifted jet flames to determine stabilisation locations and found that the modification of lifted flame stability is feasible through acoustic excitation (Figure 4.1). In a later study, Chao *et al.* (2002) established that the stabilisation of flame propagation and recession of a lifted flame is an oscillating cycle which can be achieved through the evolution of acoustically generated large-scale vortex structures.

4.1.2 Cavitation Bubbles

The generation of ZNMF jets has also been achieved using ultrasonic transducers submerged in liquids to produce non-linear acoustic cavitation and streaming, which transmit longitudinal compression waves through waveguides (Sheen *et al.*, 1989). Sheen *et al.* (1989) observed that the concurrent occurrence of fluid streaming (fluid

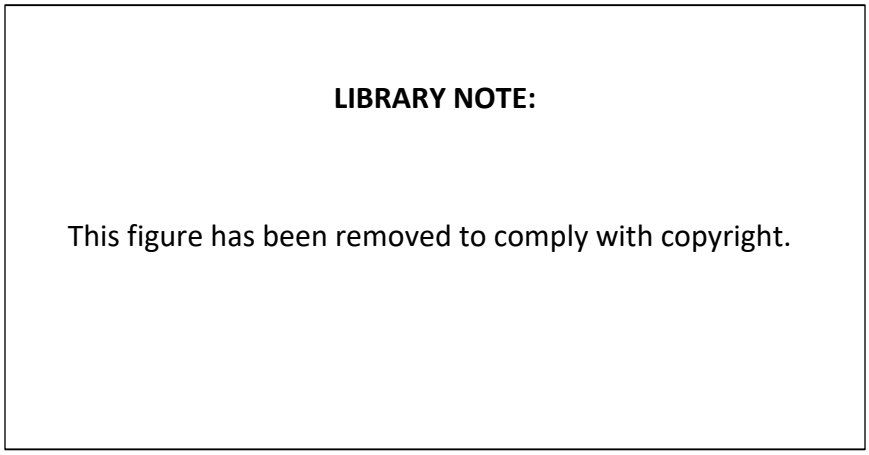


Figure 4.1: Large-scale vortices in the upstream region of a lifted flame (a) Planar images of lifted a flame - (i) unexcited, (ii) excited at 670Hz, (iii) excited at 1200Hz (Chao & Jeng, 1992) (b) Typical jet flow visualisation of the entrainment process (Chao *et al.*, 2002).

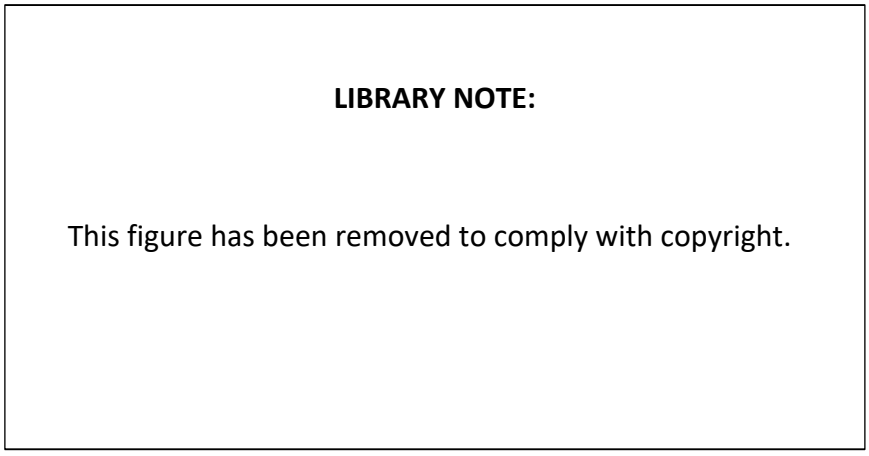


Figure 4.2: A ZNMF jet from an ultrasonic transducer (a) Dye is entrained radially from an injection port near the edge of the diaphragm; (b) Jet formation mechanism: (i) flow about a cavitation bubble (ii) momentary jet due to the collapse of a cavitation bubble (James *et al.*, 1996).

motion induced by the transmission of sound) and the formation of cavitation bubbles on the surface of the transducer results in the formation of a ZNMF jet. Although fluid streaming can be present even in the absence of cavitation bubbles, it is unclear whether there is sufficient fluid turbulence generated under these conditions to produce a ZNMF jet. James *et al.* (1996) investigated ZNMF jets using a resonantly-driven diaphragm submerged in water, mounted flush on a flat plate. The formation and evolution of a ZNMF jet was observed at the centre of and perpendicular to the submerged diaphragm (Figure 4.2a). This round turbulent jet was produced entirely from radially entrained fluid and was present only when the excitation amplitude exceeded a certain threshold and when a small cluster of cavitation bubbles were present at the diaphragm. Although the jet formation mechanism was not resolved, James *et al.* (1996) presented two plausible explanations based on the idea that the ZNMF jet is formed by a train of vortex ring clusters, owing to a secondary flow induced by the presence of cavitation bubbles. The authors postulated that the time-periodic formation of cavitation bubbles displaces vorticity from the boundary layer of the diaphragm which in turn leads to the formation of turbulent vortices that coalesce to generate a turbulent ZNMF jet (Figure 4.2b(i)). Alternatively, ZNMF jets can also be due to the formation of strong momentary jets during the collapse of cavitation bubbles. The collapse of these bubbles can be accompanied by the formation of jets that are directed away from the actuator (diaphragm) surface, which in turn leads to the evolution of clusters of vortex rings (Figure 4.2b(ii)).

4.1.3 Diaphragm Systems

A ZNMF jet can be produced through a time-periodic ejection and suction of a working fluid through an orifice in a flow boundary. One approach is to have the orifice form one of the surfaces of an otherwise sealed shallow cavity where the flow is driven by a diaphragm built into the cavity walls (Figure 4.3a). This approach to ZNMF generation has primarily been investigated using gaseous working systems. For instance, Smith and Glezer (1998) investigated the formation and evolution of a plane turbulent jet that was generated by the interactions of a train of counter-rotating vortex pairs (Figure 4.3b), while Muller *et al.* (2001) examined the flow structure and performance

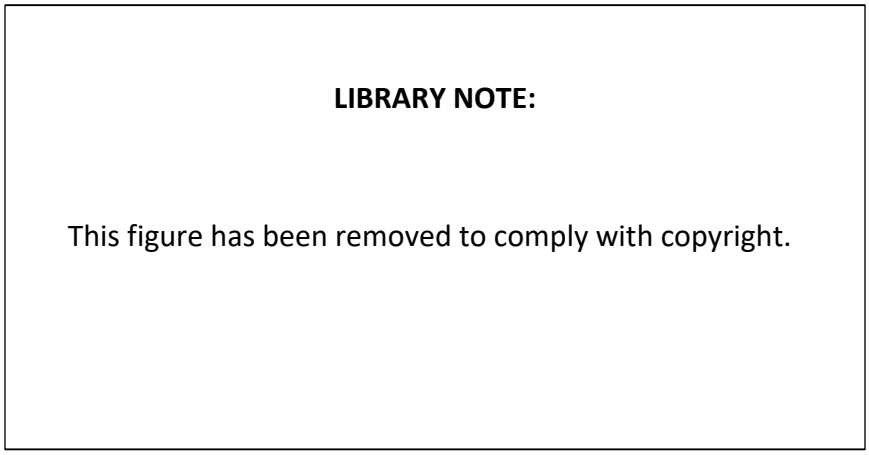


Figure 4.3: A ZNMF jet from a sealed cavity (a) Schematic diagram of the setup (b) Schelieren image of the jet at 1140Hz excitation (Smith & Glezer, 1998).

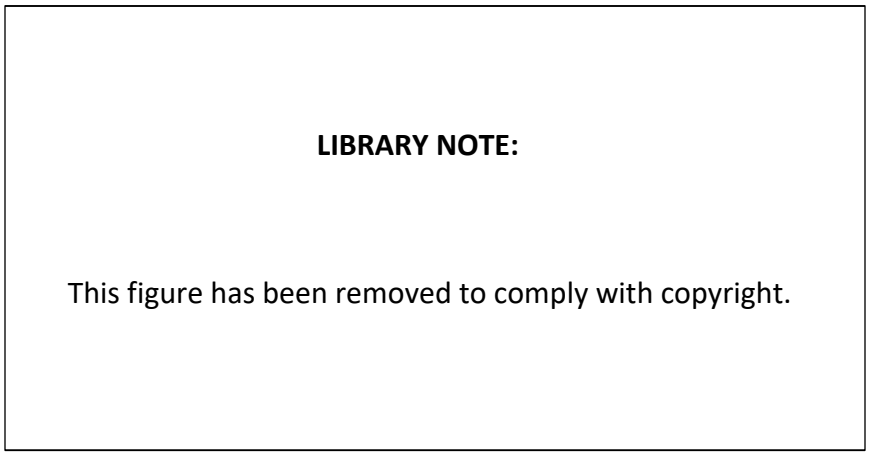


Figure 4.4: Piston-cylinder generated vortex ring (a) Schematic diagram (b) Visualisation using fluorescent dye (Allen & Auvity, 2002).

of axisymmetric ZNMF jets and established that these flow characteristics are dominated by the dynamics of vortical structures. In addition, ZNMF jets generated in this manner have been investigated for possible flow control applications. Smith and Glezer (2002) and Jabbal *et al.* (2006) examined the impact of these ZNMF jets on quiescent flow and their potential as a jet vectoring device. Crook *et al.* (2000), Lee *et al.* (2003) and McCormick (2000) examined the feasibility of using ZNMF jets as a device for controlling separation and turbulence levels in an adverse pressure gradient boundary layer.

4.1.4 Piston Systems

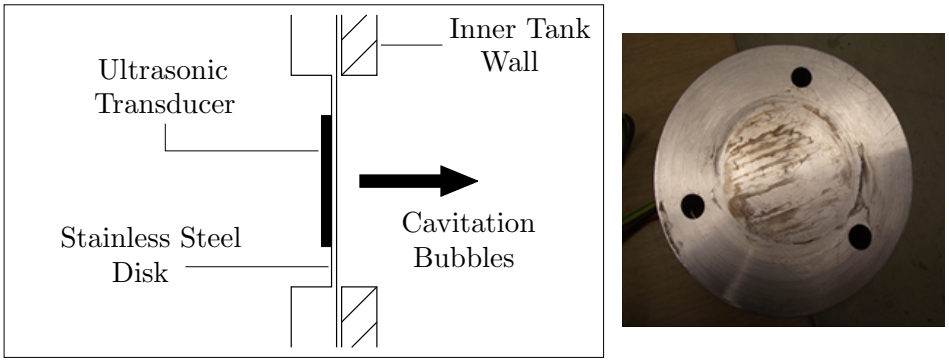
Another approach to producing ZNMF jets is through a time-periodic sinusoidal motion of a piston within a cylindrical tube, driving fluid through a flow boundary outlet (Figure 4.4a). During the outflow/expulsion phase, fluid is forced out of the outlet, while during the inlet/suction phase fluid is sucked back into the outlet to replenish the fluid that was expelled in the expulsion phase. In order for ZNMF jets to be produced using this approach, the piston-cylinder setup must be able to deliver sufficient energy to the vortices generated, such that they are able to convect away from the outlet under their self-induced field (Allen & Auvity, 2002). Glezer (1988) classified the conditions under which such a vortex generator produces either an initially laminar ring, which may or may not undergo instability and transition into a turbulent ring, or an initially turbulent ring. Gharib *et al.* (1998) then demonstrated that there exists a universal time-scale (formation number) which dictates the characteristics of the vortex rings formed in a piston-cylinder setup.

There have been a number of studies that generated ZNMF jets using piston-cylinder arrangements: Cater and Soria (2002) studied the structure and flow qualities of ZNMF jets; Allen and Auvity (2002) investigated the effect of piston vortices on primary vortex rings (Figure 4.4b); and Gordon *et al.* (2004) who examined the interactions of ZNMF jets with cross-flows. These studies established that the structure of ZNMF jets is directly influenced by the amplitude and the oscillatory frequency of the piston motion, and that the piston-cylinder setup is highly effective at generating ZNMF jets in liquids.

4.1.5 Evaluation of ZNMF Systems

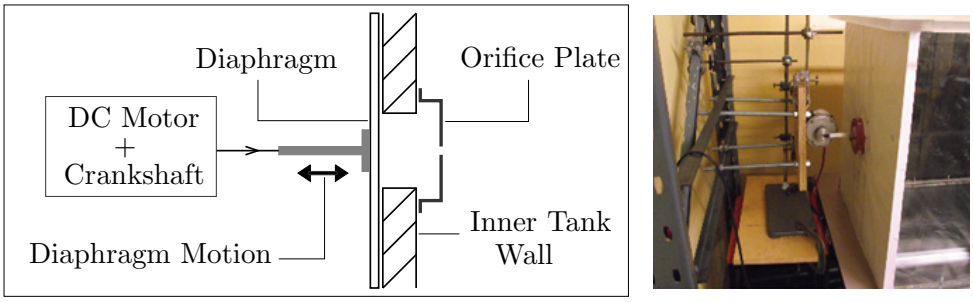
In the current work, the different methods of generating ZNMF jets were evaluated experimentally. Cavitation bubbles were generated using a 50W ultrasonic transducer with a frequency response of 40kHz, and tested within the range of frequencies used by James *et al.* (1996) (Figure 4.5). The limitation of this method is that only highly turbulent ZNMF jets could be generated since the growth and collapse of the cavitation bubbles occur on extremely small length- and time-scales. Based on the experiments undertaken, large-scale vortex structures with the necessary length-scales could not be produced within the frequency ranges needed to generate cavitation bubbles, rendering this method of ZNMF jet generation not viable.

The evaluated diaphragm-orifice setup consisted of a neoprene diaphragm and an acrylic orifice-cylinder chamber, set in motion by a 77W Direct Current (DC) motor with a rated current of 4.6A and a stall torque of 0.18N·m (Figure 4.6). With a linear displacement of 40mm on the diaphragm, fluid was expelled from the acrylic chamber to generate vortex rings. The limitation of applying this method in liquids is that insufficient impulse is transferred to the working fluid due to the flexibility of the diaphragm, thereby preventing the vortices generated from overcoming the suction forces during the ingestion stroke of the crankshaft setup. In addition, the DC motor used was a brushed motor that consisted of a stationary set of magnets in the stator and an armature. This setup prevents the motor from holding its position accurately when it experiences a resistance (such as the resistance from the diaphragm and the fluid) from the system it is exciting. Consequently, the output speed of the motor (frequency of diaphragm excitation) was not always identical for a given voltage input. Although this issue may be resolved by using a bigger motor and/or a stepper motor, the flexibility of the diaphragm causes an inconsistent transfer of impulse between the motor and the working fluid. These discrepancies prevent coherence and consistency in the vortices generated, reducing repeatability, and thereby making this method inadequate for the current research.



(a) (b)

Figure 4.5: (a) Schematic diagram of the ultrasonic transducer setup (b) Cavitation damage on the disk used.



(a) (b)

Figure 4.6: The diaphragm and orifice plate approach (a) Schematic diagram (b) Experimental setup.

The piston-cylinder setup evaluated was one that was developed based on the setup used by Gharib *et al.* (1998) and Cater and Soria (2002). An RS 440-470 stepper motor was used to drive a crankshaft setup that was connected to a piston housed within a cylindrical nozzle. The use of a stepper motor provides sufficient consistency and repeatability in terms of the output speed of the motor that is lacking in DC motors. In addition, the piston-cylinder setup also avoids the problems with diaphragm stiffness, thereby enabling the frequency and volume of fluid displaced to be better controlled. The nozzle, connected directly to a water tank, enabled large-scale vortex structures to be generated in the working fluid when the piston-cylinder setup was actuated. The resulting fluid structures generated were comparable to those published by Gharib *et al.* (1998) and Cater and Soria (2002). In addition, the fluid structures generated were highly repeatable, making this approach suitable for the experimental work in the current research.

The piston-cylinder approach of generating large-scale vortical structures was implemented in the present experimental work since it has been successfully used in other studies as an effective method of generating ZNMF jets. Details regarding the development of a piston-cylinder rig for the current research are presented in the following section.

4.2 Development of a Vortex Generator

4.2.1 Vortex Generator Outlet

The vortex generator outlet can be one of two types: an orifice, or a nozzle. For an orifice, the cylindrical outlet is a hole in a plane wall, whereas for a nozzle, the outlet is a cylindrical tube projected perpendicularly out from a plane wall (Figure 4.7). Studies have reported considerable differences in the vortical structures generated by these two types of outlets (Auerbach, 1991; Irdmusa & Garris, 1987; Syed & Sung, 2009a). Auerbach (1991) and Irdmusa and Garris (1987) suggest that a vortex ring from an orifice (orifice ring) entrains less fluid than a vortex ring from a nozzle (nozzle ring) as the presence of

the orifice floor generates vorticity of the opposite sense which impedes the influx of entrained flow into the vortex ring. Agreeing with this view, Syed and Sung (2009a) suggest that a greater mass of ambient fluid is entrained into a nozzle ring because the entire periphery of the ring is exposed to the ambient fluid during the vortex formation stage. Conversely, an orifice ring is shielded from the ambient fluid by the orifice floor at the exit plane, leading to the formation of a smaller vortex ring in terms of its mass and/or volume and its smaller size allows orifice rings to propagate faster than nozzle rings.

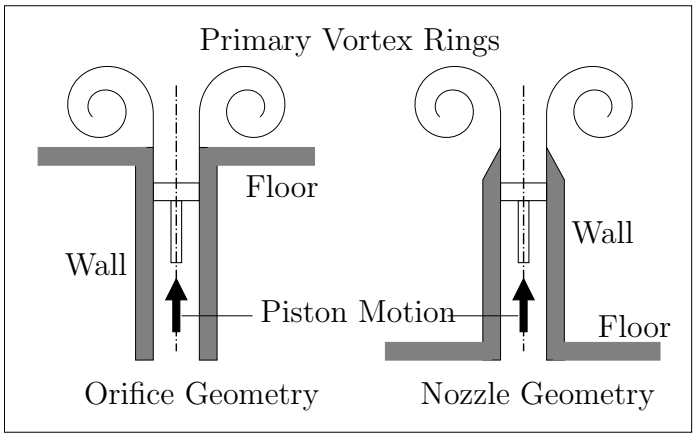


Figure 4.7: Cylindrical outlets of piston-cylinder vortex ring generators.

Syed and Sung (2009a) further infer that due to the slower propagation speed of nozzle rings, more ambient fluid is entrained into the nozzle rings per unit of propagation distance compared with orifice rings, an inference in agreement with Irdmusa and Garris (1987). Auerbach (1991) reports that streak lines of orifice rings are often twisted and irregular due to the disruption caused by negative secondary vorticity generated by the presence of the orifice wall. Syed and Sung (2009a) speculate that the wake of an orifice ring is not well defined due to the fact that orifice rings propagate faster than nozzle rings. These authors conclude that since orifice rings attain more circulation and entrain less ambient fluid, they should propagate faster and through longer distances before they are fully dissipated, when compared with nozzle rings. However, the experiments conducted in the presented research are intended for observing and understanding the occurrence of the preferential concentration mechanism, through the use of large-scale

vortical structures to induce directed motion of particles in suspension. Therefore, for the purposes of the current research, nozzle-generated vortices are considered to be more suitable as they possess more rotational kinetic energy and entrain more ambient fluid, which in turn allows the preferential concentration mechanism to act on more particles at any given instance. In addition, nozzle rings have a lower tendency to be affected by instabilities induced by the presence of the orifice floor, resulting in much clearer visualised streak lines compared with orifice rings. These properties of nozzle rings are highly advantageous in the current research as they ensure that preliminary experimental work can be conducted with minimal flow complexities. Experiments for the current research therefore employed the nozzle geometry for the generation of large-scale vortical structures.

4.2.2 Nozzle Exit Geometry

Syed and Sung (2009b) established that the dependence of the fluid entrainment fraction on the exit-wedge angle, θ, is insignificant since ambient fluid is continually ingested into the vortex ring as it propagates downstream until the vortex ring is fully dissipated. Therefore, experiments in the current research implemented a nozzle setup with $\theta = 20^{o}$ and a nozzle inner diameter, D, of 20mm, a setup previously used by Gharib *et al.* (1998) who successfully generated clear, laminar vortex rings. The nozzle wall thickness used in this work was 10mm.

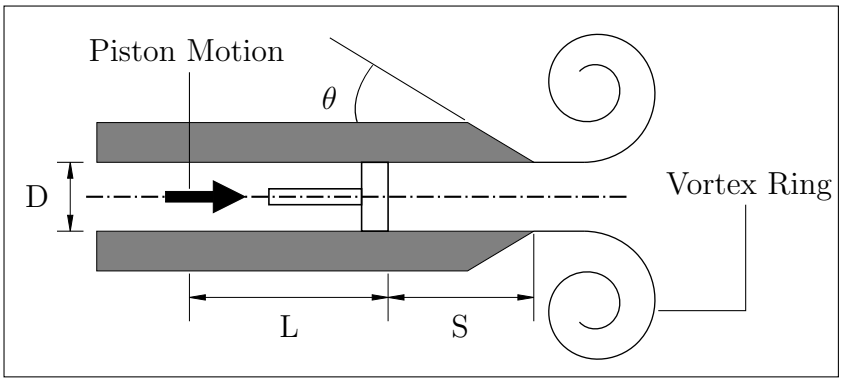


Figure 4.8: Basic parameters of a nozzle for the piston-cylinder setup.

4.2.3 Driving Mechanism

Experiments undertaken for the present research involved the examination of large-scale coherent structures generated as a single vortex ring and as a series of successive vortex rings. Two different driving mechanisms were employed to actuate the piston-cylinder rig: a crankshaft and a Marsh Bellofram diaphragm cylinder (here after referred to as a Bellofram). The crankshaft setup is well suited for experiments needing ZNMF jets generated at variable frequencies. However, the manner in which the rig operates (it is only capable of holding a limited volume of the particle suspension at any given time) prevents a continuous generation of particle-laden vortex structures as required in a number of experimental investigations. In addition, this setup also requires ambient fluid to be sucked into the piston-cylinder chamber to replenish fluid that has previously been expelled to generate vortex rings. The suction phase of the piston motion introduces additional fluid motion that would otherwise be absent in an acoustically-excited particle-laden jet. Consequently, for experiments that required the vortex rings to be seeded with particles and that required the replication of flow conditions comparable to those of acoustically excited particle-laden jets, a Bellofram was used in place of the crankshaft setup.

Crankshaft

A crankshaft setup, controlled by a stepper motor, was used to provide the reciprocating piston motion needed to generate a ZNMF jet (consisting of a series of successive vortex rings) at various excitation frequencies. This particular setup required the consideration of additional geometrical parameters to ensure that the piston, located near the nozzle exit, would have minimal adverse effects on the vortex rings produced at the nozzle exit.

Piston Exit Distance The motion of a piston through a cylinder contributes to the formation of a vortex ring (the primary vortex) but as soon as the piston stops, a secondary vortex ring (the piston vortex) is formed on the piston surface due to the removal of the boundary layer from the cylinder wall in front of the advancing piston (Allen &

Auvity, 2002; Allen & Chong, 2000; Cater *et al.*, 2004). Studies by Allen and Auvity (2002) and Cater *et al.* (2004) confirm that if the piston remains within the cylinder, piston vortices have insignificant influence on the development of the primary vortex ring. However, once the piston vortex is ejected into the fluid system, the piston vortex interacts with and changes the properties of the primary vortex ring: an interaction which can contribute to the premature transition of an initially laminar primary vortex ring into a turbulent one. Allen and Auvity (2002) established that when the ratio of the distance between the piston and the flow outlet to the outlet diameter, $S/D > 0.3$ (Figure 4.8), the piston vortex remains inside the cylinder and does not influence the primary vortex. Experiments by Cater *et al.* (2004) using $S/D = 1$, produced laminar primary vortex rings without the emergence of the piston vortex. Therefore, to ensure that the vortical structures investigated in the current research are not complicated by the presence of piston vortices, $S/D = 1$ was implemented in the piston design.

Piston Stroke Length The ratio of the piston stroke length to the outlet diameter, L/D (Figure 4.8) dictates the presence of a trailing jet following vortex rings generated by both nozzles and orifices. The present study utilised $L/D = 2$ since Gharib *et al.* (1998) established that below the critical value of $L/D = 4$, vortex rings without a trailing jet are produced. Other studies by Cater *et al.* (2004) and Walker *et al.* (1987) successfully generated single laminar vortex rings using $L/D = 2$ and $0.75 < L/D < 3.41$ respectively.

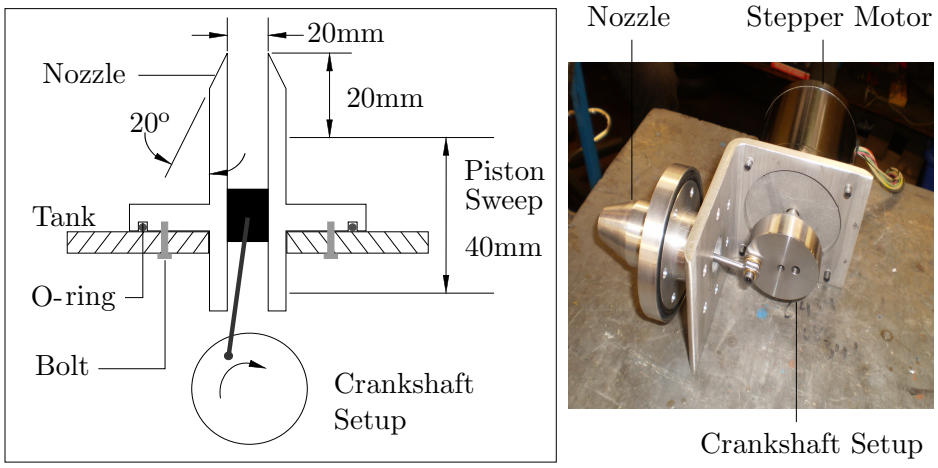
Stepper Motor Initial evaluation of a DC motor to drive the piston-cylinder setup determined that DC motors could not provide sufficient consistency and repeatability of the experimental results. Since positional accuracy and torque were considered important for the current research, stepper motors were considered as an alternative. Stepper motors have been successfully used in studies investigating piston vortices (Allen & Auvity, 2002; Cater *et al.*, 2004). The use of a stepper motor proved advantageous since they enable absolute control over the motor speed (and hence the excitation frequency of a piston), providing rotational displacements with an accuracy of up to half a motor step, as well as experimental repeatability. The stepper motor used was an RS 440-470, powered at 2.5V and 4.5A, which produced a

full-step resolution of 1.8 degrees. The stepper motor driver, which was custom made for this research, utilised paired LMD 18245 T drivers with a 55V integrated circuit and an ATMEL 8-bit AVR microcontroller 32. A 64-step micro stepping arrangement was used to generate 3200 steps per revolution in the stepper motor. Torque compensation has been included in the stepper motor driver to ensure that constant torque can be reliably maintained even at half-step locations.

Vortex Generator with Crankshaft Setup The nozzle outlet was manufactured using stainless steel, with an inner diameter, D, of 20mm at the exit. An exit-wedge angle of 20^o was adopted and a piston stroke length of $2D$ was used to obtain $L/D = 2$. The minimum distance between the nozzle exit and the piston head (at maximum displacement) was set at D. A schematic diagram of the critical dimensions of the piston-cylinder system is presented in Figure 4.9. Using the crankshaft setup to drive the piston, the fluid excitation frequency (that is, the frequency at which the vortex structures are generated) is defined based on the revolution of the crankshaft, with one full revolution of the crankshaft giving a full sweep cycle motion of the piston head within the cylinder.

Bellofram

The Bellofram consists of a linear bearing piston rod, a piston and a Neoprene diaphragm enclosed within a steel housing. Working fluid within the Bellofram is sealed off from the moving parts of the cylinder by the diaphragm, and is expelled by a piston face that is driven by a linear bearing rod. The cylinder has a cross sectional area of 23200mm^2 (36in^2) and a maximum piston stroke length of 152mm (6in). The piston rod is linearly traversed by a threaded rod with a pitch of 2mm/rev, which is in turn controlled by a stepper motor. The stepper motor used is a Step-Syn 4A bi-polar stepper motor, which provides a full-step resolution of 1.8 degrees. The stepper motor driver was custom made for this research and utilised a Bipolar Stepper motor drive board and an MW S-150-24 power supply. This configuration enables variation in motor speed, the temporal duration of the piston stroke, the time delay between successive strokes and the number of individual strokes. The Bellofram and stepper motor assembly was mounted



(a) (b)

Figure 4.9: (a) Critical dimensions of the nozzle and piston-cylinder rig with the crankshaft setup (b) The piston-cylinder system with the crankshaft setup.

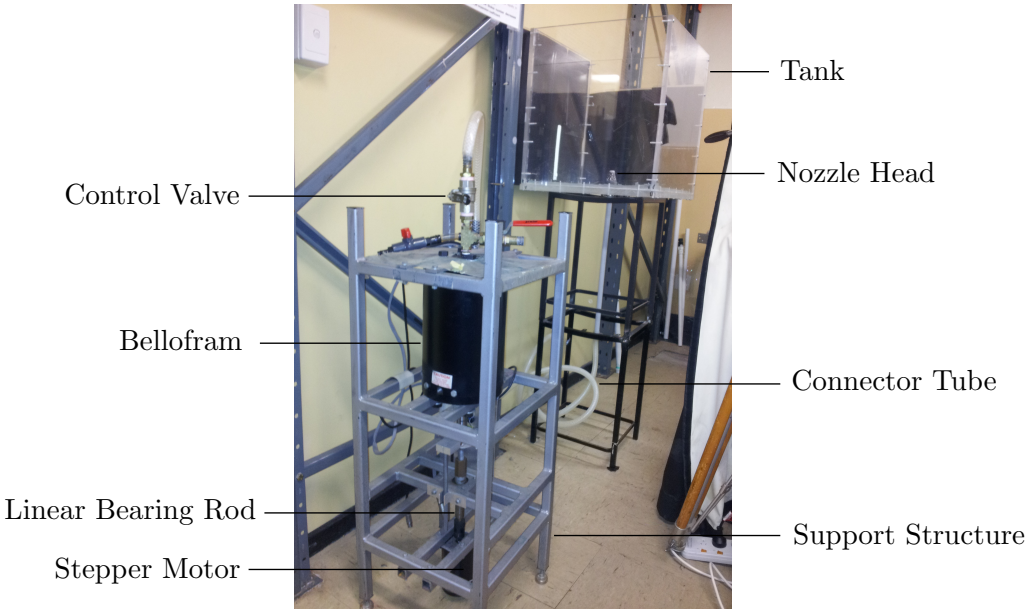


Figure 4.10: The experimental rig layout of the nozzle and the Bellofram.

vertically in a steel frame, and connected directly to the nozzle head (Figure 4.9), along with the water tank via a high pressure, reinforced connector tube (Figure 4.10).

Although the Bellofram also uses a piston as its basis of operation, it differs from the crankshaft setup in several aspects:

- The Bellofram is equipped with a significantly larger volume cylinder compared to the nozzle exit diameter, allowing for the generation of a series of continuous vortex rings (which requires a significant volume of working fluid to be expelled from the cylinder);
- Given that this cylinder does not require regular and continuous fluid replenishment, the need for the suction phase during the operation of the Bellofram is negated. That is, vortex rings are generated through a series of continuous half-cycles of a piston motion, involving only the fluid expulsion phase;
- Since the Bellofram is driven by a controlled stepper motor, this modification allows for accurate variations in vortex propagation velocities, the generation of a single or a series of short duration pulses, as well as pulses with various duty cycles.

In using the Bellofram setup, both frequency and stroke length were adjusted to produce L/D ratios and Re_f that were comparable with the arrangement using the crankshaft.

4.3 Experimental Arrangement

Although different experimental conditions were tested, a number of parameters pertaining to the rig, experimental layout and experimental procedures were consistent over all the experiments. This section details the similar conditions under which the experiments were conducted.

4.3.1 Tank

A study by Walker *et al.* (1987) investigating the impact of a vortex ring on a wall established that when a vortex ring is within a distance from a wall that is comparable with its diameter, the characteristics of

the vortex ring are significantly affected by the presence of the wall. The authors found that within this range, unsteady boundary-layer effects begin to develop and strengthen in this region. In order to limit the influence of the sidewalls and the endwall (the free fluid surface) on the vortical structures investigated in the current research, the size and depth of the water tank were chosen so that the walls were at least $10D$ from the location where the vortices were generated. This constraint significantly limited the wall effects on the vortex ring characteristics, an outcome established by Cater *et al.* (2004). The 20mm nozzle affixed at the base and in the centre of a 500mm × 500mm × 500mm water tank (driven by either the crankshaft setup or the Bellofram, depending on the nature of the experiments), provided a $12.5D$ offset distance from each wall. The tank was constructed from 10mm acrylic sheet to enable flow visualisation and laser diagnostic work (Figure 4.11 and Figure 4.12).

4.3.2 Solid Phase

The experiments used various measurement and visualisation techniques to examine the particle-fluid interactions and the preferential concentration mechanism. Different types of particles were required to accommodate the different experimental techniques used.

Polystyrene Particles

In a number of experiments, spherical polystyrene particles with a mean particle size of 0.7mm ± 0.1mm, suspended in filtered room-temperature water, were used. These particles were individually identifiable by the naked eye, making them easy to track and suitable for some of the qualitative experimental investigations. Particle sizes are significantly larger than the Kolmogorov-scale turbulence, ensuring that these particles are susceptible to the influences of the large-scale turbulence in the fluid flow field. These particles have a specified density of $\rho_p = 1060$ kg/m^3, a density which is comparable to the density of water whilst still enabling particle mass and inertia to have some influence over the two-way coupling interactions. Both the particle volume loading, ϕ, and the particle mass loading, β, were kept within the order of 10^{-4} (for a water volume of 0.1m^3) in an attempt to

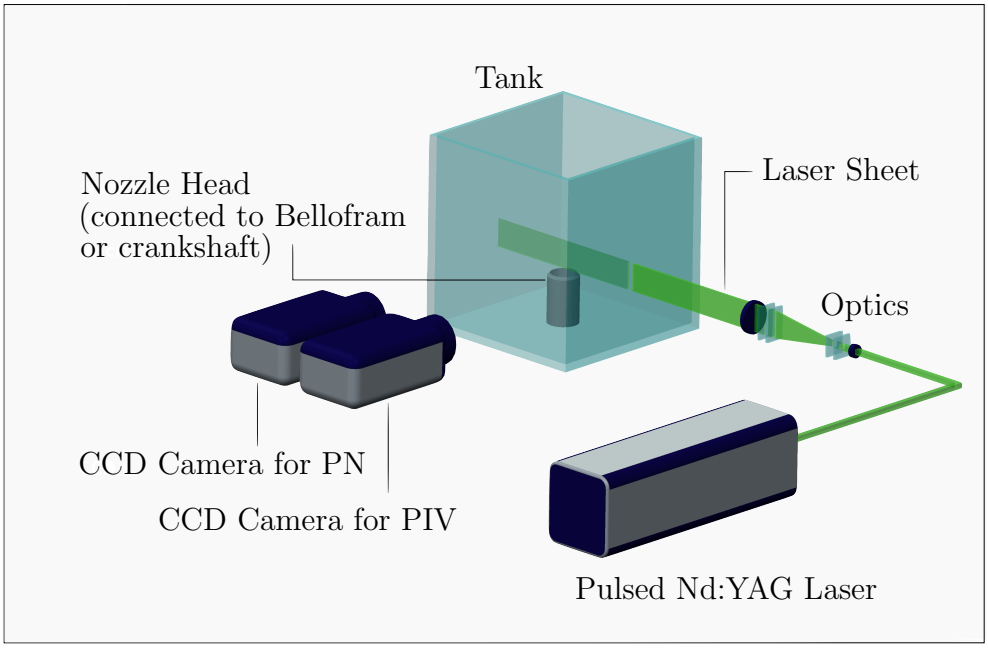


Figure 4.11: Schematic diagram of the experimental equipment and setup.



Figure 4.12: The layout of the experimental rig - crankshaft setup.

keep the particle-fluid interactions within the two-way coupling regime for the examination of turbulence-induced directed particle motion in these experiments. However, within these ϕ and β constraints, the particle number density in the flow field was insufficient for the laser diagnostic techniques to produce valid measurements. In these instances, polyamide particles with smaller diameters were used.

Polyamide Particles

Also suspended in filtered room-temperature water, the polyamide particles were spherical with a mean particle diameter of 20μm $\pm$ 15μm. These particles have a specified density of $\rho_p = 1030$ kg/m^3, a density which is comparable with the density of water, enabling them to remain neutrally buoyant. By reducing the size of the particles used, with ϕ and β kept to the order of 10^{-4}, the particle number density within the system was able to be increased. This increase in particle number density allowed more detailed qualitative and quantitative visualisation and examination of the interaction between the particles and the vortex rings using the selected laser diagnostic techniques. The smaller particle diameters also mean that the working fluid in the Bellofram could be seeded with these particles, enabling particle-laden vortex structures to be generated for some experiments.

It should be noted that the ϕ constraint (of the order of 10^{-4}) corresponds to the two-way coupling regime previously identified by Elgobashi (1991, 1994). This classification is used as a guide (as this claim has yet to be substantiated experimentally) in the current experiments to limit the complexity of the particle-fluid interactions to the two-way coupling regime. No such classifications have been proposed for β and the order of 10^{-4} constraint was selected based on the β values used by published two-way coupling studies by Elgobashi (1991, 1994). The review of the literature indicated that the β and ϕ parameters are highly inter-dependent; a classification incorporating both ϕ and β has yet to be established, and no definitive criteria have been defined to aid this process. An investigation into the roles of these parameters in the two-way coupling interactions is beyond the scope of investigation of the presented research.

4.3.3 Experimental Layout

The laser system used was a pulsed Nd:YAG laser, emitting 532nm (second-harmonic output) at 10Hz, generating a laser sheet of 1mm thickness and 50mm height. For the PIV measurements, a Kodak Megaplus ES 1.0 (8-bit pixel depth) CCD camera (1008 pixels × 1018 pixels) with a Nikon AF Nikkor 70mm-300mm f/4-5.6D lens was used to image an area of 500mm × 500mm to record the entire tank. Results focusing on the nozzle region used an image area of 56mm × 56mm. The PIV analysis of the raw PIV image pairs were conducted using PIVView (v1.75) software and an interrogation window of 32 pixels × 32 pixels with a 50% window overlap used. Checks were conducted to ensure that peak locking did not occur and that the maximum particle displacement did not exceed 8 pixels (i.e. 25% of 32 pixels corresponding to the size of the interrogation window). A inter-frame time interval of 2.5ms was implemented to achieve this constraint and length calibration conducted to confirm that the PIV analysis parameters match experimental parameters.

Measurements for the PN technique used a Redlake Megaplus II (10-bit dynamic range) CCD camera (2048 pixels × 2048 pixels) with a Nikon AF Nikkor 24mm-120mm f/3.5-5.6D lens to image an area of 500mm × 500mm to record the entire tank. Results focusing on the nozzle region used an image area of 56mm × 56mm. Both cameras were triggered simultaneously so as to enable synchronised PIV and PN measurements to be obtained.

Examination of the vortex structures at the different stages of development required repeated measurements to be taken at the same time (in relation to the stages of development of the vortex ring). The necessary experimental repeatability was developed through the implementation of a bespoke timing circuit that synchronised both cameras and the piston-cylinder rig to be triggered in phase with the laser pulses. The addition of this timing circuit allowed both PIV and PN measurements to be recorded at the same instant (in relation to the developmental phase of the vortex structures) for every test run, whilst all other parameters and conditions were kept constant.

In addition, images that were acquired during the first pulse from the laser (double laser pulses are required for the PIV technique) were analysed for particle tracking and flow visualisation purposes. These images provided instantaneous representations of particle distributions within the large-scale vortex structures. As a consequence, individual particles and vortex structures were also clearly identifiable from these images, allowing the trajectories of specific particles to tracked and analysed. These images were digitally inverted to improve the clarity of the data presentation.

4.4 Summary

This chapter discussed the development and implementation of the experimental rigs and apparatus required for the present research. Procedures and conditions used in the experimental investigations were also presented. Further experimental details pertaining to specific experiments and test runs are discussed in the following chapters.

5 Preferential Concentration

In fluids containing dense inertial particles, the occurrence of the preferential concentration mechanism can be and has been described by mass-momentum exchanges between the particle and fluid phases (see Chapter 2). The experimental investigation outlined in this chapter examines the interaction of individual particles with a vortex structure in order to substantiate existing theories on the preferential concentration mechanism. From these results, more information regarding the driving mechanism behind the preferential concentration phenomenon is acquired, leading to further experiments exploring the feasibility of using preferential concentration to un-mix particles in a fluid suspension. This chapter presents details and outcomes of the associated experimental work.

5.1 Particle Tracking Experiments

Previous studies into preferential concentration have been limited to dense inertial particles. As a consequence, centrifugal forces and hence particle density (relative to the fluid phase) were believed to be responsible for the observed behaviour. In order to substantiate these theories and claims, neutrally-buoyant particles (particles with minimal mass and inertia influences) were used in the present experiments to determine whether directed particle motion can still be achieved due to the preferential concentration mechanism.

5.1.1 Experiment-Specific Details

The investigation described here used water as the working fluid and polyamide particles ($\rho_p = 1030$ kg/m^3 and $d_p = 20\mu$m $\pm$ 15μm) as the seeding, the Bellofram setup to generate vortices, and both the PIV and PN techniques to obtain velocity and concentration measurements simultaneously. Details of the experimental layout were discussed in Chapter 4. Single-pulsed vortex rings to be examined in this experiment were generated at different pulse duration varying from 0.4s to 1.4s, at intervals of 0.2s (Figure 5.1). It is noted that the corresponding L/D ratio of these pulses lie within the range of 0.48 to 1.68, which is well within the range of formation numbers that generate a single ring, as defined by Gharib *et al.* (1998).

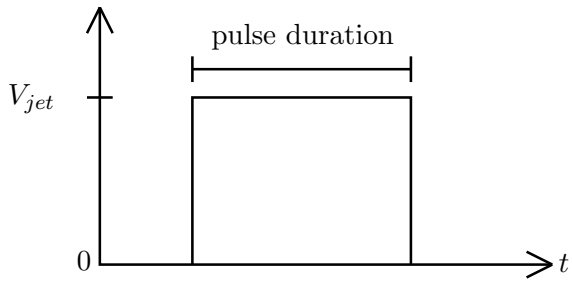


Figure 5.1: Single-pulses used for current experiments, with pulse duration varying from 0.4s to 1.4s, at intervals of 0.2s.

During the preparation of the working fluid, the occurrence of particle agglomeration was evident. Particle agglomeration allowed effective particle sizes of up to 2 orders of magnitude larger than the mean particle diameter to be obtained, thereby resulting in a larger distribution of particle sizes (polydisperse particles). The larger sizes of these agglomerated structures, when compared with an individual polyamide particle, also enabled them to be easily identified and tracked. Hence, in addition to the quantitative data obtained from the PIV and PN measurements, the recorded images were also used to track and analyse the trajectories of specific agglomerated structures as they interacted with their respective vortex ring structures throughout the evolution and the propagation of the vortex ring.

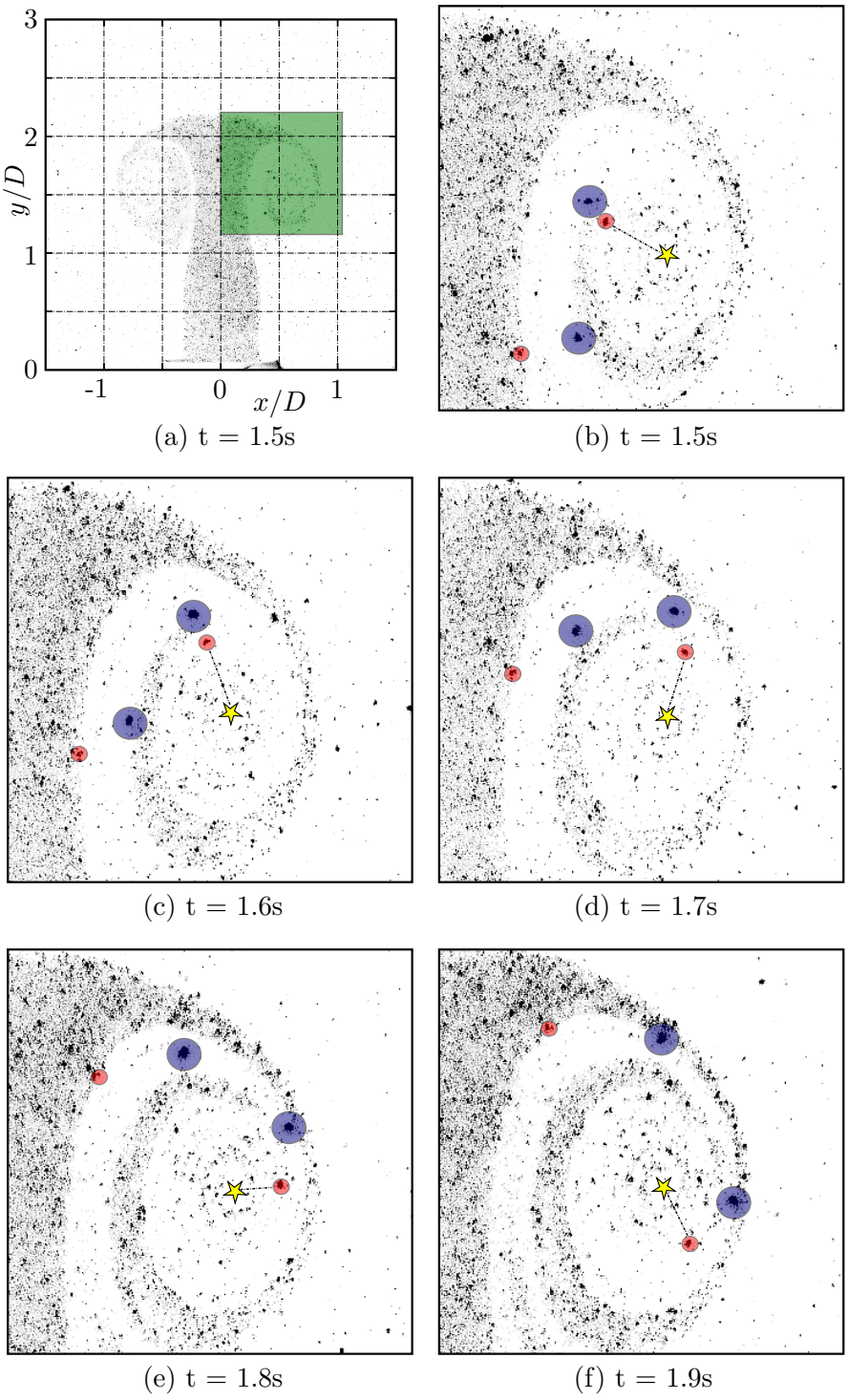
The use of a planar imaging technique to visualise a three-dimensional vortex ring presented certain limitations in spite of the axisymmetric geometry. The presence of secondary flow within the rings meant that particles tended to drift in and out of the imaging plane (i.e. the laser sheet), so that they did not remain within the imaging plane long enough to provide the desired amount of working data. Consequently, the data that could be acquired through particle tracking were limited to short time durations (typically a small number of successive flow visualisation images). A total of 15 test runs were conducted for each fluid excitation frequency so as to acquire sufficient, usable particle tracking data. A select number of test runs discussed in the current chapter are chosen specifically due the clarity of particle tracking data recorded.

5.1.2 Results and Discussion

Figure 5.2 shows two particle agglomerations within a vortex, generated using a pulse duration of 0.8s, tracked over a timeframe of 0.4s. The L/D ratio for this pulse is 0.96, and the flow Reynolds number for this test is large at $Re_f = 830$ (based on the translation velocity of the ring and the maximum ring diameter). These figures feature zoomed-in imaging areas of $1.05D \times 1.05D$ in order to improve the clarity of the information presented. The first instance, featured at t = 1.5s, shows the imaging area with its origin located at $x/D = 0, y/D = 1.15$ (Figure 5.2a). The imaging area presented follows the propagation of the vortex along the vertical axis; hence, the final imaging area featured at t = 1.9s had its origin location at $x/D = 0, y/D = 1.8$ (Figure 5.2e). Since the particles tracked are essentially agglomerated polyamide particles that are not spherical in shape, the sizes of these agglomerations are determined in terms of their effective particle diameter (should the particle have been spherical). These particles (both with effective diameters of approximately 0.5mm, circled and highlighted blue Figure 5.2) were observed to be thrown radially outward from a region near the vortex core to the periphery of the vortex structure. Two smaller agglomerates, circled and highlighted red (of diameters approximately half of those highlighted blue) were also tracked for comparison. The star symbols are to indicate vortex core locations. The vortex examined is laminar and propagating at constant convection velocity. The fact that the large particles (highlighted blue)

are slipping relative to the small particles (highlighted in red, which do not show slip) confirms that they are partially affected by fluid motion and do not follow the motion of their respective fluid elements. The tracking of these particles was terminated after t = 1.9s (Figure 5.2) as they drifted out of the imaging plane (i.e. laser sheet). Therefore, it is unclear if these particles remained at the edges of the vortex structure or if they left the vortex structure completely at longer times. Further analysis is therefore required to determine whether particles vacate vortex cores and to move to regions of low vorticity.

Preliminary examination of these outcomes implies the effect of centrifugal forces and particle inertia as the driving forces of this particular particle behaviour, and this is a deduction that is assumed by various studies involved in the preferential concentration mechanism (as outlined in Chapter 2). However, this turbulence-induced directed particle motion is exhibited by neutrally-buoyant particles which have a negligible particle inertia contribution under these flow conditions. Consequently, these results seemingly contradict the use of centrifugal forces to explain the occurrence of the preferential concentration mechanism. Despite uncertainties pertaining to the outcome of the particles tracked in Figure 5.2 (whether they stay or leave the vortex structure), there have been other instances observed in the current study whereby particles from the vortex ring were observed to leave the fluid structure completely (this is not a common occurrence). Figure 5.3 features particle concentration measurements from the PN technique, which enabled the trajectory of two distinct agglomerated particles (circled in black) to be tracked. The concentration measurements have been normalised against the highest absolute concentration recorded within the system for each individual experimental run i.e. different peak values for different experimental runs. Therefore, Figure 5.3 also provides an indication of the relative distribution of particle concentration within the working fluid. These agglomerated particles that were initially part of the vortex were observed to migrate around the vortex ring, heading towards the wake region, where the continual propagation of the vortex leaves these agglomerated particles behind. On the opposite side of the ring (the left side), the concentration of particles in the vortex wake region was also observed to increase over time (Figure 5.3f-i), indicating that particles were directed to accumulate in the wake regions and were eventually left behind as the vortex moved away.



(a) t = 1.5s (b) t = 1.5s

(c) t = 1.6s (d) t = 1.7s

(e) t = 1.8s (f) t = 1.9s

Figure 5.2: Trajectory tracking of two large agglomerated particles (highlighted blue) and two small agglomerated particles (highlighted red) within a vortex laden with particles, generated using a pulse duration of 0.8s, with $Re_f = 830$.

Figure 5.4 and Figure 5.5 present the trajectory of an agglomerated structure with an effective particle diameter of approximately 0.8mm (circled in black) for a time duration of 2.2s. Two portions of the fine particle streaks or 'braids' within the vortex are highlighted in red and blue for clarity. The imaging area used to present these images is $0.9D \times 0.9D$ and the first image at t = 2.3s was located with its origin at $x/D = 0, y/D = 0.65$ (Figure 5.4a). Following the propagation of this vortex structure along the vertical axis, the final image at t = 4.5s was located at $x/D = 0, y/D = 1.7$ (Figure 5.5f). The particle tracked, circled in black, is observed to move back and forth between the red braid and the blue braid of particles. This agglomerated structure presented with a similar behaviour to those in Figure 5.2 with big particles that do not follow the same trajectories as the small particles, that is the big particles are observed to slip radially outwards from the vortex core to the outer edges of the vortex (Figure 5.4c). However, the agglomerated structure does not remain at the outer edges of the vortex once it is flung out from the vortex core (as postulated by other studies in the literature, particles move towards and accumulate in regions of high strain and low vorticity). Instead, this structure is observed to slip across multiple braids to move towards the vortex core (Figure 5.5a), only to be flung outwards once more into the edges of the vortex (Figure 5.5f); an outcome that is unexpected and has not been reported in earlier studies.

These experimental observations create further uncertainties regarding the use of particle inertia and centrifugal forces to explain directed particle motion due to the preferential concentration mechanism. The main reason causing uncertainties is that this line of reasoning does not explain the particle trajectories featured in Figure 5.4 and Figure 5.5, whereby the particle at the edge of the ring moves towards the vortex core before returning to the edge of the vortex structure. The use of neutrally-buoyant particles negates the contribution of particle mass and inertia in their trajectories, thereby challenging the postulation that centrifugal forces are solely responsible for the particle motion in the preferential concentration mechanism. It stands to reason that existing preferential concentration theories based solely on particle inertia and centrifugal forces are unable to explain the present observation.

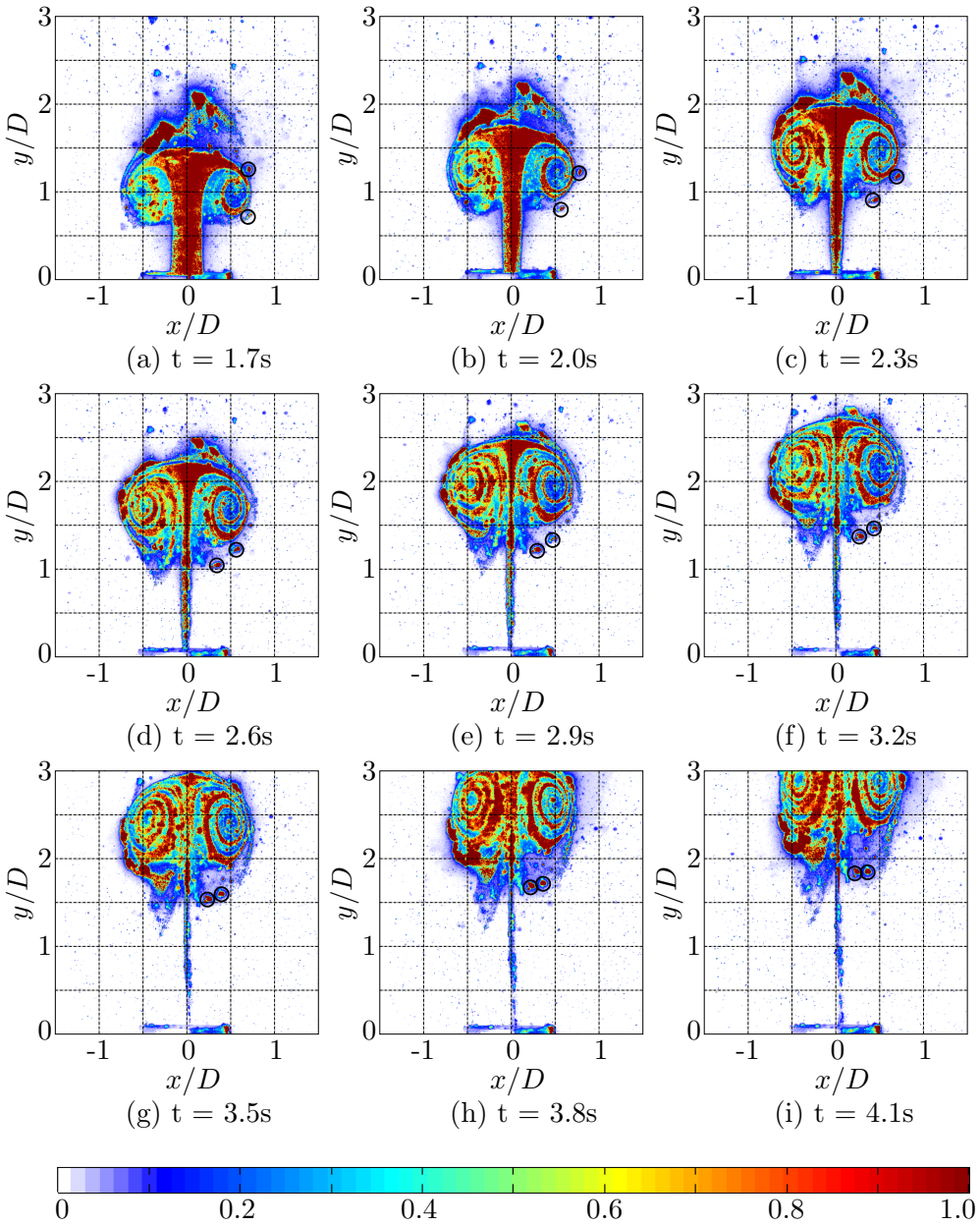
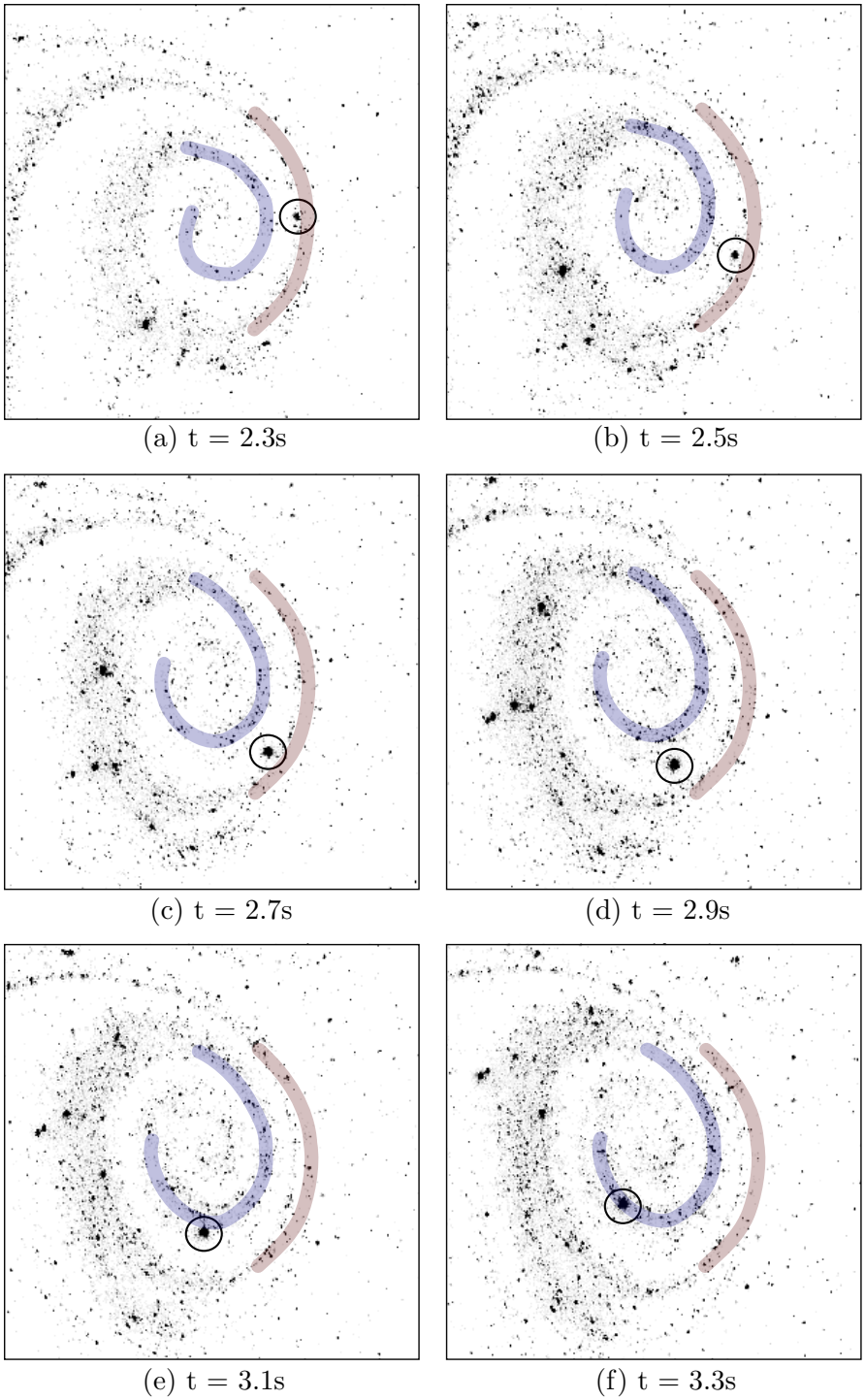


Figure 5.3: Trajectory tracking of agglomerated particle structures and particle concentration measurements of a particle-laden vortex ring, generated using a pulse duration of 1s, with $Re_f = 1040$.

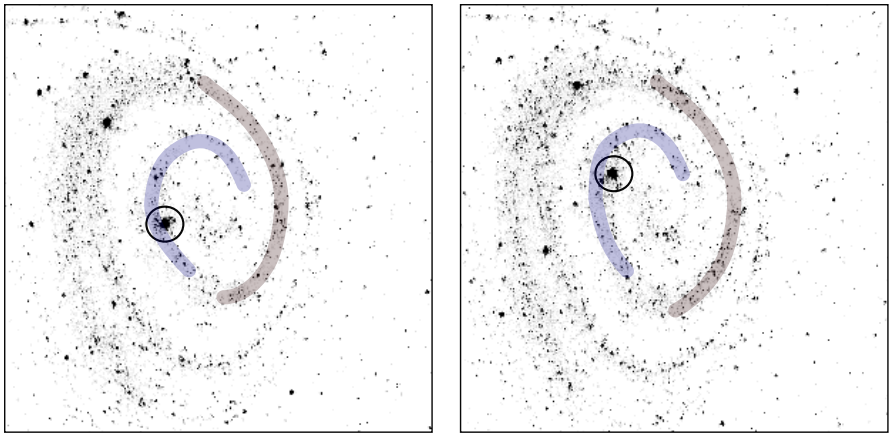


(a) t = 2.3s (b) t = 2.5s

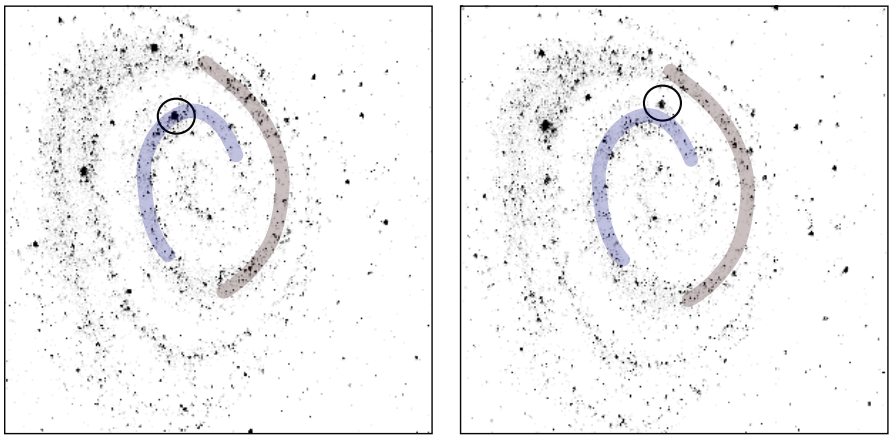
(c) t = 2.7s (d) t = 2.9s

(e) t = 3.1s (f) t = 3.3s

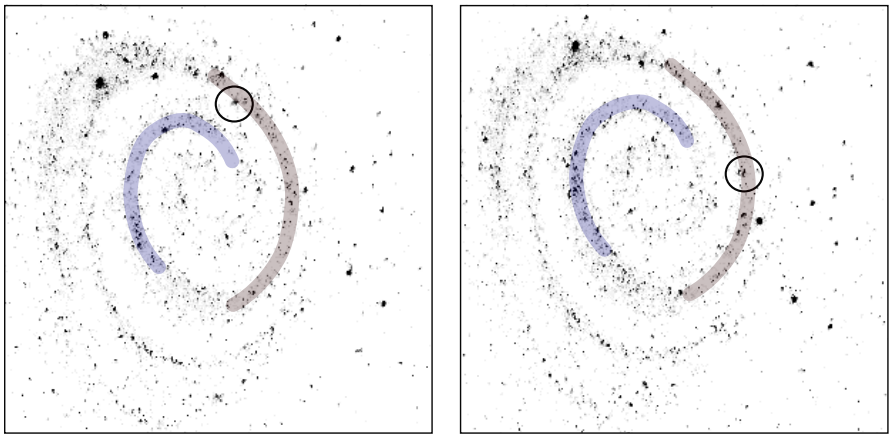
Figure 5.4: Trajectory tracking of agglomerated particles in a particle-laden vortex, generated using a pulse duration of 0.4s, with $Re_f = 415$ - part A.



(a) t = 3.5s (b) t = 3.7s



(c) t = 3.9s (d) t = 4.1s



(e) t = 4.3s (f) t = 4.5s

Figure 5.5: Trajectory tracking of agglomerated particles in a particle-laden vortex, generated using a pulse duration of 0.4s,with $Re_f = 415$ - part B.

The radius of the agglomerated particles (as well as the non-agglomerated particles within the braids) is observed to vary as it progresses through its trajectory within the vortex. This may be an indication that the agglomerated particles are affected by the presence of secondary flow within the vortex, causing it to drift forwards and backwards in the imaging plane. However, parallax errors due to the CCD camera's line of sight and the area of the imaging plane recorded was determined to be 0.04%, causing a 10^{-6}m variation in the displacement measurements of the agglomerated particles. Since the minimum displacements of the agglomerated particles were measured to be an order of magnitude larger than the contribution of parallax errors (i.e. average displacements were within the 10^{-5}m range), the impact of parallax errors on the particle tracking data is therefore negligible. Therefore, it is unlikely that the observed trajectories are the result of secondary flow.

The trajectories of the agglomerated particle structures featured in Figure 5.2, Figure 5.4 and Figure 5.5 confirm that these structures move in a directed manner, a result of their interactions with their respective vortex rings. The particles are small in comparison to the time scale of the vortex ring and that the particle volume loading used is dilute enough that particles are not affected by the presence of other particles i.e. four-way coupling not considered. On the other hand, particles are observed to agglomerate which may be the consequence of localised particle-particle interaction due to variations in local particle volume loading throughout the fluid flow. Although four-way coupling may be occurring in a localised manner, it does not fully explain the interaction of the agglomerated particle structure with the vortex structures.

The influences of Brownian motion are disregarded since these effects are insignificant on particle sizes above 1μm (Barnes *et al.*, 1989). Particles larger than this range would have particles response times much larger than the mean collision time such that the effect of Brownian motion can be neglected in comparison to the dispersion by fluid turbulence (Wang & Maxey, 1993). It is possible that the particle behaviour observed may depend on whether they are in the rotational core or in the irrotational flow outside. In addition, if the particles were

in the transition zone (part rotational, part irrotational), it is possible that the shear in the flow would have an effect.

Saffman (1965) established that particles moving through a very viscous liquid (where all particle-scale Reynolds numbers are assumed to be small compared to unity) would experience a shear lift force (often called the Saffman lift). The direction of this lift force is in the direction where the fluid's relative velocity is greater and as such would cause particles to drift across streamlines. Similarly, if Magnus lift force due to particle rotation were to be considered, the resulting lift force is also directed to where the fluid's relative velocity is greater. Results from the current work however do not support the behaviour of particles experiencing either Saffman lift or Magnus lift forces. Instead the agglomerated particles are observed to move across streamlines in the directions where the fluid's relative velocities are higher *and* lower in certain instances. Therefore, neither Saffman lift nor Magnus lift is unable to fully explain the particle behaviour observed.

In another study, Saffman (1956) also considered the effects of liquid inertia causing particles suspended in a sheared viscous liquid to take up preferred orientations, relative to the motion of the undisturbed liquid. This analysis demonstrated that the inertia of liquid does effect particle motion, however, the effects of liquid inertia on particle motion is orders of magnitude too small to account for any of the experimental observations. Saffman (1956) then suggested the non-Newtonian properties of the liquid as a contributing factor. Noting that current results have particle agglomerates occurring in the flow field, it is possible that the variation in local particle volume loading would affect local viscosity gradients and as such the bulk properties of the suspension may be to some extent behaving in a non-Newtonian manner. It is however unclear at this stage how non-Newtonian liquids (viscosity) are able to affect particles to move in a directed manner.

Further to the above discussion, since particle density (relative to fluid density) is inconsequential to the microstructural considerations involved in particle-fluid surface interactions (Barnes *et al.*, 1989; Mueller *et al.*, 2010; Stickel & Powell, 2005), it is deduced that the hydrodynamic forces acting on these agglomerated particle structures play a significant role in the behaviour exhibited by these structures.

Hydrodynamic forces are dependent on particle volume and particle surface area (Barnes *et al.*, 1989), and therefore provide an indication of the influence particle-fluid surface interactions have on directed particle motion. These agglomerated structures, having larger surface areas, would be more susceptible to the effects of fluid viscosity and pressure gradients when compared with an average size polyamide particle. As a consequence, it is reasoned that the particle-fluid surface interactions would have a significant influence over how these agglomerated structures respond to a vortex structure, leading them to move in a directed manner.

Based on the reasoning that particle-fluid surface interactions are capable of inducing directed motion in particles, it follows that these interactions may have significant influence over the preferential concentration mechanism. This proposition may help shed some light on current experimental observations which existing preferential concentration theories based solely on particle inertia and centrifugal forces are unable to explain.

5.1.3 Conclusions of the Particle Tracking Experiments

Current experiments provided observations of some unexplained behaviour in the interaction between particles and fluid structures. This behaviour cannot be explained by conventional concepts of preferential concentration based solely on particle mass and inertia. One possibility is that there are other factors such as particle-fluid surface interactions that play a significant role behind the preferential concentration mechanism. Alternatively, it is plausible that the directed particle motion observed may be due to factors that are not associated with the preferential concentration mechanism. Further experiments will be necessary to substantiate these postulations.

5.2 Preferential Concentration Experiments

Results from the particle tracking experiments indicate that particles are able to move in a directed manner. The present investigation examines possible factors, besides particle mass and inertia, which may be contributing to the directed motion in particles that may or may not be associated with the preferential concentration mechanism.

5.2.1 Experiment-Specific Details

The Bellofram setup was used to generate single pulsed vortex structures with different pulse duration varying from 0.4s to 1.4s, at intervals of 0.2s (Figure 5.1). Particle velocity profiles and concentration measurements were obtained using the PIV and PN techniques respectively. Polyamide particles (ρ_p = 1030 kg/m^3 and d_p = 20μm $\pm$ 15μm) were seeded in the working fluid in three different manners: (i) Case A - only the ambient fluid is seeded; (ii) Case B - only the vortex ring is seeded; and (ii) Case C - both the vortex ring and the ambient fluid are seeded with particles. The three different ways of particle seeding were applied to each of the six different pulse durations tested, with 10 test runs done for each case (i.e. a total of 180 test runs). Note that these test conditions are different from those evaluated in Section 5.1. The general flow and particle distribution characteristics were experimentally consistent and comparable for every case evaluated. Changes in the distribution of particle concentration will provide an indication that particles are accumulating in specific regions in/around fluid turbulence structures. This enables the feasibility of using the preferential concentration mechanism to un-mix particles in a fluid suspension to be established.

In order to produce vortex rings laden with particles, fluid in the Bellofram and the connecting tube were seeded with Polyamide particles. The fluid in the tank and the Bellofram were prepared under identical laboratory conditions to ensure negligible temperature differences between the two fluids. The particle suspension was

subjected to ultrasonic sonication to obtain a mono-disperse distribution of polyamide particles for the experiments. Ratoarinoro *et al.* (1992) established that sonication, the application of sound energy to agitate particles in a fluid sample, is highly effective at preventing the agglomeration of particles. High frequency pressure (sound) waves applied to a particle-liquid suspension produce high vibrational forces on the particles, thereby preventing agglomeration and generating a mono-disperse distribution of particles in a fluid. A mono-disperse distribution of particles ensures that the particle-fluid surface interactions are approximately uniform for the particles subjected to the preferential concentration mechanism in the present investigation.

5.2.2 Results and Discussion

Figures 5.6 - 5.8 feature a time series of ensemble-averaged velocity fields of a vortex generated with a pulse duration of 0.4s (Figure 5.1), in the three different ways the working fluid was seeded. These figures represent the ensemble average over 10 repetitions of each case. With vortices generated using a pulse duration of 0.4s, the flow Reynolds number for this test is $Re_f = 415$ (based on the translation velocity of the ring and the maximum ring diameter) with an L/D ratio of 0.48. The first column presents data from Case A - where only the ambient fluid is seeded, the second column presents data from Case B - where only the vortex ring is seeded, and the third column presents the data from Case C - where both the vortex ring and the ambient fluid are seeded with particles. The ensemble-average PIV measurements were acquired using the sum of the correlation functions (i.e. the ensemble correlation) whereby prior to peak searching, all correlation functions are added up in order to suppress noise efficiently. The difference between this approach to the averaging of vector fields is that outliers in the individual vector fields will not affect the final result since their peaks are suppressed due to the summation of the correlation function prior to ensemble-averaging the vector fields. Velocity measurements were recorded from t = 0.1s to t = 2.1s, at time intervals of 0.4s. Despite keeping ϕ to the order of 10^{-4} in the fluid that was seeded with particles, the number density of the velocity vectors within the vortex structure was seemingly higher in Case C, compared with Cases A and B (this is more obvious later in the time series i.e. in Figure 5.8). This

outcome is to be expected for Case C since both the ambient fluid and the fluid forming the vortex ring are seeded with particles, thus minimising the dilution of the particle number density within the vortex ring as it evolves with time. Consequently, the velocity vectors for Case C include both the motion of particles from within the vortex ring itself and particles from the ambient fluid that are entrained into the vortex ring, resulting in a seemingly higher number density of velocity vectors in the vortex ring when compared with Cases A and B.

The time series of PIV measurements from Cases A, B and C indicated that the vortices were propagating at comparable velocities. The vortex in Case C was noted to be slightly ahead of Cases A and B later in the time series (Figure 5.8f) and the possibility of this issue being due to variations in test run starting times was considered. However, the starting position of the piston in the Bellofram was identical for every test run and the vortices for all three cases were recorded at the same time delays after the Bellofram was pulsed. The PIV data in Figure 5.6 - 5.8, ensemble-averaged velocity profile measurements along different y/D locations and at various times were determined for all three particle loading scenarios.

Figure 5.9 shows the velocity profiles measured at the nozzle outlet during the start of the experiments, corresponding to the PIV measurements in Figure 5.6. The velocity profile for Case A at t = 0.1s was determined to have a peak velocity of 0.04m/s while for Cases B and C, this value was found to be 0.03m/s (Figure 5.9a). Despite similarities in the distribution of the velocity profile, there was an approximately 20% variation in magnitude between the three cases. The variation was determined based on the largest deviation of the peak velocity of the individual cases when compared with the peak velocities of all three particle loading cases. Comparing the velocity profiles at t = 0.5s, the variation in magnitude between the three cases reduced to approximately 7%, with Cases A and C having a peak velocity of 0.11m/s and Case B with 0.1m/s (Figure 5.9b).

Figure 5.10 shows the velocity profile through the vortex cores for all three particle loading cases at various times. The variation in peak velocity is observed to be 14% at t = 1.3s, 8% at t = 1.7s and 9% at t=2.1s, with the peak velocity for Case C being higher than Cases A

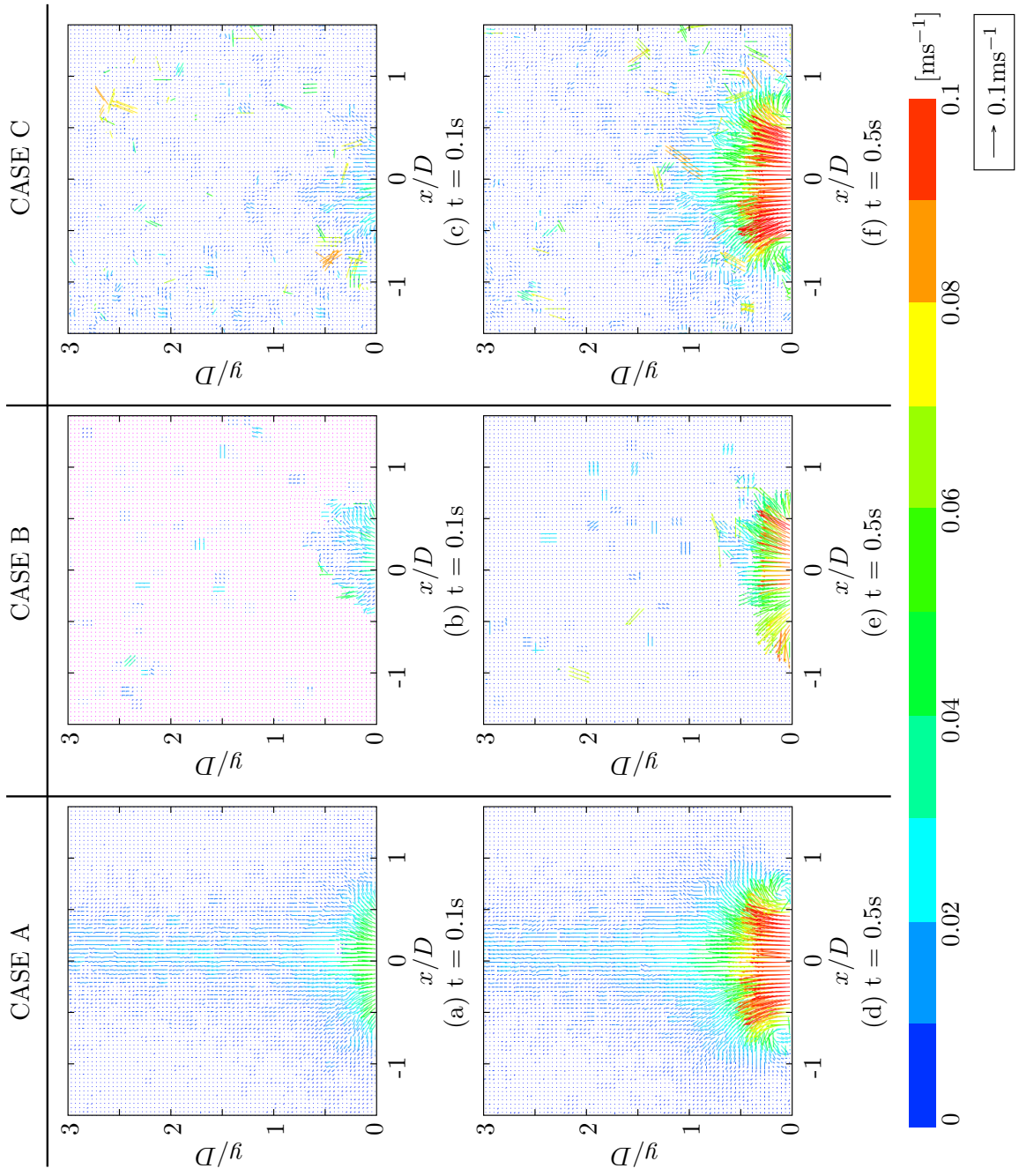


Figure 5.6: Ensemble-averaged velocity measurements of a vortex generated using a pulse duration of 0.4s with $Re_f = 415$, propagating into a working fluid for different particle loading cases - part A.

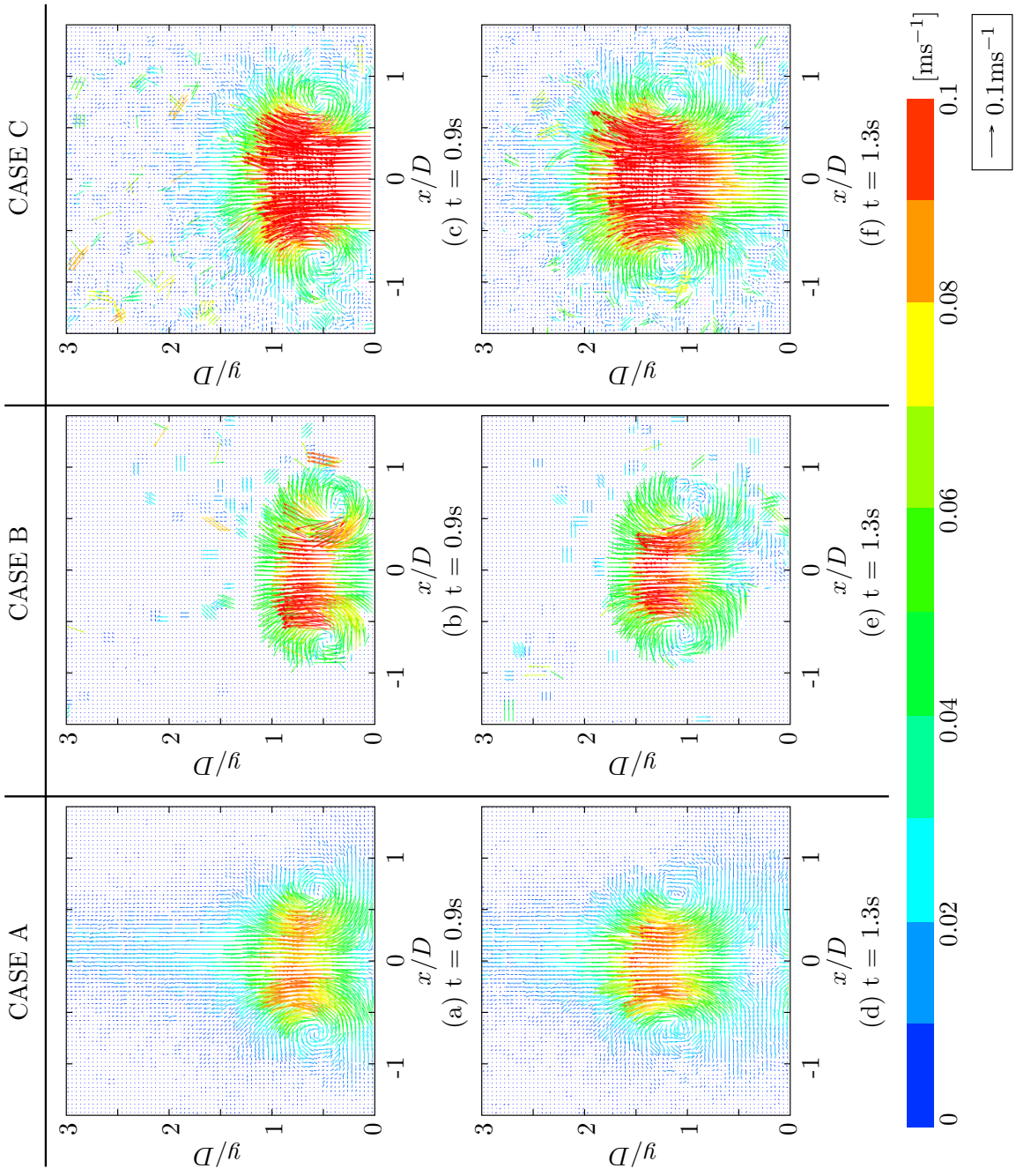


Figure 5.7: Ensemble-averaged velocity measurements of a vortex generated using a pulse duration of 0.4s with $Re_f = 415$, propagating into a working fluid for different particle loading cases - part B.

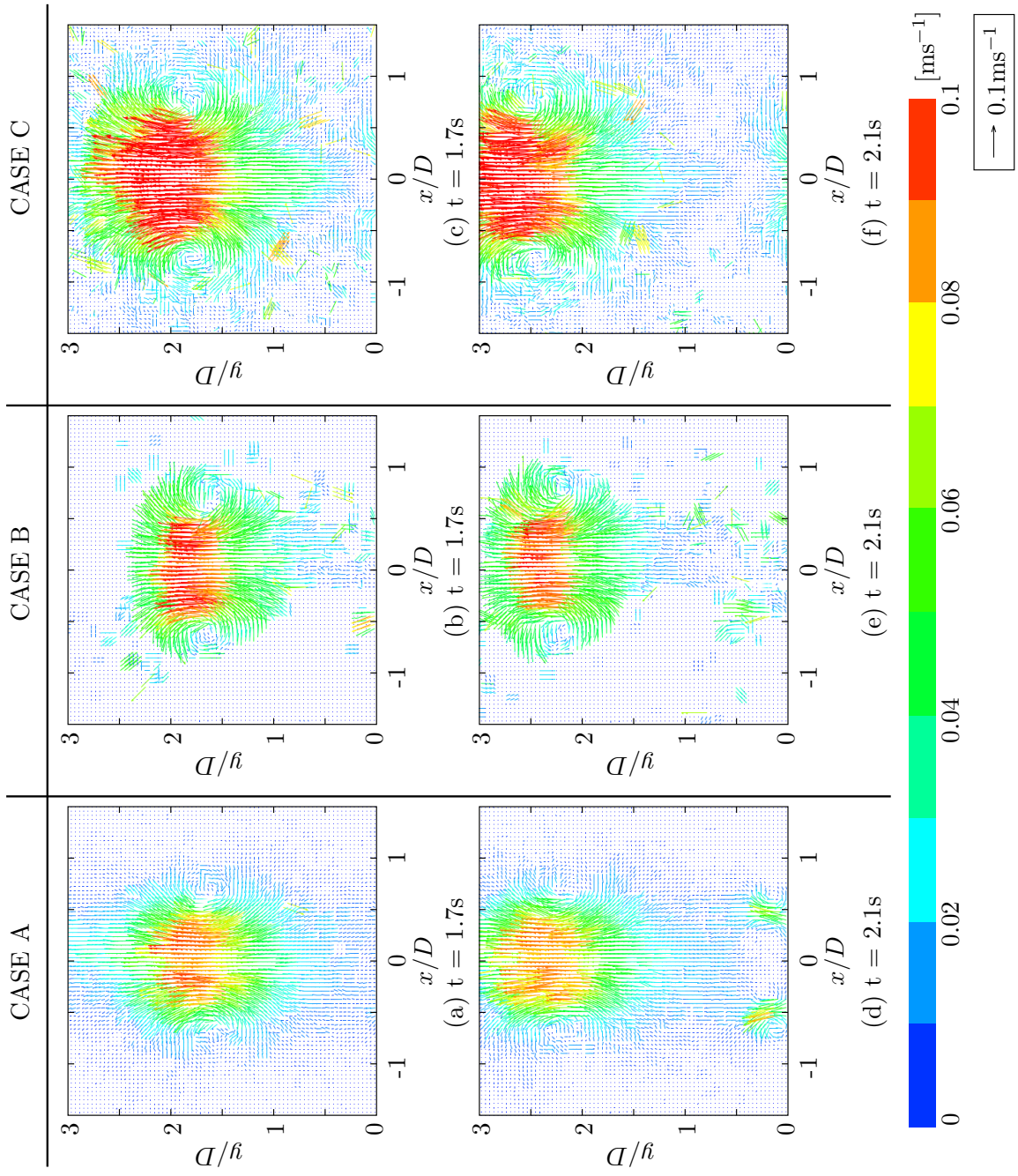
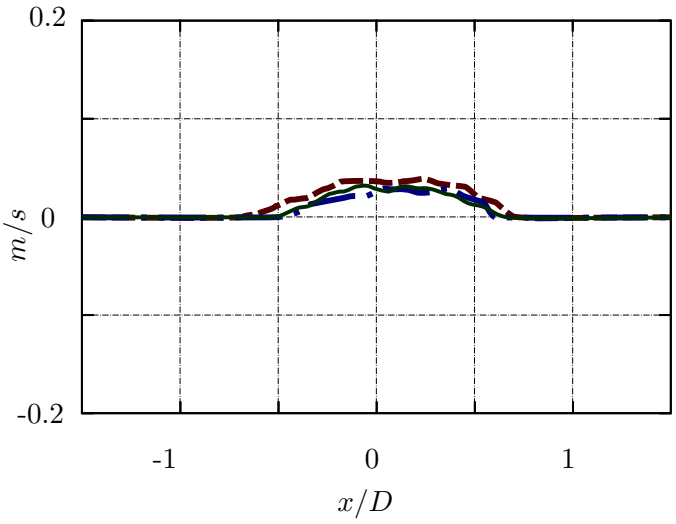
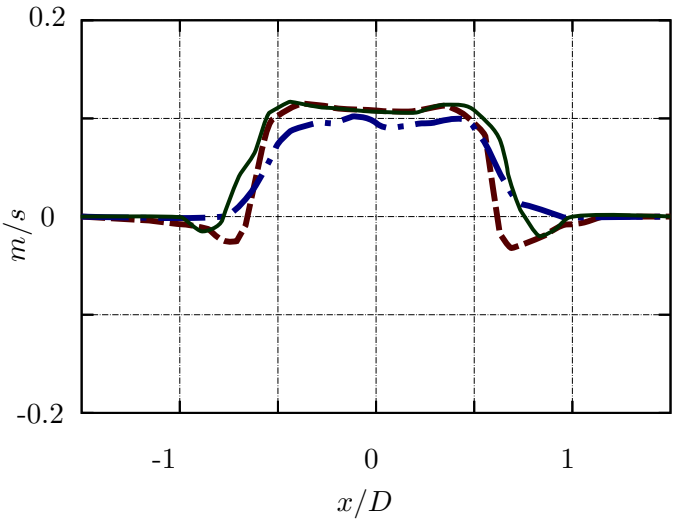


Figure 5.8: Ensemble-averaged velocity measurements of a vortex generated using a pulse duration of 0.4s with $Re_f = 415$, propagating into a working fluid for different particle loading cases - part C.



(a) t = 0.1s



(b) t = 0.5s

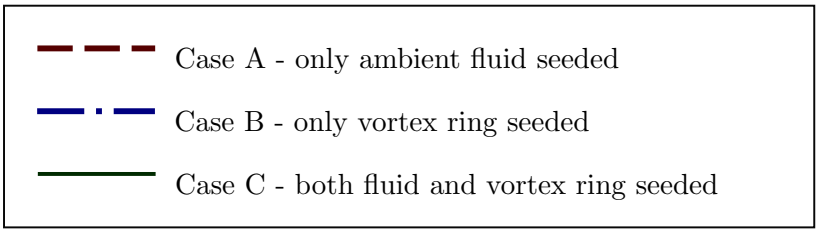


Figure 5.9: Ensemble-averaged velocity profiles at the nozzle exit for a vortex generated using a pulse duration of 0.4s, with $Re_f = 415$.

and B in all these instances. Despite these variations, the peak velocity is of the same order of magnitude and the overall distribution of the velocity profiles for all three cases in Figure 5.10 were found to be comparable. Comparing the data from Figure 5.9 and Figure 5.10, the 'lead' in peak velocity in Case A was subsequently 'lost' to Case C and no significant deviation in the general trend of the velocity profiles was observed. These outcomes indicate that the discrepancy in initial flow conditions (Figure 5.9) did not significantly impact the subsequent development and propagation of the vortices generated. However, it is interesting to note that the peak velocity for Case C is consistently higher than Cases A and B, despite starting with a lower peak velocity (Figure 5.9a). Checks were conducted to ensure that no significant deviation was observed in the general trend of the instantaneous velocity profiles and the ensemble-averaged velocity profiles presented. The instantaneous velocity profiles were within ± 0.015 m/s of the ensemble-average velocity profile, giving an acceptable 10% error margin associated with experimental error.

Table 5.1: Average vortex diameter of ensemble-averaged velocity profiles through vortex cores for a vortex generated using a pulse duration of 0.4s, with $Re_f = 415$.

	Case A	Case B	Case C
t = 1.3s	9.5mm	8.8mm	10.7mm
t = 1.7s	9.9mm	9.5mm	10.9mm
t = 2.1s	10.0mm	10.2mm	12.0mm

Table 5.1 shows the average vortex diameter determined from the velocity profiles in Figure 5.10. These values were determined by first establishing the mid-point between the highest and lowest velocities within a given profile, which provides an approximation to the centre of the shear layer. The x/D values corresponding to these mid-points are then used to determine the average vortex diameter for a given case. Results from Table 5.1 and the velocity profiles in Figure 5.10 show that the vortex ring diameter for each particle loading case increases

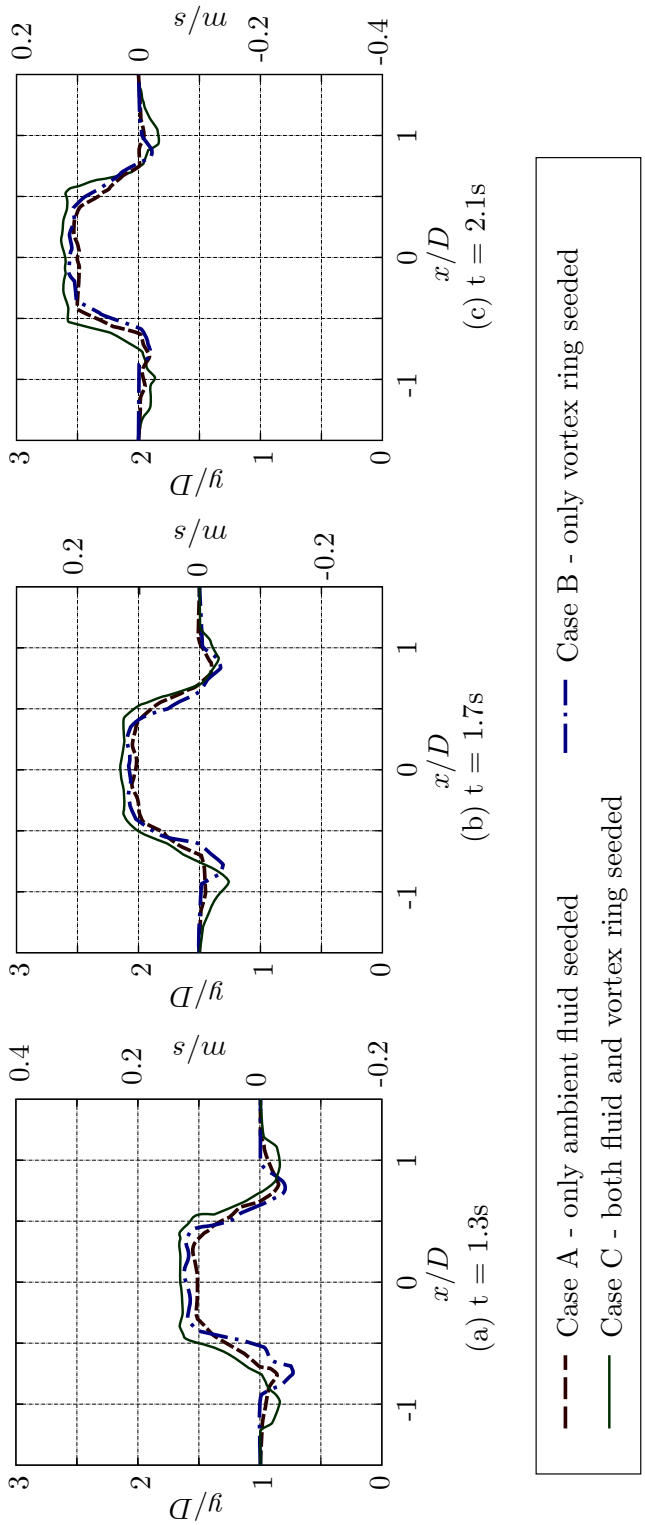


Figure 5.10: Ensemble-averaged velocity profiles through vortex cores for a vortex generated using a pulse duration of 0.4s, with $Re_f = 415$.

with time, with Case C consistently presenting with the largest vortex diameter.

Table 5.2: Propagation velocity of ensemble-averaged velocity profiles through vortex cores for vortex generated using a pulse duration of 0.4s, with $Re_f = 415$.

	Case A	Case B	Case C
t = 0.9s	0.0167ms^{-1}	0.0133ms^{-1}	0.0122ms^{-1}
t = 1.3s	0.0192ms^{-1}	0.0177ms^{-1}	0.0169ms^{-1}
t = 1.7s	0.0206ms^{-1}	0.0194ms^{-1}	0.0218ms^{-1}
t = 2.1s	0.0214ms^{-1}	0.0205ms^{-1}	0.0229ms^{-1}

Table 5.2 shows the instantaneous propagation velocity of the vortex rings determined from the vorticity plots (Figure 5.11 and 5.12). The propagation velocity was obtained by tracking the locations of the maximum absolute vorticity, which is assumed to coincide with the centre of the vortex-ring core. Results from Table 5.2 show that the propagation velocity of the vortex rings for all three particle loading cases increases with time. The vortex ring in Case A presented with the fastest initial propagation velocity, with Case C eventually gaining the highest propagation velocity.

It is possible that the variation in vortex propagation velocities between the three cases could be due to some form of correlation between particle concentration and the fluid flow velocity field. Therefore as a starting point, consideration is given to the general equations of motion for incompressible Newtonian fluids. The Navier-Stokes equations are expressed in vector notation as:

$$\rho\left(\frac{\partial \boldsymbol{v}}{\partial t} + \boldsymbol{v}\cdot\boldsymbol{\nabla}\boldsymbol{v}\right) = -\boldsymbol{\nabla}p + \mu\nabla^2\boldsymbol{v} + \mathbf{f} \tag{5.1}$$

along with the continuity equation

$$\nabla \cdot \boldsymbol{v} = 0 \tag{5.2}$$

where $\boldsymbol{v}$ is the fluid velocity vector, p is the fluid pressure, ρ and μ denote the fluid density and dynamic viscosity respectively, $\mathbf{f}$ is the body force per unit volume, and ∇^2 is the Laplacian operator. From Equation 5.1, the term $\mu\nabla^2\boldsymbol{v}$ indicates that changes in fluid viscosity would have an impact on fluid motion. Hence, when particles are introduced into a fluid flow field (whether in the ambient fluid only, or the vortex structure only, or both), the overall fluid viscosity would in turn be affected. This would lead to a follow on effect on the overall fluid flow field. In particular, localised changes in fluid viscosity due to instantaneous local particle concentration variation would also have an impact on the instantaneous local fluid flow field. Hence, the different fluid velocity flow fields observed due to the variation in the manner in which the fluid flow field is seeded with particles is not unexpected.

Following from the above discussion and to appreciate the effect of viscous diffusion on vorticity dynamics, it is useful to examine the vorticity transport equation, obtained by taking the curl of the Navier-Stokes equation (Equation 5.1). The vorticity equation is expressed in vector notation as:

$$\frac{D\boldsymbol{\omega}}{Dt} = (\boldsymbol{\omega} \cdot \boldsymbol{\nabla})\boldsymbol{v} + \nu\nabla^2\boldsymbol{\omega} \tag{5.3}$$

where ν is the kinematic viscosity and vorticity, $\boldsymbol{\omega}$, of a flow field with velocity vector, $\boldsymbol{v}$, is defined by:

$$\boldsymbol{\omega} = \boldsymbol{\nabla} \times \boldsymbol{v}(u, v, w) \tag{5.4}$$

Equation 5.3 describes the transport and generation of vorticity of an incompressible flow. The term $(\boldsymbol{\omega} \cdot \boldsymbol{\nabla})\boldsymbol{v}$ is the vortex stretching term and represents the enhancement of vorticity by stretching. This is the mechanism by which turbulent (kinetic) energy associated with large scale structures is transferred (dissipated) to smaller scale structures.

The last term in Equation 5.3 describes the effects of viscous diffusion on the vorticity distribution. This indicates that as a result of viscosity, the vorticity of a flow tends to diffuse in space. From this equation, the vorticity of fluid flowing along a streamline will only change for one of two reasons, either by vortex stretching or due to the diffusion of vorticity. Noting that the contributions of viscosity can be important in low Reynolds number flow, it is anticipated that the different manner in which particles are introduced into the fluid flow field in the current body of work would have an evident effect on vortex dynamics due to the differences in overall fluid viscosity throughout the flow field. As before, differences in the localised fluid viscosity due to variation in the instantaneous local particle concentration is anticipated to affect the development and dissipation of the vortex rings examined.

Data from Table 5.1 and Table 5.2 show that the different particle loading cases affect the evolution and propagation of vortex rings. In order to establish the effects of particle loading on the preferential concentration mechanism, consideration must be given to the correlation between particle loading and fluid entrainment into the vortex ring. The entrainment of ambient fluid into the vortex ring leads to the growth of both the volume and mass of the vortex ring over time. Maxworthy (1972) identified that the propagation velocity of the ring must decrease with time to ensure that momentum is conserved as the vortex diameter grows. This postulation is in line with observations where the average propagation velocity of a vortex decays exponentially with distance instead of translating at a constant velocity once it is fully formed (Glezer & Coles, 1990; Lim & Nickels, 1995; Maxworthy, 1972).

$$U_T = \frac{\Gamma}{4\pi r}\left\{\log\left(\frac{8r}{2\sqrt{\nu t}}\right) - \frac{1}{2}(1-\gamma+log2) + O\left[\left(\frac{\nu t}{r^2}\right)^{1/2}\log\left(\frac{\nu t}{r^2}\right)\right]\right\} \quad (5.5)$$

where Γ represents the total circulation around the vortex core, r is the radius of the vortex, ν is the kinematic viscosity, t is the time measured from the instant at which the core is infinitely thin, and γ is Euler's constant. Equation 5.5 has been demonstrated to correspond to the Kelvin formula for the velocity of a circular vortex ring of a small cross section in a perfect fluid (Saffman, 1970 and 1971):

$$U_T = \frac{\Gamma}{4\pi r}\left\{\log\left(\frac{8r}{\delta}\right) - \frac{1}{4} + O\left(\frac{\delta}{r}\right)\right\} \quad (5.6)$$

where Γ represents the total circulation around the vortex core, r is the radius of the vortex, δ is the radius of the cross section of the vortex core. Consideration of Equation 5.5 suggests that an increase in viscosity, will increase the vortex core size by $(\nu t)^{1/2}$, which would reduce the vortex translational velocity by $-\ln(t)$. It follows that viscous diffusion would cause the vortex cores to grow and eventually come into contact at the axis of symmetry, annihilating the vorticity, thus further reducing the vortex translational velocity. Equation 5.6 indicates that this notion is probable, since an increase in vortex core diameter would lead to a reduction in vortex translational velocity.

In terms of the reduction in vortex translational velocity, Maxworthy (1972) also suggested that the decrease in ring translational speed may be due to vorticity from the ring being continuously deposited in the wake. Therefore, although the total impulse in the flow filed remains constant, the decrease of the ring impulse is accompanied by a corresponding increase of the impulse in the wake region i.e. circulation of the ring continuously decreases. The ejection of vorticity into the wake would reduce the vortex circulation and thus the vortex translational velocity. Such shedding of vorticity into the wake was also observed by Dabiri and Gharib (2004), Gharib *et al.* (1998) and Weigand and Gharib (1997), with Stanaway *et al.* (1988) (as cited by Lim & Nickels, 1995) establishing that the accumulated vorticity in the wake regions is quickly destroyed by viscous dissipation. James and Madnia (1996) confirmed the validity of Maxworthy's hypothesis using direct numerical simulation of a viscous, laminar ring.

Given that particle number density affects fluid viscosity (Section 2.2.5), it follows that the manner in which the working fluid is seeded would affect the structure and behaviour of the vortex ring, which in turn affects particle behaviour. These affects may be more evident when the working fluid is unevenly seeded such that there are different bodies of fluid with significantly different particle number densities. The interfaces where these bodies of fluid come in contact, e.g. the shear layer of a seeded vortex with ambient fluid that is not seeded, would result in a variation in local particle number density and hence local fluid viscosity within the vicinity of those interfaces. Analysis of the vorticity fields corresponding to the flow fields featured

in Figure 5.6, Figure 5.7 and Figure 5.8 is required to explore these ideas further.

Based on the definition of vorticity in Equation 5.4, vorticity fields estimated from two dimensional PIV data are therefore formed using the out-of-plane vorticity component, $\boldsymbol{\omega}_z$, expressed as:

$$\boldsymbol{\omega}_z = \frac{\partial v}{\partial x} - \frac{\partial u}{\partial y} \tag{5.7}$$

Since PIV data are sampled on a two-dimensional, evenly spaced grid, finite differencing is employed in the estimation of the differential terms required (Equation 5.7) for the vorticity fields (Raffel *et al.*, 2007). In examining the different standard differentiation schemes applicable to PIV, Raffel *et al.* (2007) identified the least-squares scheme as the most suitable method for estimating the first derivatives of PIV data. The least-squares scheme is described by the second order finite different scheme given by:

$$\left(\frac{\mathrm{d}f}{\mathrm{d}x}\right)_i \approx \frac{2f_{i+2} + f_{i+1} - f_{i-1} - 2f_{i-2}}{10\Delta x} \tag{5.8}$$

where $\mathrm{d}f/\mathrm{d}x$ is the first derivative of a function $f(x)$ sampled at discrete locations $f_i = f(x_i)$. It is noted that the least-squares approach has a tendency to smooth the estimate of the differential because the outer data $f_{i\pm2}$ are more weighted than the inner data $f_{i\pm1}$ (Raffel *et al.*, 2007). Consequently, this estimation scheme is designed to reduce the effect of the random errors, that is, the measurement uncertainties due to noise associated with the velocity data acquired through PIV (Raffel *et al.*, 2007).

Applying the least-squares scheme to the derivatives in the vorticity (Equation 5.7) yields the least-squares vorticity estimate (Hassan *et al.*, 2007a and 2007b):

$$(\omega_z)_{i,j} \simeq \frac{p(v) - q(u)}{10\Delta} \tag{5.9}$$

where $\Delta = \Delta x = \Delta y$ since grid spacings are equal in the two-dimensional velocity data.

Functions $p(v)$ and $q(u)$ in Equation 5.9 are expressed as the following:

$$p(v) = 2v_{i+2,j} + v_{i+1,j} - v_{i-1,j} - 2v_{i-2,j} \tag{5.10}$$

$$q(u) = 2u_{i,j+2} + u_{i,j+1} - u_{i,j-1} - 2u_{i,j-2} \tag{5.11}$$

Equation 5.9 is applied to the PIV data, using the algorithm developed by Hassan *et al.*, (2007a and 2007b), in the present research to estimate the vorticity fields. The velocity measurements from the PIV data in Figure 5.6, Figure 5.7 and Figure 5.8 are used to estimate the associated vorticity fields, shown in Figure 5.11 and Figure 5.12.

The magnitude of the largest detectable constant-vorticity contour was observed to vary between 50 and 80s^{-1}. In order to improve the clarity of presentation, constant-vorticity contours below 5s^{-1}, which constitute approximately 10% of the data field, were suppressed for all the vorticity fields. Figure 5.13 provides a comparison of a vorticity plot with data suppression and a corresponding plot without data suppression. It was noted that the suppression of the low constant-vorticity levels did not significantly impact the quality of information provided by the resulting vorticity plots.

The vorticity associated with the generation and propagation of the vortex ring is as expected - with the convection of vorticity being preserved along the vortex propagation path, and simultaneous diffusion of vorticity occurring over time, outwards from the vortex propagation path. The vorticity plots in Figure 5.11 and Figure 5.12 are in agreement with the results presented by Gharib *et al.* (1998) for cases when $L/D < 4$. Vorticity in the trailing region is observed to dissipate quickly after the formation of the vortex ring.

An inconsistency is noted in the vorticity plots of Case B (Figure 5.11h) having an envelope of vorticity, which is of the opposite sense to the primary vortex, surrounding the primary vortex. The envelope of

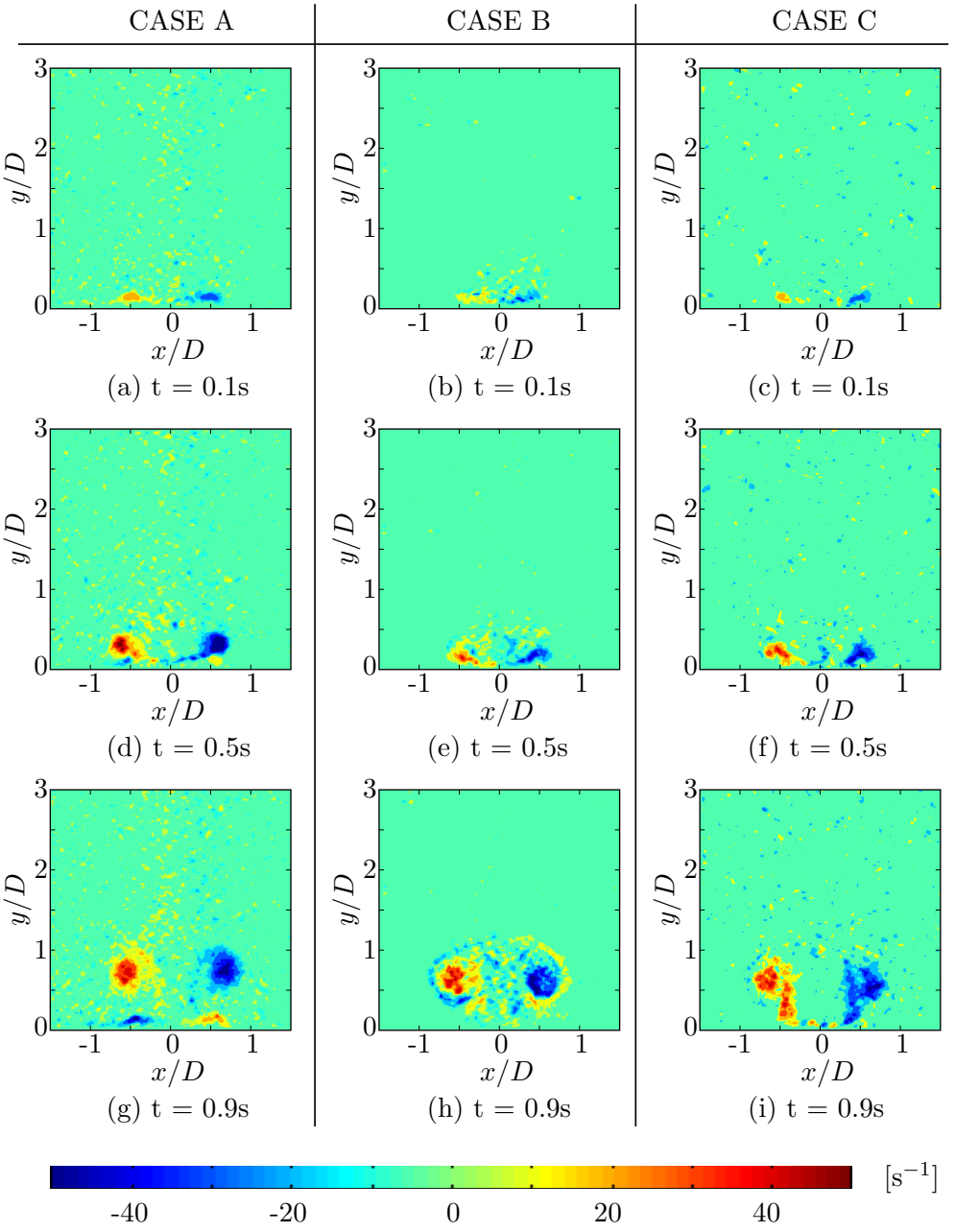


Figure 5.11: Ensemble-averaged vorticity plots of a vortex generated using a pulse duration of 0.4s, propagating into a working fluid for different particle loading cases: (i) Case A - particles in ambient fluid, (ii) Case B - particles in a vortex ring, and (iii) Case C - particles in a vortex ring and ambient fluid - part A.

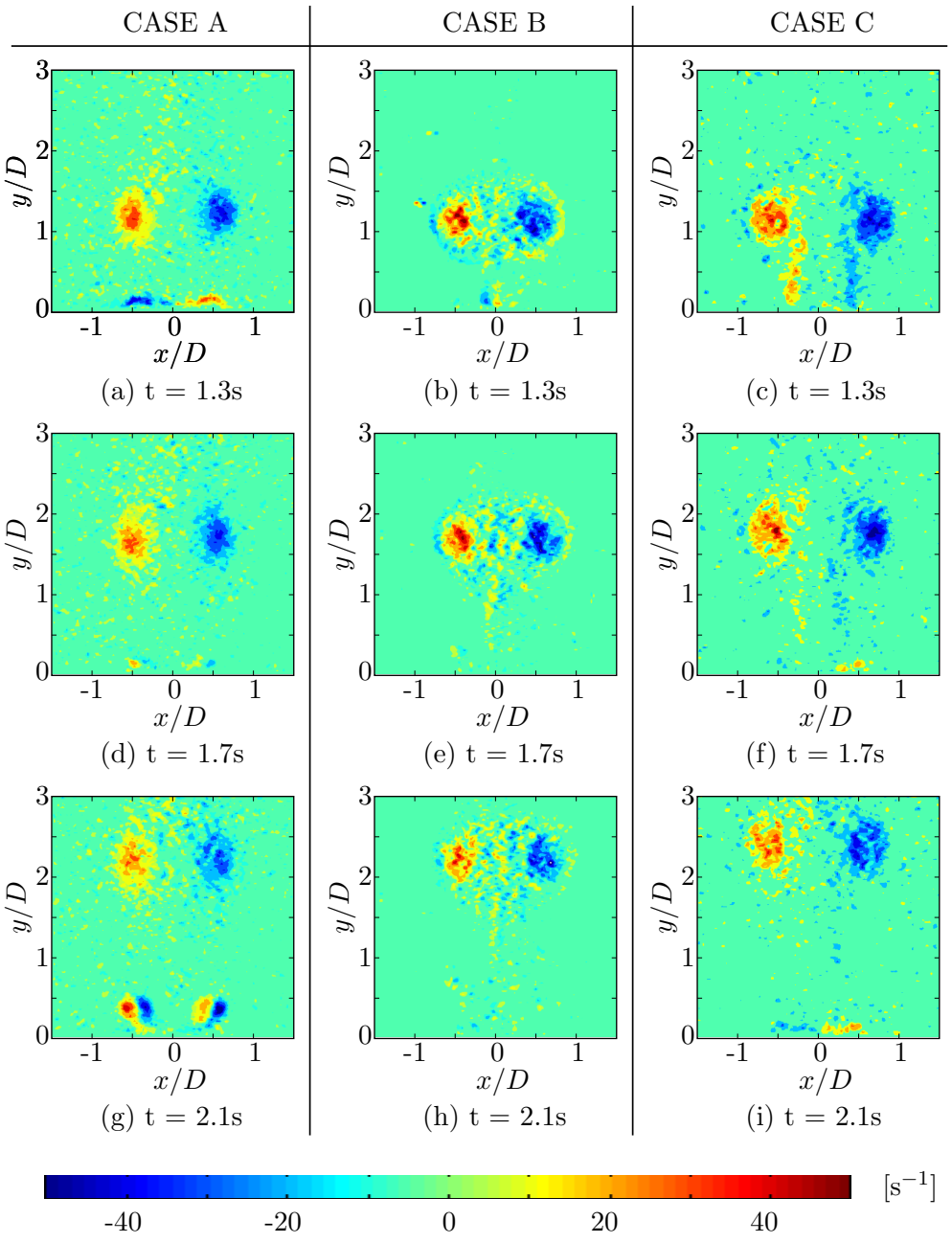


Figure 5.12: Ensemble-averaged vorticity plots of a vortex generated using a pulse duration of 0.4s, propagating into a working fluid for different particle loading cases: (i) Case A - particles in ambient fluid, (ii) Case B - particles in a vortex ring, and (iii) Case C - particles in a vortex ring and ambient fluid - part B.

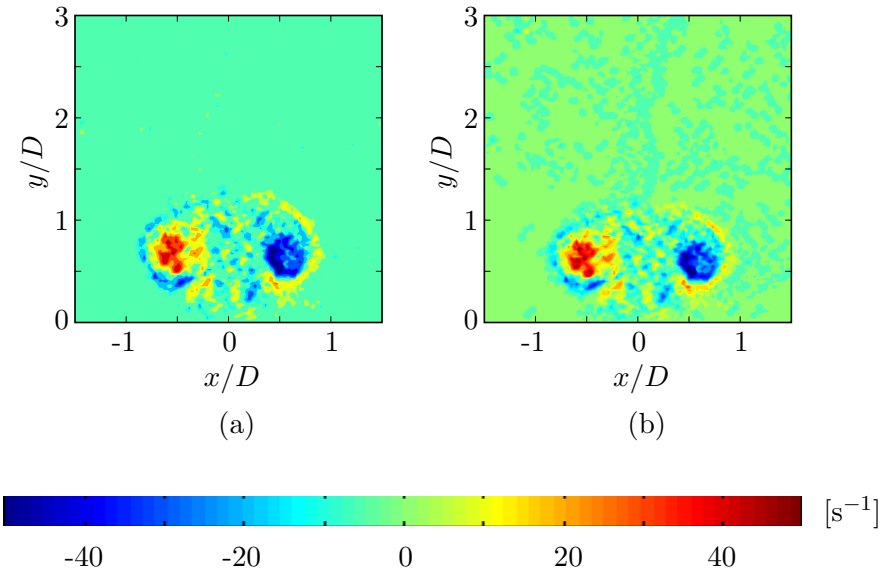


Figure 5.13: Vorticity plots of a vortex generated using a pulse duration of 0.4s, at $t = 0.9s$ for Case B: a) with low constant-vorticity levels suppression b) without suppression.

vorticity remains evident throughout the development and propagation of the vortex in Case B, and it is noted that this envelope of vorticity is only present in Case B but absent in Cases A and C.

Figure 5.14 provides a comparison of the vorticity plots generated from the ensemble-averaged velocity field against an instantaneous velocity field, with the presence of the vorticity envelope evident in both instances. This envelope of vorticity surrounding the primary vortex was present in all the vorticity plots associated with the instantaneous velocity measurements from the PIV data. Therefore, the occurrence of the envelope of vorticity surrounding the primary vortex is not the consequence of random outliers affecting the ensemble-averaged data. Comparing the vorticity plots in Figure 5.14, it is noted that the general distribution of vorticity is comparable between ensemble-averaged and instantaneous data. However, there is a disparity in the magnitude of the vorticity contours, particularly in the vortex envelope, with the instantaneous plot (Figure 5.14b) exhibiting larger magnitudes compared with the ensemble-averaged plot (Figure 5.14a). This disparity is due to the fact that the vortex envelope is not at the exact same location in every instantaneous

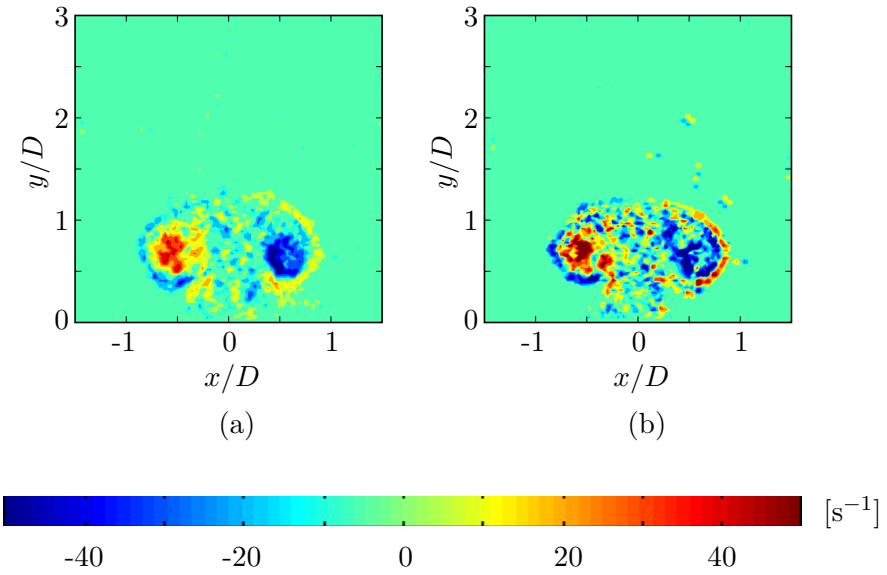


Figure 5.14: Vorticity plots of a vortex generated using a pulse duration of 0.4s, at $t = 0.9s$ for Case B: a) ensemble-averaged b) instantaneous.

vorticity field. Consequently, the ensemble-averaging process is observed to reduce the associated magnitude of the vortex envelope in the ensemble-averaged vorticity field. The impact of the ensemble-averaging process on the vortex circulation is therefore evaluated to ensure the validity of the results generated in subsequent data analysis procedures.

In regards to the occurrence of the vortex envelope in Figure 5.11 and Figure 5.12, the difference between Case B compared with Cases A and C is that particles are not present in the ambient fluid but only in the vortex. With the entrained fluid fraction of a vortex ring averaging at approximately 40% at any given time (Dabiri & Gharib, 2004; Auerbach, 1991), the local particle concentration within the vortex ring is considered to increase for Case A, decrease for Case B due to ambient fluid entrainment, and to remain unchanged for Case C.

It is possible that this diffusion of particles, spreading outwards from the vortex, would have the capacity to affect the local effective viscosity in the boundary regions between the vortex and the ambient fluid (Section 2.2.5). Such changes in the local effective viscosity at the

boundary of the vortex may in turn affect the normal diffusive process of vorticity, thus contributing to the observed envelope of vorticity around the primary vortex. The plausibility of this idea requires further analysis to substantiate this possibility.

Alternatively, the vortex envelope could be an artefact of the seeding and PIV method used to obtain the vorticity plots. Case B only had the vortex ring seeded with particles, therefore, clean ambient fluid being convected into the vortex ring as it develops and propagates may cause an apparent velocity jump in PIV measurements within the boundary regions between the vortex and the ambient fluid. The apparent velocity jump from the PIV data in turn translates into an apparent envelope of vorticity, which is of the opposite sense to the primary vortex surrounding the primary vortex observed within the vorticity plots. Since this artefact is associated with the seeding of the fluid, and the manner in which the vortex rings being seeded is the focus of the present research, there is no means of confirming or disproving that this artefact is the cause of the vortex envelope observed within the vorticity plots.

Further examination of the ensemble-averaged vorticity plots (Figure 5.11 and Figure 5.12) highlights the occurrence of secondary vortices in the trailing regions of the primary vortices. Secondary vortices are observed near the piston nozzle in Case A (Figure 5.12g and also in Figure 5.8d for the velocity measurements) and possibly a highly dissipated pair in Case B (Figure 5.12). Secondary vortices which have similar circulation to the primary vortex ring have been observed by Akhmetov (2001) and Allen and Auvity (2002), with Akhmetov (2001) noting that the trailing jet behind the primary vortex ring rolls itself up into a secondary vortex ring, then moves behind the primary vortex ring and dissipates rapidly. Allen and Auvity (2002) postulated that these secondary vortices are the piston vortex, formed due to the removal of the boundary layer from the cylinder wall in front of the advancing piston head. However, the use of the Bellofram setup as well as the use of 0.5m of high pressure, reinforced hose and PVC pipe separating the Bellofram and the nozzle outlet makes it highly unlikely that the observed secondary vortices (Figure 5.8d) are piston vortices.

There have been a number of instances where secondary vortices are generated with the opposite circulation from the primary vortex ring, with its axis corresponding to the nozzle-exit plane (Didden, 1979; Weigand and Gharib, 1997). These secondary vortices, also known as stopping vortices, are found to be formed when the piston is brought to an abrupt halt, causing the separation of the primary vortex which subsequently forms a boundary layer at the corner of the geometry creating the primary vortex (Allen & Auvity, 2002). This boundary layer separates from the outlet and rolls up in the form of a vortex sheet and subsequently into a vortex ring, termed stopping vortex (Didden, 1979; Lim & Nickels, 1995 ; Lugt, 1983). Lugt (1983) only acknowledges the piston vortex as being a secondary vortex structure but presented an image of a primary vortex ring, followed by what seems to be a superposition of both the piston vortex (Allen & Auvity, 2002; Akhmetov, 2001) and the stopping vortex (Didden, 1979; Weigand & Gharib, 1997). It is worth mentioning that studies examining the factors dictating the occurrence (or suppression) of either the piston vortex or the stopping vortex, as opposed to both these structures occurring simultaneously, are limited, and the effects both of these secondary structures have on the characteristics and the trajectory of the primary vortex is still an unanswered question. Notwithstanding such paucity of information in the literature, this line of investigation is beyond the scope of the present research.

The strength of a vortex ring is determined through its circulation, Γ, and this parameter can be defined as:

$$\Gamma = \oint_{C_o} \boldsymbol{v} \cdot \mathrm{d}\boldsymbol{l} \tag{5.12}$$

where $\boldsymbol{v}$ is the local velocity vector and $\mathrm{d}\boldsymbol{l}$ is an incremental displacement around a closed path C_o.

In two dimensions, Equation 5.12 can be expressed in the form of:

$$\Gamma_{vel} = \oint_{C_o} (u\mathrm{d}x + v\mathrm{d}y) \tag{5.13}$$

with Equation 5.13 referred to as the velocity integral in the following discussion.

The Γ parameter can also be expressed in terms of the curl of the velocity vector:

$$\Gamma = \int\int_{S_o} (\boldsymbol{\nabla} \times \boldsymbol{\upsilon}) \cdot \mathbf{n} \mathrm{d}S_o \tag{5.14}$$

where S_o is a surface enclosed by C_o and $\mathbf{n}$ is a unit vector orthogonal to S_o. In two dimensions, Equation 5.14 can be expressed in the form of:

$$\Gamma_{vor} = \int\int_{S_o} \omega_z \mathrm{d}S_o \tag{5.15}$$

Equation 5.15 is referred to as the vorticity integral in the following discussion.

The circulation, estimated using two dimensional data from PIV measurements, can be evaluated using either the velocity integral, Γ_{vel}, or the vorticity integral, Γ_{vor}. For a given path of integration, the evaluation of Γ_{vel} (Equation 5.13) can be completed using integration schemes such as the trapezoidal approximation or Simpson's rule (Raffel *et al.*, 2007). An integration path centered at the position of maximum vorticity was determined to be sufficient for clearly defined vortical structures, provided that no other vortices are included in the integration contours (Raffel *et al.*, 2007). In the evaluation of Γ_{vor} (Equation 5.15), the path of integration is chosen along the lowest detectable constant-vorticity contour of either the positive or negative sense in order to get a value close to the actual circulation of the vortex. The study by Gharib *et al.* (1998) established that in the absence of a trailing jet, the choice of vorticity contour level did not significantly affect the total circulation level as long as the contour level chosen contained the desired vorticity region.

These two estimates of the circulation, that is, through the evaluation of Γ_{vel} and Γ_{vor}, will differ from each other and from the true value of the circulation since data are only available at certain points in the flow (i.e. discretised two-dimensional data field). Circulation obtained through Γ_{vel} and Γ_{vor} are equal only when the velocity and vorticity are analytically defined. The evaluation of either Γ_{vel} or Γ_{vor} requires an appropriate path of integration in order to determine the circulation of individual vortex ring cores in the present research. The algorithm developed by Hassan *et al.* (2007a) and Hassan *et al.* (2007b) selects a constant-vorticity contour encapsulating the required vortex ring core, and this region is defined as the Region of Integration (ROI). The area of this region is used as the area S in the evaluation of Γ_{vor} (Equation 5.15) while the perimeter of this region is used as the closed curve C in the evaluation of Γ_{vel} (Equation 5.13).

The circulation estimator Γ_{vor} is directly dependent on the vorticity estimation scheme used since the vorticity is integrated within the ROI to calculate circulation for this approach. In contrast, the evaluation of Γ_{vel} is indirectly dependent on the vorticity estimation scheme as vorticity is only used to determine the path of integration for the circulation calculations in this approach. Since the least-squares vorticity estimation scheme is used in the present work, errors associated with both Γ_{vor} and Γ_{vel} will be dependent on this scheme. In examining the total errors associated with these two approaches of determining circulation, Hassan *et al.* (2007a) established that Γ_{vel} is superior to Γ_{vor} in estimating circulation when the least-squares vorticity estimation scheme is used. Consequently, the circulation estimator Γ_{vel} is implemented in the present research using the computational algorithms developed by Hassan *et al.* (2007a) and Hassan *et al.* (2007b).

In the current study, the peak vorticity values are between 50s^{-1} and 80s^{-1}, so the threshold level of 5s^{-1} represents a small fraction of the maximum. The threshold value was chosen as it was sufficient to exclude background noise in the vorticity field (Figure 5.15). Contour level of 5s^{-1} therefore was used as the path of integration in the circulation calculations for the different particle loading cases.

Figure 5.15a shows a vorticity plot, from which a constant-vorticity contour level is selected to determine the circulation of the vortex core

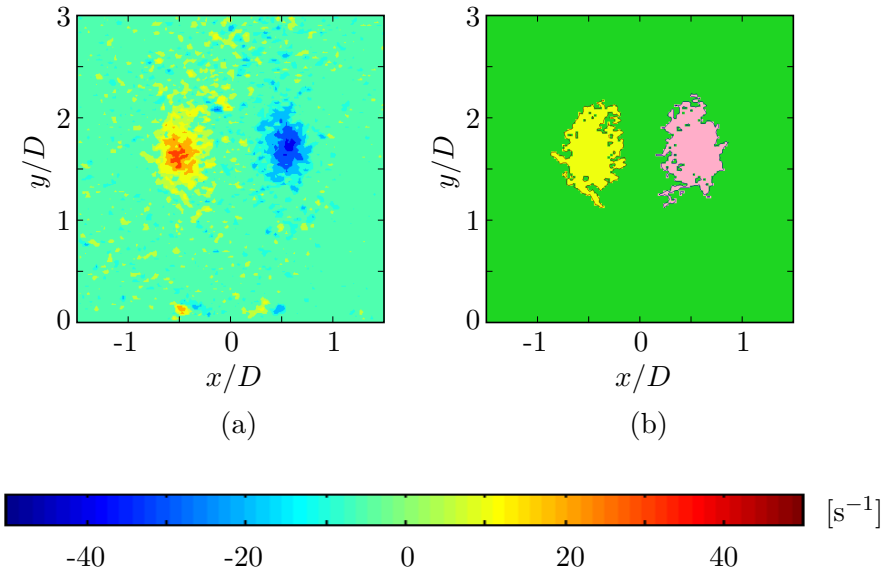


Figure 5.15: Vortex generated using a pulse duration of 0.4s, at $t = 1.7s$ for Case A: a) vorticity plot c) region of integration used to determine the path of integration for the circulation calculations.

for either the positive or the negative sense. In Figure 5.15b, the yellow area indicates the core with a positive circulation, while the pink area indicates the core with a negative circulation. An outline surrounding these areas shows the constant-vorticity contour used as the path of integration to calculate Γ_{vel}.

Figure 5.16 shows the circulation of the vortex rings for Cases A, B and C over time. Positive and negative circulation values for each particle loading case correspond to the measured values from the positive and negative vortex cores respectively. The circulation magnitudes for the positive and negative cores are comparable for each of the particle loading cases, an outcome to be expected from axisymmetric fluid structures. The total discharged circulation, that is the maximum circulation values achieved (Figure 5.16), were comparable across all three particle loading cases. This outcome indicates that the vortex generation process and the structures produced in all three particle loading cases were highly comparable, thereby further supporting the validity of the experimental results presented.

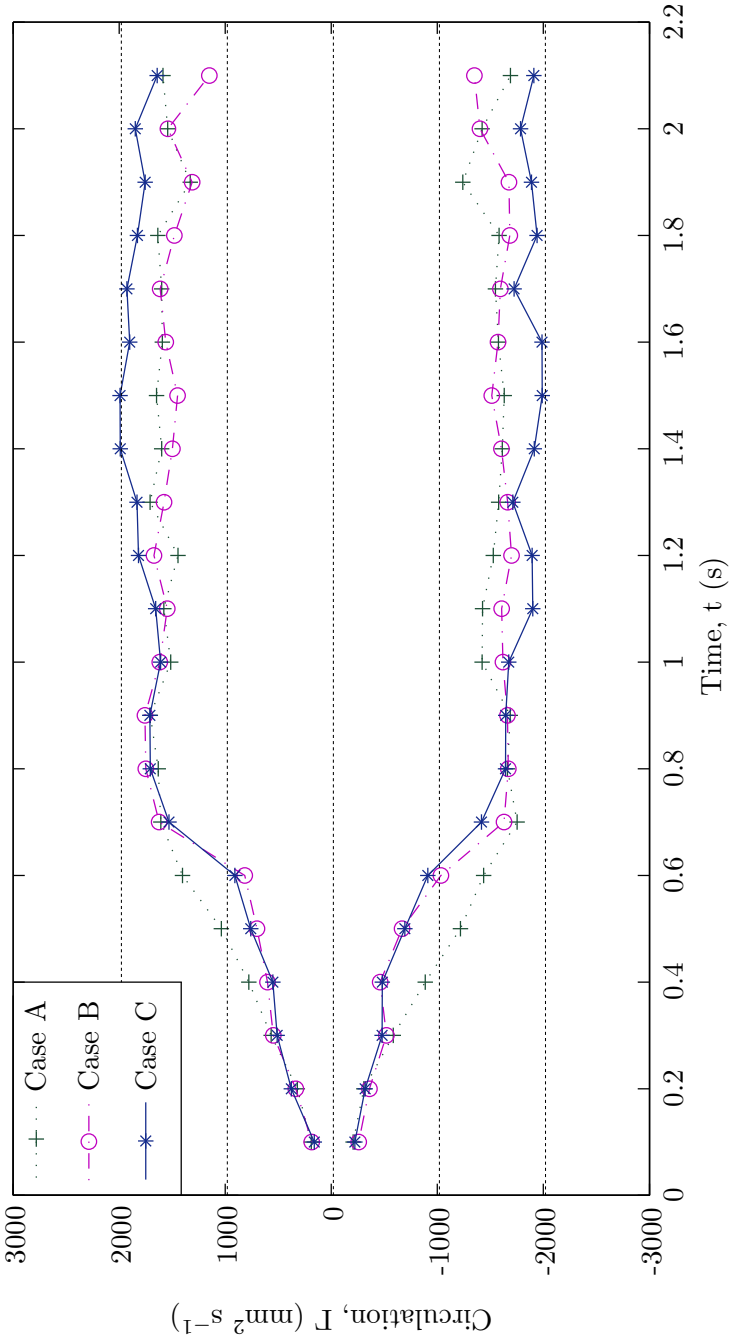


Figure 5.16: Ensemble-averaged vortex ring circulation of vortices generated using a pulse duration of 0.4s, propagating into a working fluid for different particle loading cases: (i) Case A - particles in ambient fluid, (ii) Case B - particles in vortex ring, and (iii) Case C - particles in vortex ring and ambient fluid.

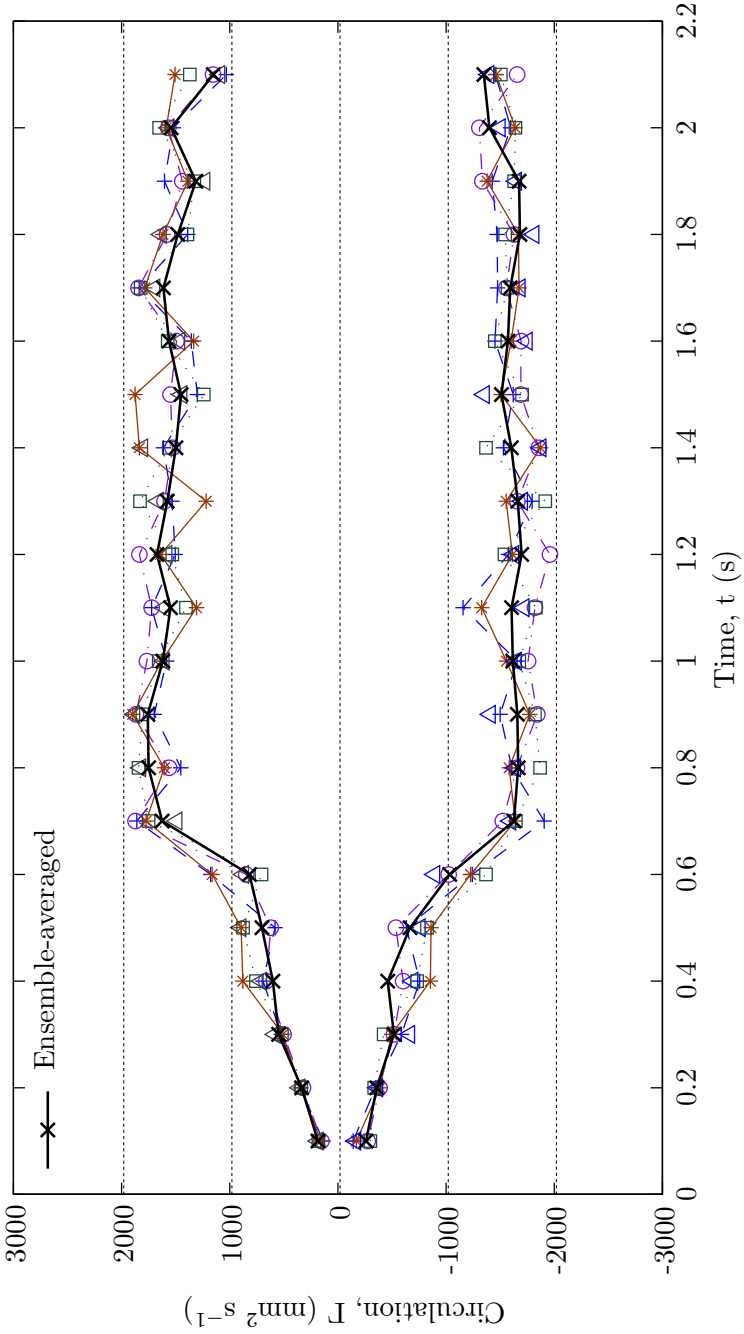


Figure 5.17: Ensemble-averaged and instantaneous vortex ring circulation of vortices generated using a pulse duration of 0.4s, for Case B - particles seeded in the vortex ring. Coloured lines indicate instantaneous vortex ring circulation values.

Further examination of Figure 5.16 shows that the circulation plot for Case A differs from Cases B and C when time is between t = 0.3s and t = 0.7s. The circulation for Case A increases with a relatively linear progression to a maximum value at approximately t = 0.8s, indicative that the vortex ring is fully formed and that circulation is no longer being imparted into the vortex ring over time. This outcome is in agreement with the findings of Gharib *et al.* (1998). In contrast, the circulation plots for Cases B and C do not present with the linear progression portion of the curve, and are currently an unexplained outcome. From t = 0.8s onwards, both Cases A and B demonstrate a gradual decay in circulation over time while Case C recorded a further increase in circulation between t = 1.0s to t = 1.4s before presenting with a gradual decrease in circulation over time. The increase in circulation recorded in Case C after the vortex ring is fully formed, remains an unexplained phenomenon yet to be explored.

The gradient of the plots after the vortex ring is fully formed is related to the rate of diffusion of vorticity (Equation 5.3 and 5.5). Given that the vortex rings are generated by the same method, it is expected that that the manner in which vorticity is ejected/shed would be identical, thus resulting in the rate of vorticity diffusion being similar. Therefore, it is as anticipated that the gradual decrease in circulation portion of the plots for all three particle loading cases would have similar gradients. However, it should also be noted that viscosity also governs the rate of diffusion of vorticity. All three particle loading cases were seeded differently, which in turn affected local particle number densities and therefore the distribution and gradients of viscosity within the vortex rings. These differences in viscosity distributions would affect the rate of diffusion of vorticity within the vortex rings, thereby also affecting the rate of decay of circulation of the vortex structures.

Identical vorticity contour levels were used as the path of integration for the circulation calculations. With the contour levels defined in this manner, it may have missed some vorticity from Cases B and C which could explain the discrepancies (the non linear progression of the circulation plots) noted in Figure 5.16. Note that Case A was initially faster (Figure 5.11) compared to Cases B and C, which could also be due to the manner in which the contour levels were defined. The integration contour is out in the ambient fluid and since Cases A and C

have particles seeded in the ambient fluid, the circulation plots for all of these cases should be similar but they are not. Additionally, the lack of particles in the ambient fluid for Case B, which may contribute to the PIV measurements registering a false velocity jump, should have given a false low in the circulation calculations but do not. It is noted that the vorticity contours are derived from velocity data acquired via the PIV measurements, which are essentially dependent on particle seeding within the vortex structures. The manner in which Cases A and B were seeded meant that there were bodies of fluid that were un-seeded with particles. Consequently, as the vortex ring rolls up and becomes fully formed, the growing mixture of seeded and un-seeded bodies of fluid would result effectively in a decrease in seeding particles within the vortex. This decrease in seeding particle number density in turn contributes to the decrease in data captured for the vorticity and thus circulation calculations. Although it is highly plausible for these factors to contribute to differences in circulation plots, it remains inconclusive as to how vorticity and circulation are affected by these factors individually.

Table 5.3 provides an overview of the results that have been presented in this section. Case A presents with the highest initial vortex propagation velocity and the highest initial growth in circulation. However, Case C eventually acquired the highest vortex propagation velocity and the highest final circulation, at which stage Case C also possessed the vortex ring with the widest diameter. These outcomes are consistent with the arguments presented in Equations 5.5 and 5.6, which identified the dependence of vortex physical characteristics such as propagation velocities and vortex diameters on fluid viscosity within the vortex structures.

It is noted that in Figure 5.11 a stopping vortex is forming in Case A but there is little evidence of this in Case C. In Figure 5.12 a stopping vortex is present in Case A but is almost absent in Case C. Based on these outcomes, particle number density which affects the viscosity distribution in the vortex rings, could impact the formation and evolution of the vortex rings. It is plausible to suppose that the changes in local viscosity induced by the different particle loading cases are disrupting or suppressing the roll-up process of the vortex ring. Changes in local particle-induced viscosity would also continuously

affect subsequent entrainment of particles as well as the shedding of vorticity. Consequently, the rates of growth of the vortex rings for the different particle loading cases would be altered, which would in turn may also affect the timing of the roll-up of the primary and secondary vortices. Collectively, these results indicate that the different particle loading cases potentially affect the development and evolution of vortices, as well as their physical characteristics such as the vorticity and circulation of the vortex rings.

The circulation plots featured in Figure 5.16 were obtained from the ensemble-averaged PIV data. Since the results from Case A are in agreement with published data, the ensemble-averaged circulation plots for Cases B and C were compared with circulation plots obtained from instantaneous PIV data in order to further examine the above discrepancy. No significant deviations were obtained in the general trend of the circulation plots compared. Figure 5.17 shows that the circulation plot for Case B obtained from the ensemble-averaged PIV data (Figure 5.16), were similar to those obtained from instantaneous PIV data. These outcomes indicate that the experiments are valid and as previously noted in the discussion relating to the vorticity plots, it is reasonable to link the discrepancies observed to the manner in which the particles were seeded into the fluid system.

5.2.3 Conclusions of the Preferential Concentration Experiments

The results confirm the validity of the experiments in that the vortex generation process and hence the vortex structures and flow conditions were comparable across all three of the particle loading cases examined. Disparities were noted in the vorticity and circulation plots, which led to the postulation that the different particle loading cases impact on local effective viscosity, thus causing these observations. The current work also indicates that other factors, besides particles mass and inertia, are able to influence particle and fluid behaviour. Further experiments are needed to determine whether there is a relationship between local effective viscosity and particle-fluid surface interactions.

Table 5.3: Physical characteristics of the vortex rings generated using a pulse duration of 0.4s for the different particle loading cases.

Case A	Case B	Case C
Highest initial peak velocity before formation	Lowest initial peak velocity before formation	
Lowest peak velocity post formation		Highest peak velocity post formation
		Largest vortex diameter
Highest initial propagation velocity post formation		Lowest initial propagation velocity post formation
	Lowest propagation velocity	Highest propagation velocity
Linear initial growth in Γ	Low initial growth in Γ	Low initial growth in Γ
Γ decays after formation	Γ decays after formation	Γ increases after formation before decaying

5.3 Summary

Preliminary experimentation discussed in this chapter highlighted interactions between particles and vortices that cannot be explained using conventional concepts of preferential concentration based solely on particle mass and inertia. Although irregularities were noted in the vorticity and circulation plots between the different particle loading cases examined, it remains unclear what is causing this observation. It is possible that the different manner of particle seeding changes the local effective viscosity within the vicinity of the vortex structures. This in turn impacts on the normal diffusive process of vorticity, which affects the development and evolution of the vortex rings as well as its physical characteristics. Understanding the implications of the current results requires further investigation to examine whether changes in local effective viscosity are associated with particle-fluid surface interactions, which may in turn affect particle and fluid behaviour. Further work is necessary to determine if such factors are able to induce directed motion in particles and to determine whether these factors are associated with a preferential concentration mechanism.

6 Particle-Fluid Surface Interactions

This chapter details experiments that examine the effect of particle-fluid surface interactions on particle and fluid properties and characteristics. The outcomes of these investigations provide additional information on how particle-fluid surface interactions are affected by local particle number density which in turn influences directed movement in particles.

6.1 Validation Experiments

Studies concerned with preferential concentration have predominantly focused on the contributions of particle inertia driving the preferential concentration mechanism. As a consequence, previous examinations into the significance of particle-fluid surface interactions in the preferential concentration mechanism are scarce. This situation makes benchmarking studies in particle-fluid surface interactions and preferential concentration difficult and unfeasible. Benchmarking is required to help facilitate the direction of the presented research and also to help establish the validity of the results obtained from the experiments.

Instead of engaging benchmarking studies, preliminary work was undertaken to replicate the experimental investigation published by Longmire and Eaton (1992) and Wark *et al.* (2000) in their investigations involving acoustically-pulsed particle-laden jets. The purpose of doing so was to provide a starting point for the presented research and to produce outcomes that were comparable with existing

findings. In addition, this process also provided a means to confirm the earlier results of the present research.

6.1.1 Experiment Specific Details

The experiments undertaken involve the examination of a series of continuous particle-laden vortex rings generated using the Bellofram setup (see Chapter 4) at rates varying from 0.4Hz to 1.4Hz, at an incremental interval of 0.2Hz, and a 1.0s time delay applied between pulses (Figure 6.1). A total of 10 test runs were conducted for each case. Note that these experimental parameters differ from those evaluated in Chapter 5.

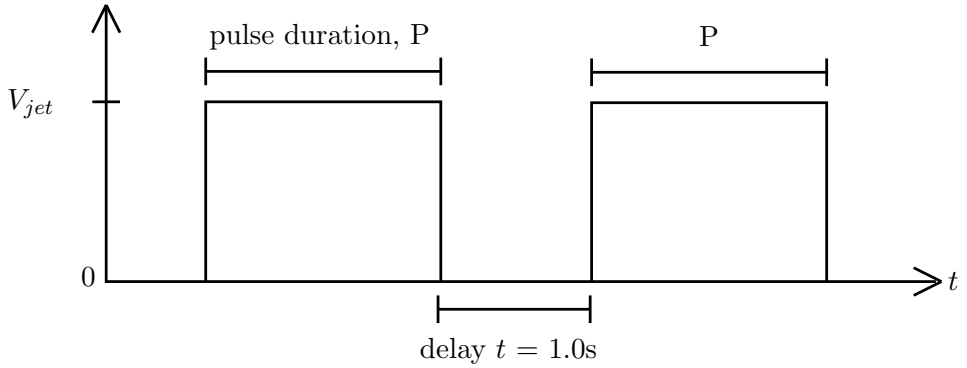
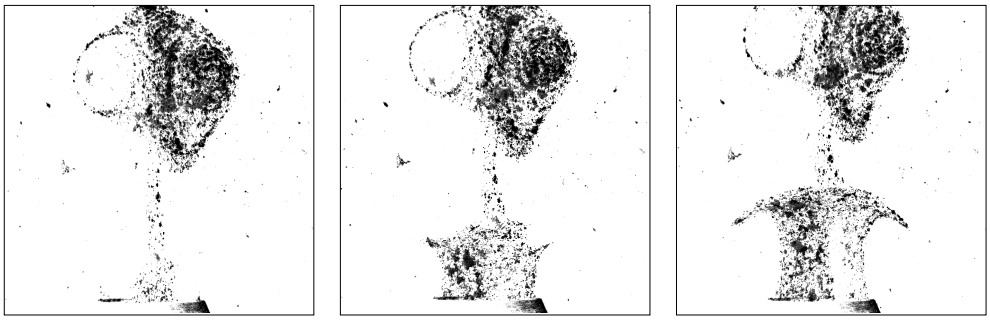
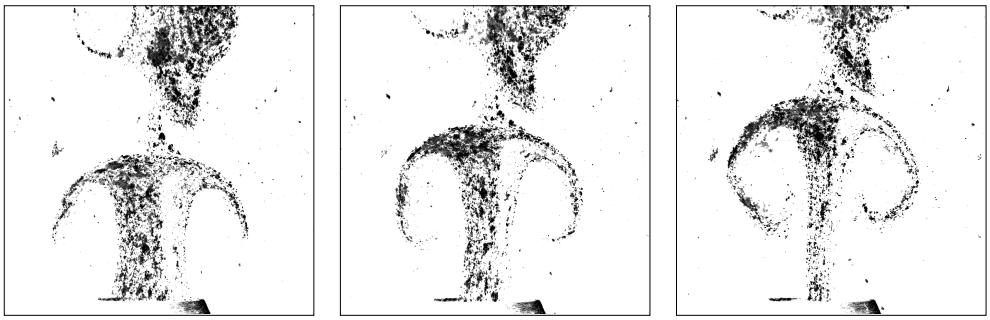


Figure 6.1: Continuous pulses used for current experiments, with pulse duration, P, varying from 0.4s to 1.4s, at intervals of 0.2s and a time delay of 1.0s between pulses.

The corresponding L/D ratios of these pulses lie within the range of 0.48 to 1.68, which is well within the range of formation numbers that generated a single ring, as defined by Gharib *et al.* (1998). Neutrally-buoyant polyamide particles (ρ_p = 1030 kg/m^3 and d_p = 20μm $\pm$ 15μm) were used to seed the vortex structures. Particle concentrations and velocity measurements were acquired using the PN and PIV techniques respectively. Details of the experimental setup are discussed in Chapter 4. Images processed for the PIV technique were also used as a means of flow visualisation, providing useful qualitative data to further support the investigation.



(a) t = 1.3s (b) t = 1.4s (c) t = 1.5s



(e) t = 1.6s (f) t = 1.7s (g) t = 1.8s

Figure 6.2: Flow visualisation of the evolution and interaction of a vortex ring with a previous vortex ring, generated using pulse duration of 0.4s with a time delay of 1.0s between successive vortex structures, with $Re_f = 415$.

6.1.2 Results and Discussion

Examination of the flow visualisation images indicated that general flow structures and particle distributions for all test runs recorded are highly comparable amongst all the excitation frequencies investigated. Discrepancies between case studies include the fact that lower fluid excitation frequencies, producing vortex structures that propagate at lower velocities, have more flow visualisation images since the camera recorded at a fixed rate. The different L/D ratios used while maintaining a 1.0s time delay between vortex pulses resulted in the different spacing between vortex rings of different case studies. Owing to the lower Reynolds number associated with slower propagation velocities, vortex rings generated at low fluid excitation frequencies presented flow structures and particle distributions with higher clarity when compared with vortex rings generated at higher frequencies. Consequently, the present discussion examines vortex structures generated using pulse duration of 0.4s with 1.0s time delay between successive pulses. Under these conditions, the flow Reynolds number for this test is $Re_f = 415$ (based on the translation velocity of the ring and the maximum ring diameter) with an L/D ratio of 0.48.

Figure 6.2 shows vortex rings that are seeded with particles but the ambient fluid was not. It is noted that the distribution of particles within the first vortex ring in Figure 6.2 was uneven, resulting in particles populating the right hand core for the first vortex. However, the development of the second vortex ring shows that particles in the fluid slug exiting the nozzle follow the evolution of the vortex ring and seem to remain within the jet fluid. The vortex ring is clearly identifiable and the non-uniform distribution of particles within their respective vortex rings evident. Comparing the image at $t = 1.5s$ (Figure 6.2c) with an image of an acoustically excited particle-laden jet from a study by Wark *et al.* (2000) in Figure 6.3, the flow structures and particle distributions are identical in both instances. Specific flow features classified by Wark *et al.* (2000) are the jet core (or jet column) and the wing regions, which correspond to the leading edges of the large-scale vortex structures. These features are observable across all the excitation frequencies investigated, with Figure 6.3b being an image

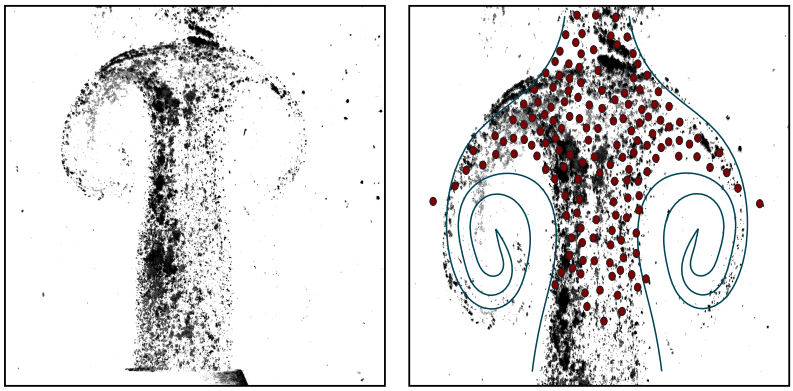
from a 1.0Hz test run provided as a reference. In all these instances, a significant proportion of particles is distributed on the leading edge of the large-scale vortex structure as well as in the jet core region (a term defined and used by Wark *et al.* (2000)). As the vortex rings evolve over time, particles that were initially concentrated on the leading edge of the vortex ring were stretched out further into the wing regions (Figure 6.2d-f). Examining the image at $t = 1.8s$ (Figure 6.2g), the particles wrap around the edges and into the vortex ring, leaving the vortex cores (regions of high vorticity) devoid of particles. Longmire and Eaton (1992) suggest that particles are pulled from the jet core region and pushed out into the downstream regions of the vortex cores where particles concentrate. Comparing the image at $t = 1.8s$ (Figure 6.2g) with an illustration of this concept superimposed onto the acquired particle distributions in Figure 6.4, the experimental results obtained in the current investigation are congruent with the concept proposed by Longmire and Eaton (1992). The particle-fluid behaviour is observed across all the excitation frequencies investigated despite the anomaly of the first vortex ring being unevenly seeded with particles in Figure 6.2 (Figure 6.4a from a test run with vortex rings generated with pulse duration of 1.0s, with 1.0s time delays between pulses, provided as a reference).

Following the evolution and propagation of successive vortex rings in this investigation, when the unevenness of the particle distribution across a particular vortex ring is significant, certain particle-fluid interactions are observed to be highlighted and amplified. It is postulated that when the particle concentration is sufficiently high in a vortex structure, fluid elements within the fluid structure can experience substantial displacements to accommodate the presence of the particles. Consequently, fluid elements between particles experience a certain level of distortion when particles and flow structures interact, resulting in the modulation of the fluid flow field, which complicates and appears to disrupt the usual formation process of a vortex ring as well as the uniformity in particle distribution within a vortex structure. Figure 6.5 features the particle concentration measurements of two successive vortex structures (the corresponding flow visualisation of these structures was shown in Figure 6.2). The concentration measurements have been normalised against the highest recorded value in order to establish the relative particle concentration distribution

LIBRARY NOTE:

This figure has been removed to comply with copyright.

Figure 6.3: (a) Acoustically excited particle-laden jet (Wark *et al.*, 2000), (b) Flow visualisation of a vortex ring at $t = 1.5s$, generated using pulse duration of 1.0s, with 1.0s time delay between pulses, and $Re_f = 1040$.



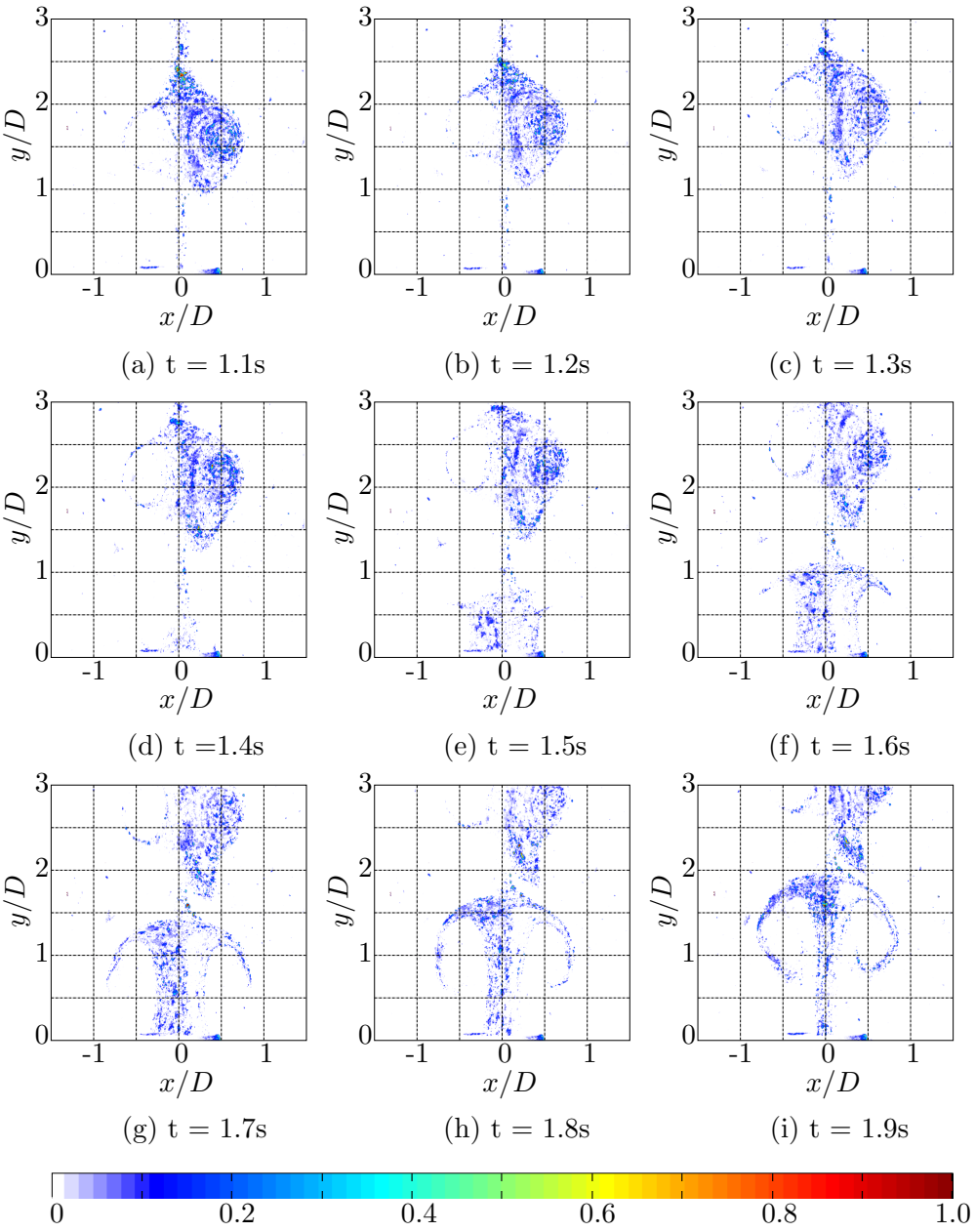
(a) (b)

Figure 6.4: (a) Flow visualisation of a vortex ring at $t = 1.5s$, generated using a pulse duration of 1.0s, with $Re_f = 1040$ (b) Illustrated concept of the particle-fluid interaction proposed by Longmire and Eaton (1992) superimposed on image (a).

within the flow field. For this particular test run, the first vortex ring recorded had a higher concentration of particles entrained into the right side of the vortex ring, when compared with the left. Particles entrained into the right side of the vortex ring were observed to fill the vortex core as well as lag behind the original flow structure, which generates a cluster of particles in the wake of the ring. When the next vortex ring was generated, the subsequent ring collided with the cluster of particles left behind by the previous vortex ring. This collision caused the particles to accumulate in the regions between successive vortex cores, in the shear layer called the braid regions. These braid regions tend to be strained as they are affected by shearing forces acting perpendicular to the jet axis in the evolution and propagation of continuous vortices (Lasheras *et al.*, 1986; Martin & Meiburg, 1991). Although these results show an accumulation of particles in the wake of the ring, it is still insufficient to substantiate the occurrence of the preferential concentration mechanism.

Figure 6.6 shows the instantaneous PIV images of the fluid structures featured in Figure 6.5d-i. These images highlight the movement of the particles within the braid regions as the second vortex ring propagates downstream. Figure 6.7 provides a more detailed view of the particle velocity vectors within the braid regions of Figure 6.6e. The PIV results featured in Figure 6.6 and Figure 6.7 indicate that particles deposited into the wake of the first vortex ring continue propagating with the ring downstream.

The accumulation of particles in the vortex braid regions (Figure 6.5) is in agreement with the conclusions presented by Kobayashi *et al.* (1992), Lazaro and Lasheras (1992), and Longmire and Eaton (1992). The subsequent propagation of the particle clusters with the vortex structures, while remaining within the vortex braid regions provides, experimental evidence that supports the findings presented by Chein and Chung (2004), Chung and Troutt (1988), and Squires and Eaton (1990, 1991) in their simulations. The tendency of particles to accumulate in regions of low vorticity and high strain has conventionally implicated particle centrifugal forces as the driver behind the preferential concentration mechanism. However, despite the good level of agreement between the results of the present work and published data, the current results are still insufficient to confirm or disprove the occurrence of the preferential concentration mechanism.



(a) t = 1.1s (b) t = 1.2s (c) t = 1.3s

(d) t =1.4s (e) t = 1.5s (f) t = 1.6s

(g) t = 1.7s (h) t = 1.8s (i) t = 1.9s

Figure 6.5: Normalised particle concentration measurements in vortex structures, generated using pulse duration of 0.4s, with a time delay of 1.0s between successive pulses, and with $Re_f = 415$.

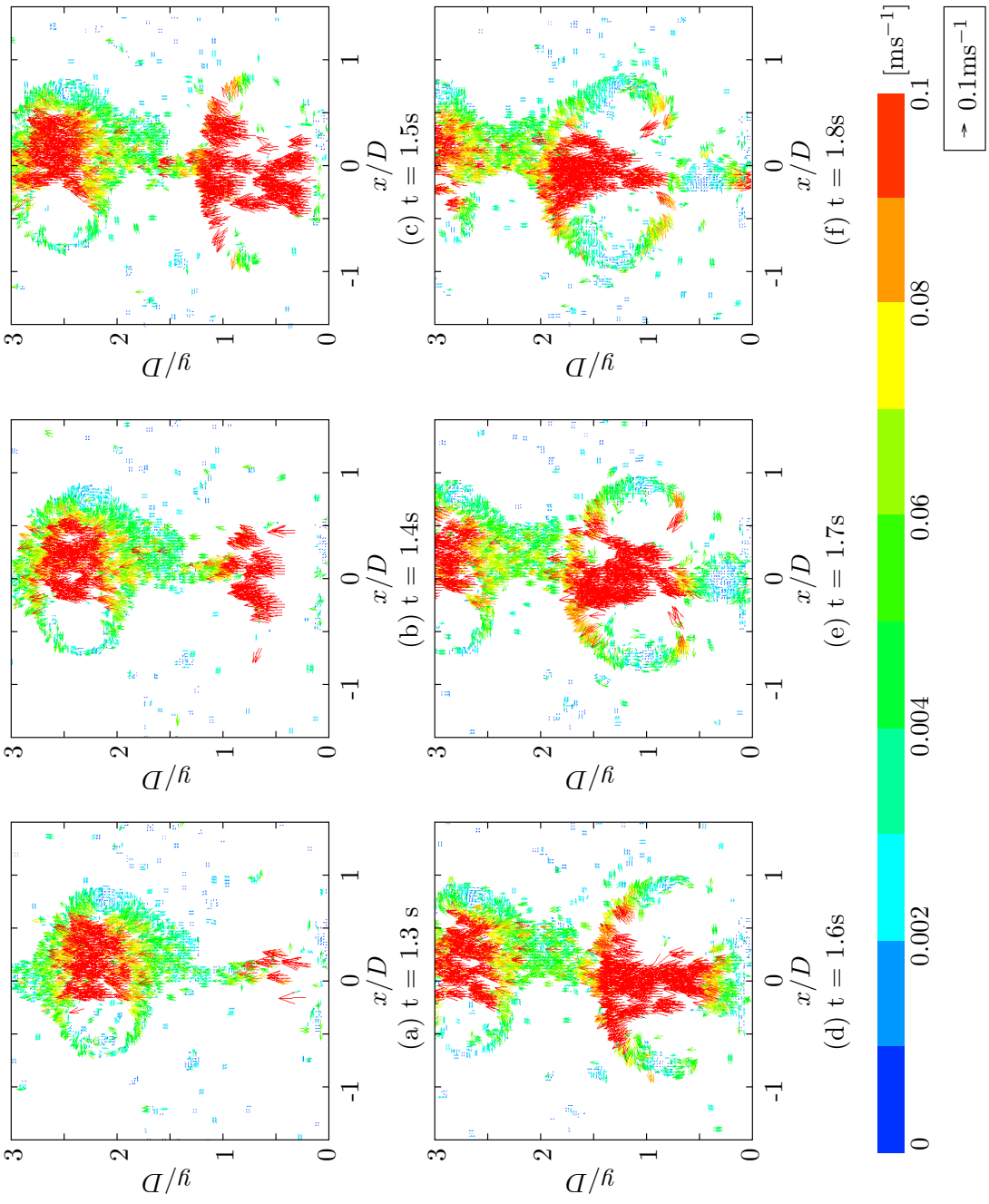
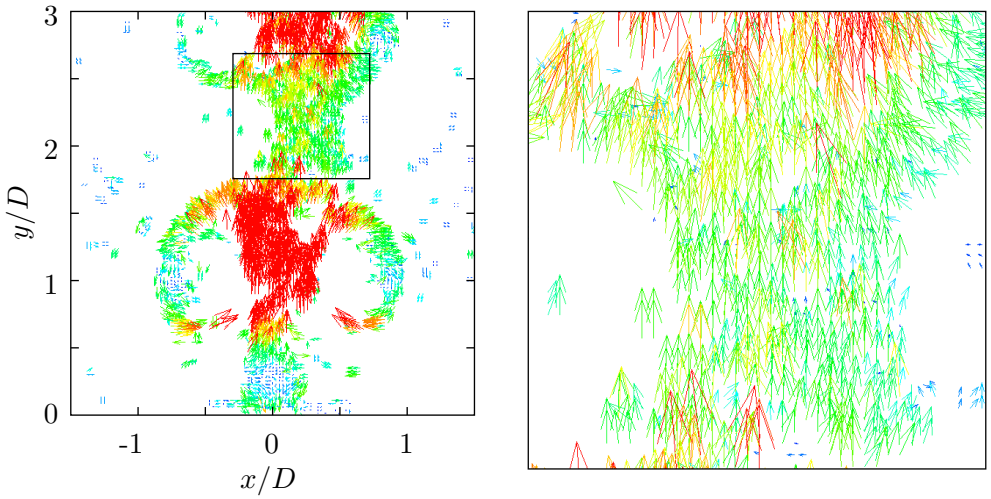


Figure 6.6: Phase-locked PIV images of vortex structures, generated using pulse duration of 0.4s, with a time delay of 1.0s between successive vortex structures, and with $Re_f = 415$.



(a) t = 1.7s (b) t = 1.7s

Figure 6.7: Close-up of the velocity vectors of particles in braid regions of Figure 6.6e.

6.1.3 Conclusion of Validation Experiments

The results of the validation experiments are congruent with published results, thereby substantiating the fidelity of the work done in the present research. However, there is still insufficient evidence to either confirm or disprove the occurrence of the preferential concentration mechanism. Current experiments also highlighted the possibility that in addition to particle centrifugal forces, there may be other factors such as particle-fluid surface interactions driving the movement of particles into braid regions. More focused experiments are undertaken to establish the influence of particle-fluid surface interactions on the possibility of inducing directed particle motion as well as to establish the occurrence of the preferential concentration mechanism.

6.2 Focused Experiments

The accumulation of particles in braid regions between successive vortices (identified in Section 6.1) did not provide conclusive evidence to either confirm or disprove the occurrence of the preferential concentration mechanism. At present, consideration is given to the possibility that the interaction between successive vortices encourages particles to accumulate within these braid regions. Examination of the redistribution of particles from within the vortex structures to the wake regions of the vortex rings is necessary to verify the occurrence of the preferential concentration mechanism. In order to test this idea, the current experiment examines the interaction of a single particle-laden vortex ring with a trail of particles placed in the propagation path of the vortex ring. The underlying idea is that this path of particles would represent particles that are deposited in the wake regions of an earlier vortex structure.

6.2.1 Experiment-Specific Details

These experiments used the Bellofram setup to generate single-pulsed vortex rings that were seeded with polyamide particles (ρ_p = 1030 kg/m^3 and d_p = 20μm $\pm$ 15μm). The vortex rings examined were generated with a pulse duration of 0.4s (Figure 5.1), with an L/D ratio of 0.48 and flow Reynolds number Re_f = 415 (based on the translation velocity of the ring and the maximum ring diameter). These conditions ensured that the vortex structures generated remain within the stable laminar phase ($Re_f < 600$) (Maxworthy, 1972). Note that these experimental parameters differ from those evaluated in the previous Section 6.1. Both PIV and PN techniques were used to measure particle concentration and particle velocity profiles. Details of the experimental layout used were discussed in Chapter 4.

6.2.2 Results and Discussion

Control test runs involved examining single-pulse vortex rings in the absence of a trail of particles ahead of the propagation front (Figure 6.8a-c). The observations in Figure /refunevena-c are a typical set of instantaneous images. It was noted that there was one instance (out of the 10 control test runs done) where the vortex rings in the control tests presented with particle deposits in the vortex wake regions (Figure 6.8d-f). The asymmetrical accumulation of particles in Figure 6.8d-f is also seen to contribute to the vortex ring turning right over time. Given that the particles used in the experiment have a density which is comparable to the density of water, it is therefore unexpected that the inertial properties of these particles would be able to cause the vortex ring to become so asymmetrical. It is possible that this asymmetry in particle accumulation may be due to a prior disturbance in the fluid flow field, where vorticity in the tank was entrained into the vortex ring. Once that occurs, the vortex ring circulation is subsequently re-distributed, causing asymmetry in the entrainment of particles from the jet. It is also possible that the presence of particles within the vortex ring changes the viscosity and therefore disrupts the rate of diffusion of vorticity, which in turn causes the vortex ring to turn. The apparent shedding of particles on the left side of the wake in Figure 6.8f may be the result of there being more

particles in the left side of the vortex, thereby disrupting the vorticity diffusion and leading to the shedding of some vorticity when compared with the right side of the ring. The influence of particles and viscosity in affecting vorticity diffusion is addressed later in this section.

Experiments involving a trail of particles placed ahead of a vortex ring proved challenging since particles had to be introduced into the fluid system with minimal flow perturbations (the particles had to have negligible initial velocities when placed in the fluid system). Particles could not be injected into these trails mechanically; instead they had to be deposited manually with great care to ensure that fluid disturbances due to the introduction of the trail of particles were minimised. PIV was performed on a trail of particles introduced into the fluid system, at t = 0.1s, just as the vortex generator was initiated. Figure 6.9a shows the velocity vectors of the trail of particles. The data indicate that the particles are moving randomly, however, the motions of the particles is so minute that it can barely be discerned using PIV. Figure 6.9b shows the velocity contours of the flow field. Data from the PIV analysis established that the maximum velocity is 1.24×10^{-2} ms^{-1}, and the majority of the particles with a velocity of this order of magnitude are within the vicinity of the nozzle. This outcome is expected, given that PIV is done just as the vortex generator was initiated and there would be flow disturbances within the outlet of the nozzle at that instant. Overall, the velocity field of the trail of particles does have a random distribution of velocities and with a mean velocity of 6.58×10^{-4} ms^{-1} amongst the particles, it is reasonable to consider that the particle sink velocity is approximately zero. In addition, due to the way in which particles were deposited manually, difficulty was faced in ensuring that the trail of particles produced was consistent in terms of geometry, location, as well as the concentration of particles within the trail across all the test runs. Therefore, all experimental data pertaining to these tests were analysed using instantaneous PN measurements, and all corresponding particle concentration measurements were used not for their absolute values, but were instead normalised against the highest recorded value in order to obtain a distribution profile of the relative particle concentration within the flow field.

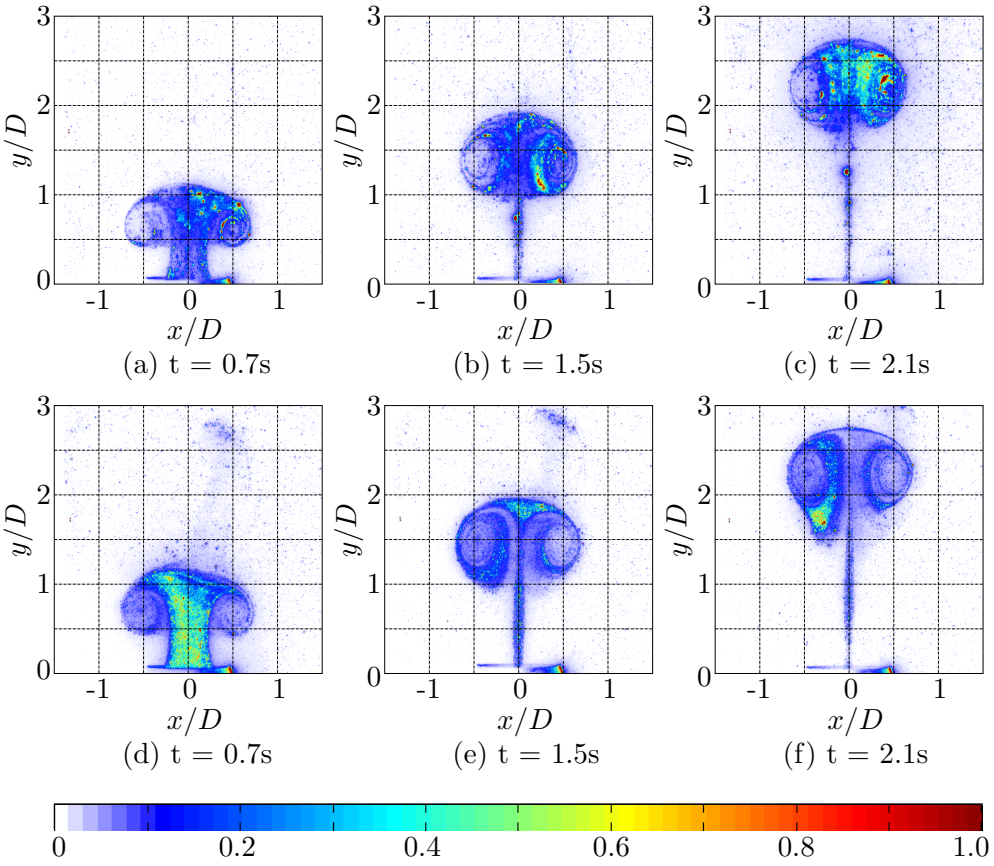


Figure 6.8: Instantaneous particle concentration measurements normalised to maximum recorded concentration values of single pulsed particle-laden vortex rings, generated using a pulse duration of 0.4s for flow case $Re_f = 415$: (a)-(c) Typical set of images, (d)-(f) Vortex ring displaying unusual behaviour.

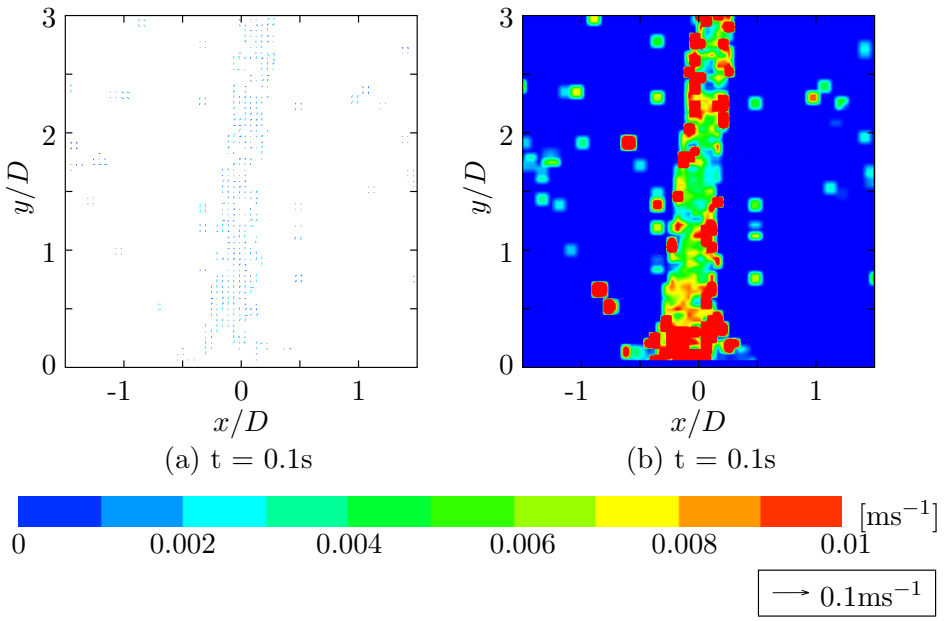


Figure 6.9: PIV image of the trail of particles featured in Figure 6.8a-c: a) velocity vectors b) velocity contours.

Figure 6.10a-c shows a vortex ring propagating through a trail of particles, at t = 0.7s to t = 2.1s of the experiment featured in Figure 6.9. As the vortex ring propagates through the trail of particles, the occurrence of particle deposits in the vortex wakes becomes a certainty with the wake deposits becoming more evident the further the vortex ring propagates (Figure 6.10a-c). The increase in the concentration of particles in wake deposits over time supports the idea that particles are directed to accumulate in these regions by the flow of fluid within the vortex ring. It is noted that that in Figure 6.10a-c, particles were distributed in a non-homogeneous manner within the vortex structure, resulting in the right side of the vortex ring possessing a higher concentration of particles compared with the left side of the ring. Consequently, a higher concentration of particles was found to deposit on the right side of the ring compared with the left. This outcome indicates that the concentration of particles deposited in the vortex wake region has a certain level of dependence on the initial particle concentration within the ring, as well as on the particle concentration of the incoming trail. Despite the non-uniform concentration of particles within the vortex structures, particles were

still found to deposit in both sides of the vortex wake regions as the vortex propagated through the trail of particles. Further test runs involved examining the effect of a trail of particles that was displaced from the axis of symmetry of the vortex to favour one side of the vortex structure (Figure 6.10d-f). The trail of particles was laterally offset to the left side of the vortex ring, and as a vortex ring propagated through this trail, particle wake deposits only occurred on the left side of the vortex ring (corresponding to the side where the trail of particles was initially located). Although the results featured in Figure 6.10 strongly indicate that the presence of particles in the propagation front of the vortex ring play an important role in the accumulation of particles in the wake of a vortex ring, the influence of the trail of particles inducing a vortex asymmetry to cause the observed experimental outcome has yet to be disproved. It is still plausible that the results in Figure 6.10d-f can be explained in a similar manner to that in Figure 6.8d-f.

The situation whereby a propagating vortex ring interacts with particles in its propagation front is encountered when particle-laden vortex rings are generated successively (the flow conditions used for the experiments discussed in Section 6.1) and in pulsed particle-laden jets, which were predominantly investigated in studies concerned with particle-fluid interactions. For the case of inertial particles, it is plausible that additional particles entrained into the vortex ring are also flung out from the vortex cores due to their inherent inertia, and as the vortex ring propagates away, these particles are left to accumulate in the wake of the ring, together with particles displaced around the vortex ring envelope into the wake of the ring. This explanation is reasonable when considering inertial particles alone, and agrees well with other studies previously published (Crowe *et al.*, 1995; Eaton & Fessler, 1994; Longmire & Eaton, 1992; Wark *et al.*, 2000). However, since the present results were produced with neutrally buoyant particles for which particle inertia is minimal, it is premature to attribute the accumulation of particles in vortex wake regions to being entirely due to particle inertia, as has been done by previously published studies.

One proposition to explain these results is that as a vortex ring propagates through a trail of particles, these particles are displaced by the vortex ring envelope, to pass around the sides of the ring. As this occurs, the relative particle concentration of the ambient fluid around

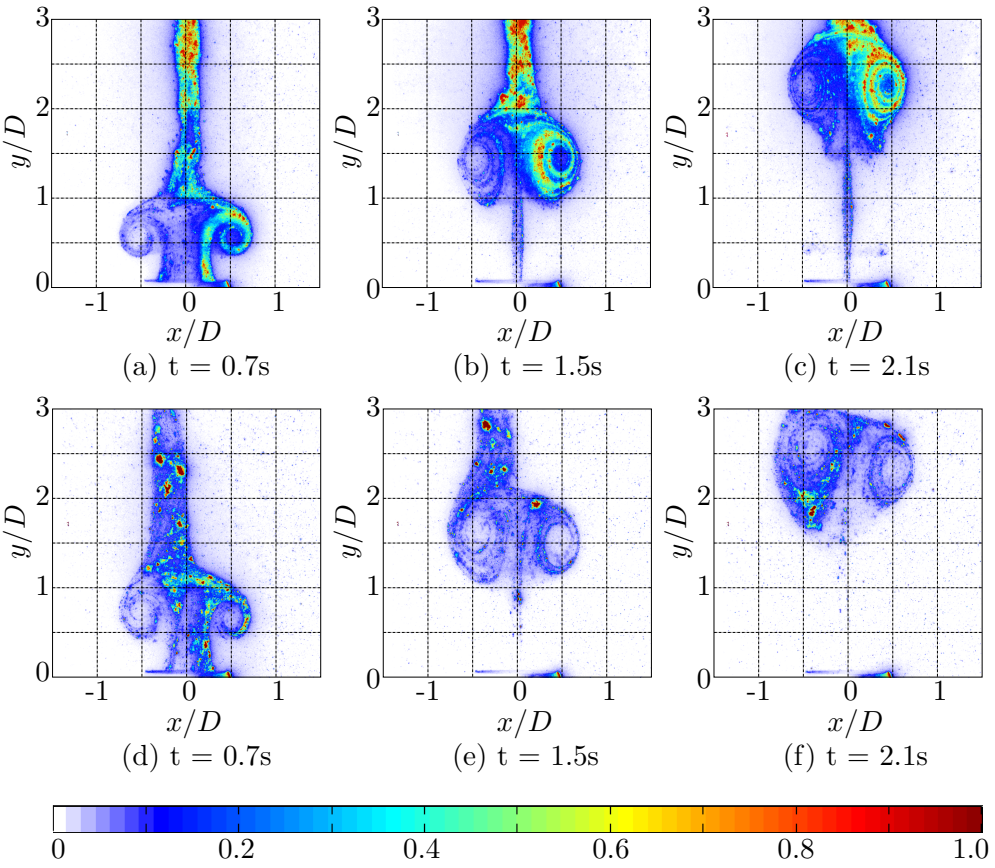
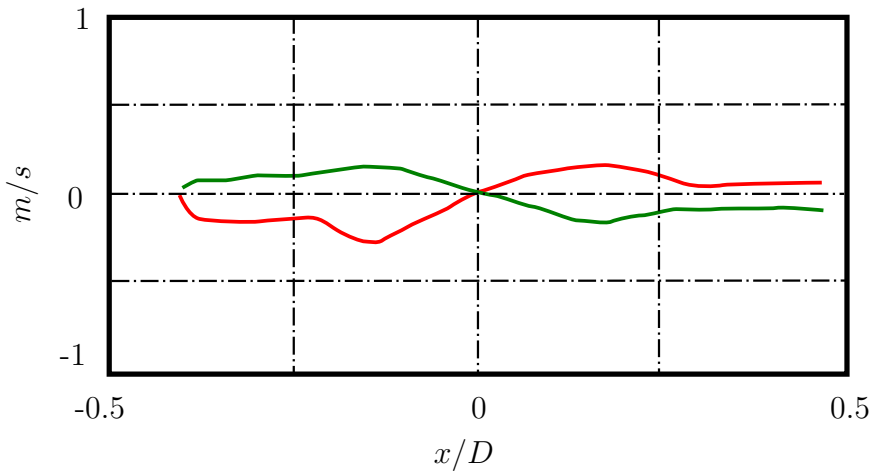


Figure 6.10: Normalised particle concentration of single pulsed particle-laden vortex rings interacting with a trail of particles in its propagation front, generated using a pulse duration of 0.4s for flow case $Re_f = 415$.

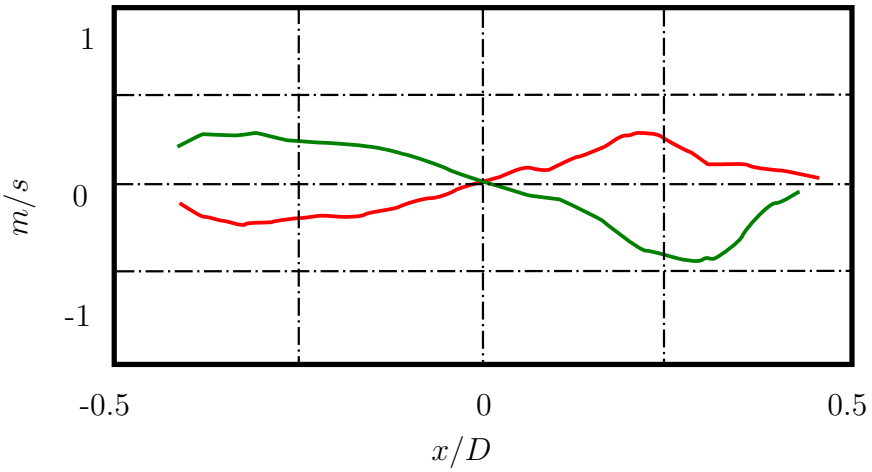
the vortex ring is significantly increased. A portion of this trail of particles will continue heading towards the rear of the vortex ring, accumulating at the wake of the ring, while the other portion would be entrained into the ring itself. Auerbach (1991) previously established that for vortex rings generated by a nozzle outlet such as the one investigated at present, approximately 40% of the fluid in the vortex ring will consist of entrained fluid. Consequently, a significant proportion of the vortex ring would consist of particles and fluid from the trail of particles, leading to an increase in particle concentration within the vortex structure itself. The impact of this increase in particle concentration within the vortex ring on particle and vortex behaviour is examined using the correlations established in Equation 5.6 and Equation 5.5, discussed in the previous chapter. Equation 5.5 shows that the vortex translational velocity depends on the vortex core size while Equation 5.6 shows that vortex core size and vortex translational velocity are associated with viscosity.

Velocity profiles through the cores of the vortex structures presented in Figure 6.10 were used to determine their respective vortex core sizes. Figure 6.11(a) presents the velocity profiles of the vortex cores featured in Figure 6.10(c), while Figure 6.11(b) presents the velocity profiles of the vortex cores featured in Figure 6.10(f). The red profiles represent the cores on the left side with a counter-clockwise rotation, while the green profiles represent the cores on the right side with a clockwise rotation. The distance between the highest and the lowest point on the velocity profiles provides an approximation of the respective vortex core sizes. Figure 6.11(a) shows that the left and right vortex cores featured in Figure 6.10(c) are effectively the same size. This outcome is as expected given that the vortex structure is propagating without any disturbances. In contrast, data from Figure 6.11(b) show that the right vortex (the green profile) is approximately 13% larger when compared with the left vortex (the red profile).

Based on Equation 5.5, a larger vortex core results in a smaller vortex translational velocity. Considering the data from Figure 6.10f and Figure 6.11(b), the right vortex is larger than the left vortex. In addition, the range of velocities (i.e. $U_{max} - U_{min}$) for the right vortex is also larger which is indicative that the circulation is larger, and that



(a)



(b)

Figure 6.11: Instantaneous velocity profiles through vortex cores featured in: (a) Figure 6.10(c), (b) Figure 6.10(f). The red profiles represent cores with a counter-clockwise rotation; the green profiles represent cores with a clock-wise rotation.

the right core is stronger compared to the left core. It is possible that different propagation velocity of the vortex cores in turn causes the entire vortex ring to veer towards the side with the larger core. It is also possible that the left core is weakened, compared to the right core, because of higher dissipation due to higher viscosity which also explains the vortex ring turning right.

This argument explains the observations in Figure 6.10f, with the vortex ring veering towards the right side, which has the larger vortex core. In addition, the correlations from Equation 5.6 show that a larger vortex core and smaller vortex translational velocity are associated with a higher local viscosity and a higher diffusion rate. These explanations indicate that changes in the particle number density within the vortex structure can affect local viscosity and the rate of diffusion of vorticity, which in turn affect the behaviour of the vortex structures as well as the particles.

Experiments where a vortex ring propagates through a trail of particles have shown that particles accumulate in the wake region of the vortex ring. In the case where the interaction of a vortex ring with a trail of particles is asymmetrical, the outflow of particles into the wake of the vortex ring is likewise observed to occur unevenly (Figure 6.10d-f). Analysis of these experiments established that a difference in vortex core sizes, with a larger core having reduced influence in induced velocities, result in different vortex translational velocities. These observations are in turn associated with differences in local viscosity and diffusion rates due to changes in the local particle number density.

Current discussions established that changes in local particle number density impacts on the particle volume fraction which in turn affects the shear rate and viscosity of a working system with particle suspensions. The movement of particles to accumulate in vortex wake regions results in particle dispersing into larger regions relative to vortex roll-up fluid layers. This particle dispersion would result in a relative decrease in particle number densities, which decreases local viscosity. Consequently, the motion of particles from regions with relatively higher shear stresses to regions of low shear stresses (the wake regions) may also be attributed to the occurrence of a shear-induced particle migration

phenomenon (Leighton & Acrivos, 1987; Stickel & Powell, 2005). This outflow of particles in the wake of a vortex ring in turn affects other characteristics of the vortex ring itself (such as, but not limited to convection velocity, vorticity field, and rate of velocity decay).

These arguments indicate that changes in particle number density, which affects local viscosity, diffusion rates, and shear rates, are able to influence the behaviour of particles and fluid in a working system. This explanation in turn establishes that there is a relationship between particle-fluid surface interactions and the directed movement of particles within vortex structures as well as the accumulation of particles in vortex wake regions. However, there are a number of reasons that can be attributed to this directed movement of particles within the vicinity of the vortex ring. In addition, the current work does not provide sufficient evidence to either prove or disprove the occurrence of the preferential concentration mechanism and as such, the link between particle-fluid surface interactions over the preferential concentration mechanism is yet to be validated experimentally.

6.2.3 Conclusion of Focused Experiments

The current investigation presented experimental outcomes and explanations that indicate the influence of particle-fluid surface interactions on the directed movement of particles within vortex structures as well as the accumulation of particles in vortex wake regions. However, the present results are insufficient to confirm the occurrence of the preferential concentration mechanism and therefore the influence of particle-fluid surface interactions over the preferential concentration mechanism is not substantiated. Nevertheless, the results indicate that an uneven distribution of particles within the vortex ring causes an imbalance in core size (perhaps even circulation), leading to turning of the vortex trajectory. This observation is attributed to the effect of particle loading on viscosity of the fluid in the vortex cores.

6.3 Summary

This chapter detailed the examination of particle-fluid surface influences on particle and fluid behaviour. Experiments utilising neutrally-buoyant particles successfully replicated the outcomes of some previously-published studies involving a series of particle-laden vortical structures that used dense, inertial particles. Further examination of the interaction of particles with individual vortex rings under different flow conditions led to a number of conclusions:

- the accumulation of particles in braid regions between consecutive vortical structures reported in previous studies indicate that there may be other factors beside particle centrifugal forces driving the movement of particles into braid regions
- changes in local particle number density within the vortex structure can affect local viscosity and the rate of diffusion of vorticity, which in turn affect particle and fluid behaviour
- the current work provided insufficient evidence to either confirm or disprove the occurrence of the preferential concentration mechanism. Therefore the role of particle-fluid surface interactions in driving the preferential concentration mechanism is yet to be substantiated experimentally.

7 Fluid Excitation Frequency

The parametric investigation described in this chapter examines the effect of fluid excitation frequency on the directed movement of particles. It is postulated that changing the fluid excitation frequency changes the way the particles and fluid interact with each other, which would in turn influence the capabilities of the preferential concentration mechanism. From the results presented in this chapter, more information regarding the influence of fluid excitation frequency on particle and fluid behaviour has been acquired, enabling recommendations to be made for future experimental investigations.

7.1 Fluid Excitation Frequency Experiments

Experiments by Longmire and Eaton (1992) and Wark *et al.* (2000) showed that the fluid excitation frequency provided a means of controlling the vortex structure behaviour, which in turn controlled the location of particle dispersion and accumulation. The current work examines the manner in which excitation frequency changes the way particles respond to fluid perturbations. The range of fluid excitation frequencies examined in the presented results was chosen such that flow conditions of $St \approx O(1)$ were obtained, since this condition is where turbulence-induced directed particle motion due to preferential concentration is likely to be most evident (see Chapter 2). The experiments used large-scale coherent structures at low Reynolds numbers to ensure that the range of turbulence scales generated is narrow and concentrated around a single length-scale.

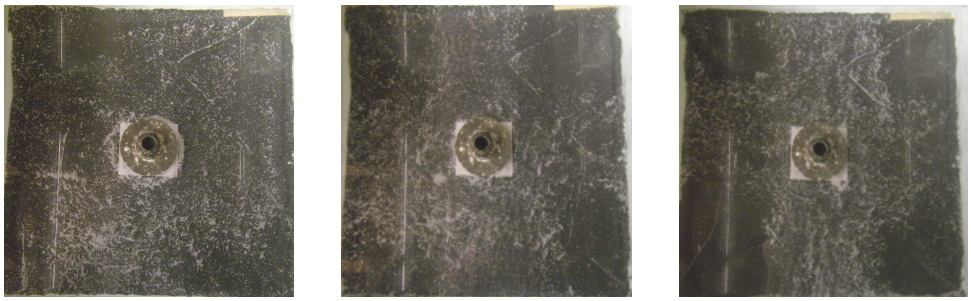
7.1.1 Experiment-Specific Details

The experiments used the crankshaft setup (see Chapter 4) to generate periodic vortex structures at frequencies ranging from 2Hz to 13Hz, at 1Hz intervals. A total of 10 test runs were recorded for each excitation frequency. Polystyrene particles (mean particle size of 0.7mm $\pm$ 0.1mm, $\rho_p = 1060$ kg/m^3) were used for this investigation and were homogeneously dispersed in water. Vortex structures were generated continuously for 15 minutes, after which the vortex generator was turned off. The particles were allowed to settle before visual inspection. For every excitation frequency evaluated, the particle settlement patterns were identical across all the test runs.

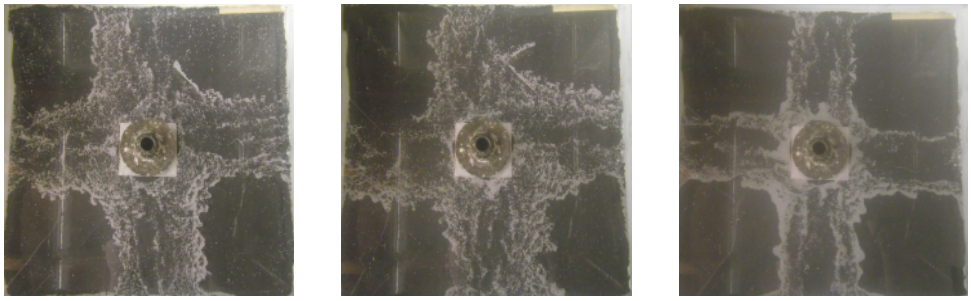
7.1.2 Results and Discussion

Figure 7.1 shows a sequence of particle settlement patterns produced by flows with increasing fluid excitation frequency. No discernible pattern was obtained visually in the particle settlement after a 2Hz and 3Hz excitation frequency was applied (Figure 7.1a-b). At 4 Hz (Figure 7.1c), there were some indications of structure in the settlement of particles although the structure was not visually distinctive. When the excitation frequency was increased from 5Hz to 13Hz, particles were observed to settle in a structured manner, generating a symmetrical pattern in both axes along the horizontal plane that became more clearly defined with increasing excitation frequency (Figure 7.1d-l). Experiments did not explore frequencies beyond 13Hz due to the physical limitations of the stepper motor. In addition, the piston-cylinder setup was run at 5Hz for 60 minutes but no change in the particle settlement pattern was observed, indicating that these results are independent of time, and had converged to a representative pattern after 15 minutes of running time.

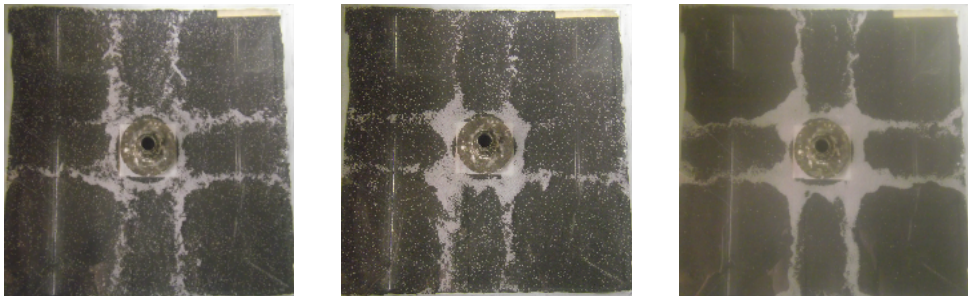
The unstructured particle settlement patterns obtained for fluid excitation frequencies of 2Hz and 3Hz indicate that the particles retained their initial homogeneous particle distribution and were not affected by the presence of large-scale vortical structures. When the fluid excitation frequency ranged from 4Hz to 13Hz, the resulting



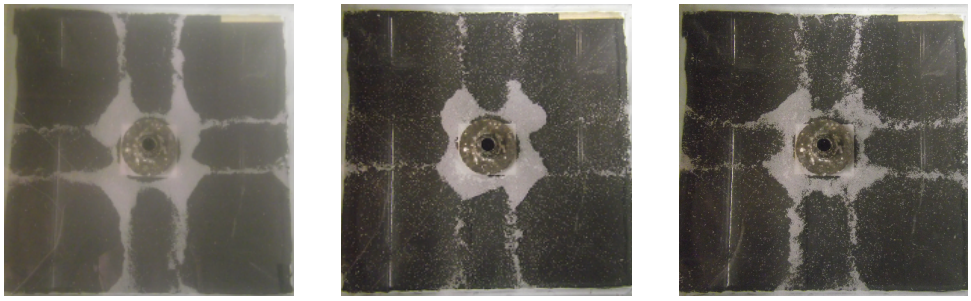
(a) $f = 2$Hz (b) $f = 3$Hz (c) $f = 4$Hz



(d) $f = 5$Hz (e) $f = 6$Hz (f) $f = 7$Hz



(g) $f = 8$Hz (h) $f = 9$Hz (i) $f = 10$Hz



(j) $f = 11$Hz (k) $f = 12$Hz (l) $f = 13$Hz

Figure 7.1: Particle settlement patterns after interacting with vortex structures generated at different fluid excitation frequencies for a period of 15 minute intervals. The views show the floor of the water tank, viewed from above. The nozzle head can be seen at the centre of the floor.

structured particle settlement patterns indicate that particles are influenced by the presence of large-scale vortical structures and are induced to move in an organised and directed manner. This observation suggests that within this frequency range, the flow conditions are such that they are suitable for the occurrence of turbulence-induced particle motion, a notion requiring the analysis of the particle Stokes number, St, for verification (Table 7.1). Equations 2.4, 2.5 and 2.10 were used to calculate particle Stokes number, St. In the determination of τ_{int} (i.e. Equation 2.10), the nozzle diameter was used for L while the propagation velocity of the vortex structure, U_v, was estimated using the distance of the piston sweep (see Figure 4.9) and the fluid excitation frequency (which was used to determine the time taken for the linear displacement of the piston i.e. the piston sweep). The manner in which the particles settled provides the locations where particles are accumulating due to their interaction with the vortical structures.

Table 7.1: The particle Stokes number at different fluid excitation frequencies.

Fluid Excitation Frequency	Particle Stokes Number, St
2Hz	0.288
3Hz	0.432
4Hz	0.576
5Hz	0.792
6Hz	0.864
7Hz	1.008
8Hz	1.152
9Hz	1.296
10Hz	1.440
11Hz	1.584
12Hz	1.728
13Hz	1.872

Table 7.1 provides St for all the fluid excitation frequencies. Excitation frequencies of 2Hz and 3Hz are provided with flow conditions whereby

$St < 1$; however the particles are still within the range of $St \approx O(1)$. Consequently, it is unlikely that the particles would follow all fluid motion perfectly, especially for small-scale turbulence. Particles follow all fluid motion and behave as flow tracers when $St \approx O(10^{-2})$ or smaller. Therefore, under the present conditions, excitation frequencies of 2Hz and 3Hz are expected to cause particles to be partially influenced by the fluid motion. Particles are in turn observed to settle in an unstructured manner, indicating that the particles were not moving in a directed manner.

Conversely, when the excitation frequency ranges from 4Hz to 8Hz, the particles were observed to settle in a structured manner, indicating that the particles move in a directed manner. These outcomes are to be expected when flow conditions are such that $St \approx O(1)$ where the motion of particles is partially influenced by fluid motion. However, when the excitation frequency ranges from 9Hz to 13Hz, where $St > 1$, particles are also observed to settle in a structured manner despite the flow conditions being such that the particles should be less responsive to the fluid's motions. It is highly possible that the variation in particle responses with different St is not so definitive and immediate, such that there would be a significant difference between particle behaviour for when $St = 1$ and $St = 1.8$. This argument may explain these unexpected outcomes which contradict the initial postulation, whereby turbulence induced directed particle motion due to preferential concentration is likely to be most evident when $St \approx O(1)$.

Other inconsistencies were also noted in the present experimental arrangement where the large-scale vortex structures generated are restricted to the centre of the tank (corresponding to the axial location of the nozzle) (Figure 4.12). If the preferential concentration mechanism (as described by published studies cited in Chapter 2) takes place, the vortical structures will direct particles to regions of high strain and low vorticity in the flow field. These locations correspond to saddle/braid regions between successive vortex structures. Therefore, when fluid excitation is terminated, it is expected that a significant proportion of the particles will settle around the nozzle of the piston at the base of the tank and this experimental outcome should be evident when $St \approx O(1)$. Particle accumulation under these conditions can then be used to substantiate the occurrence of directed particle motion due to the preferential concentration mechanism. However, the unexpected

manner in which the particles settle at the base of the tank suggests the possibility of other factors causing the observed particle settlement that may be unrelated to the preferential concentration mechanism.

Additionally, the change in particle behaviour as $St \rightarrow 1$ suggests a corresponding change in the particle-fluid dynamics, in which the Stokes number has little to do with the results obtained. Fluid flow patterns are established by fluid excitation, which in turn result in the observed structured settling of particles on the base of the tank. The structured settling of particles may be due to directed particle motion associated with the preferential concentration whilst particles are within the fluid flow field; or that all particles sinking to the base of the tank are swept into structured patterns by the fluid motion in which case the directed particle motion is not associated with the preferential concentration mechanism.

The unexpected manner in which particles settle and form structured patterns at frequencies from 4Hz to 13Hz indicates that the latter is likely to be the contributing factor for the observed results. This idea is highly likely considering that at frequencies $<$ 4Hz, particles remain settled in an unstructured manner, possibly due to insufficient fluid excitation, causing the fluid flow pattern not to occur or to be too unsteady to form a consistent pattern. Alternatively, velocities in the fluid flow field may be too low, i.e. less than the settling velocity of the particles, or too slow to sweep the particles along the floor of the tank to enable the patterns to form. In order to evaluate this idea further, the polystyrene particles used in the current research were replaced with polyamide particles (with a mean particle size of 20μm $\pm$ 15μm, $\rho_p = 1030$ kg/m^3) in the current experimental arrangement. Subsequent experimental results show that these particles settled in an unstructured manner for the entire frequency range evaluated.

To determine the particle settling velocity, Stokes Law was used:

$$U_{settling} = \frac{2(\rho_p - \rho_f)gr^2}{9\mu_f} \tag{7.1}$$

where ρ_p is the particle density, ρ_f is the fluid density, μ_f is the fluid dynamic viscosity and ρ_p is the particle radius. Applying Stokes Law,

the settling velocities for the polyamide and polystyrene particles in the present experimental arrangement are $O(10^{-6})\text{ms}^{-1}$ and $O(10^{-2})\text{ms}^{-1}$ respectively. With the fluid flow field having velocities of the order of $O(10^{-1})\text{ms}^{-1}$, these being five orders of magnitude faster than the settling velocity of the polyamide particles, it follows that the fluid flow field would have dissipated significantly before the particles are able to settle to the base of the tank. Consequently in the case of polyamide particles, any uneven distribution of particles within the tank due to the fluid motion would have been lost through particle diffusion as the particle-fluid system would have re-established particle distribution equilibrium by the time the particles settled to the base of the tank. As a result, the polyamide particles are observed to settle in an unstructured manner, being unaffected by the fluid flow field and fluid excitation velocities.

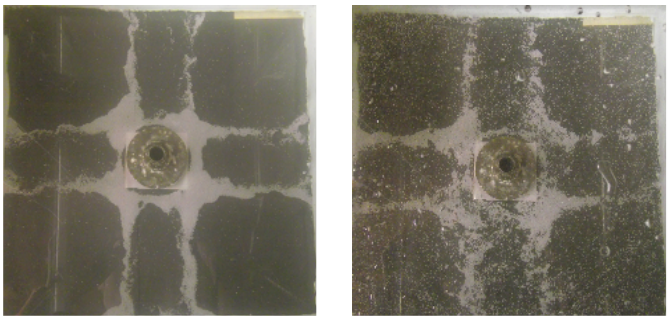
In contrast, the settling velocity of the polystyrene particles is comparable with the velocities of the fluid flow field. Since it would take the polystyrene particles (Figure 7.1) an average of 50s to settle in a 500mm deep tank, having experiments with vortex structures generated continuously for 15 minutes would mean that all the particles would have settled once the vortex generator was turned off. It is likely that, as the fluid flow field moves the particles, the particles are able to settle fast enough for them to retain a structured distribution within the tank. It is also likely that the large-scale vortical structures in the tank would sweep the particles, once they had settled on the base of the tank, into low velocity areas. Both explanations would require the fluid's motion to be fast enough to move the particles to enable the structured patterns to form, thus explaining the observation that structured particle settlement is only observed when the fluid excitation frequency is above 4Hz. These explanations are able to account for the unexpected manner in which the polystyrene particles settle at the base of the tank being affected by the fluid excitation frequency. Therefore, it is highly likely that the structured settling of particles that has been observed is due to the particles being affected by the sweeping fluid motion either as they sink or once they have sunk to the base of the tank, and is not due to the preferential concentration mechanism.

These experimental outcomes do not, at present, provide sufficient evidence to demonstrate or support the occurrence of the preferential

concentration mechanism. However, the absence of evidence is also insufficient to disprove the existence of the mechanism within the current experimental arrangement i.e. for particles in a fluid suspension. In addition, there are numerous considerations that may have contributed to the unexpected experimental results observed. For instance, aside from differences in settling velocities, the polystyrene and polyamide particles also have very different diameters. Particles with larger diameters may be more susceptible to the influences of particle-fluid surface interactions compared with particles with smaller diameters, which in turn affect fluid and particle behaviour. Although the present work provides further support to the outcomes of Chapter 6, which indicated that particle-fluid surface interactions affect fluid and particle behaviour, the occurrence of the preferential concentration mechanism is yet to be established in the current research. Consequently, the influence of particle-fluid interactions on the preferential concentration mechanism remains inconclusive at this stage.

The initial conjecture regarding contributing factors affecting the way particles settle was that the surface motion of the fluid phase (wave-like motion) interacting with the corresponding reflections from the tank walls produces some form of stationary wave front at the locations where particle settlement occurs. In order to confirm this speculation, experiments were repeated with the addition of a false ceiling placed in the tank. An acrylic sheet, used as a false ceiling, was placed on the surface of the fluid phase in order to suppress any surface wave motion caused by the continuous generation of vortex structures by the piston-cylinder setup. During this test run, the motor was driven at 10Hz. The particle settlement pattern obtained using the false ceiling was comparable with that obtained without the false ceiling (Figure 7.2). This result indicates that the surface motion of the fluid phase and its reflections are not the cause of the symmetrical pattern observed.

Due to the symmetrical nature of the particle settlement patterns, it was thought that the tank geometry might influence particle settlement. This hypothesis would be supported if a different form of particle settlement pattern were to be obtained from a tank with different geometry. Modifications were made to the existing



(a) (b)

Figure 7.2: Particle settlement at $f = 10$Hz (a) Without a false ceiling (b) With a false ceiling.



(a) (b)

Figure 7.3: (a) Cylindrical tank setup (b) Particle settlement at $f = 10$Hz.

experimental tank to allow a test run to be conducted using an acrylic cylindrical tank with a diameter of 0.75m (Figure 7.3a). During this test run, the motor was driven at 10Hz and the polystyrene particles settled in an unstructured manner, without any discernible pattern to indicate directed motion in the particles (Figure 7.3b). This outcome is interesting for two main reasons. Firstly, building on the outcomes of Longmire and Eaton (1992) and Wark *et al.* (2000), it is expected that particles would still settle at the centre of the tank (i.e around the nozzle even in an axi-symmetric tank) if the preferential concentration mechanism were occurring. Secondly, aside from indicating that tank geometry causes the cross-symmetry in particle settlement, there is also a possibility that tank geometry may play a role in facilitating the other factors contributing to these structured particle settlements. More experimentation was undertaken to establish how tank geometry affected the occurrence of particles settling in a structured manner, and this will be discussed in Section 7.2.

7.1.3 Conclusions of Fluid Excitation Frequency Experiments

The present work attempted to examine the preferential concentration mechanism on a large scale, with experiments focusing on particle movement within a tank as opposed to particle movement within the vicinity of the vortex structures (Chapters 5 and 6). The results from this work show that fluid excitation frequencies from 4Hz to 13Hz, with $St \approx O(1)$ as well as $St > 1$, provided flow conditions such that particles are able to respond to fluid turbulence and move in a directed manner. Additionally, the change in particle behaviour as $St \rightarrow 1$ suggests that Stokes number has an insignificant effect on the corresponding change in the particle-fluid dynamics observed. Results indicate the possibility that a number of different factors are contributing to the directed motion in particles which subsequently leads to the observed structured settlement of particles. However, there is insufficient evidence to indicate that these directed motions in particles are associated with the preferential concentration mechanism. Consequently, the influence of the various factors identified, such as particle settling velocities and particle-fluid surface interactions, on the preferential concentration mechanism remains unsubstantiated.

Further experiments aimed at establishing the occurrence of the preferential concentration mechanism while concurrently isolating and examining the various factors contributing to the mechanism is necessary and warranted. However, these experiments are highly challenging experimentally and are beyond the scope of the present experimental arrangement. Nonetheless, for the purposes of completeness of the research for this thesis, the next set of experiments aims to examine how tank geometry influences fluid and particle motion, causing the particles to settle in a structured manner.

7.2 Additional Experiments

These experiments aim to determine how the tank geometry influences fluid and particle motion, which in turn causes the particles to settle in a structured manner. In order to do so, the flow structures generated during the experiments described in Section 7.1 were examined using dye-based visualisation to provide an understanding of the 3D fluid flow field within the tank.

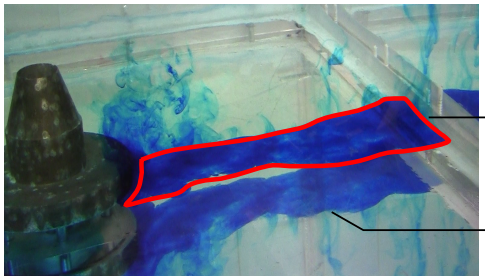
7.2.1 Experiment-Specific Details

The experiments utilised the crankshaft setup (see Chapter 4) to generate periodic vortex structures at a frequency of 2Hz. Dye visualisation experiments were carried out at this frequency to ensure that the flow turbulence was minimal, thereby producing the clearest possible flow visualisation images. The dye-based flow visualisation technique used undiluted Brilliant Blue, non-toxic food dye. This dye provided good contrast and a fluid density comparable to water, making it suitable for the current investigation. Due to the axi-symmetry of the flow structures produced by the nozzle, dye was introduced to the water tank in one quadrant at a time.

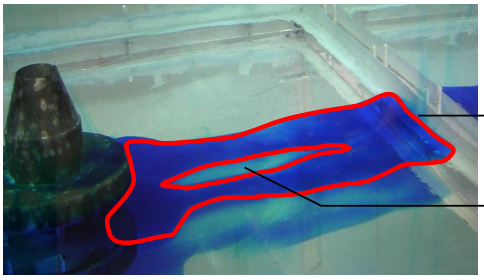
7.2.2 Dye Visualisation Results

Figure 7.4 shows the movement of a streak of dye, laid between the piston and the tank wall, in a straight line perpendicular to the tank wall while the piston system was driven continuously. The location of the dye is outlined in red for clarity, with its reflection at the base of the tank. The streak of dye initially widened and a vacant area was observed to appear within the streak (Figure 7.4b). Figure 7.4c shows that this vacant area eventually developed into a clear strip, separating the dye into two distinct streaks. These two dye streaks remained distinguishable, with no visible change after another 5 minutes of fluid excitation, indicating that a steady-state condition had been achieved. These results are indicative of some form of fluid motion along the vacant path. The locations of these two dye streaks are identical to the particle accumulation pattern at these locations, as shown in Figure 7.1. These observations indicate that particles settling on the base of the tank behave as the dye does, accumulating along areas of flow convergence of the surface flow.

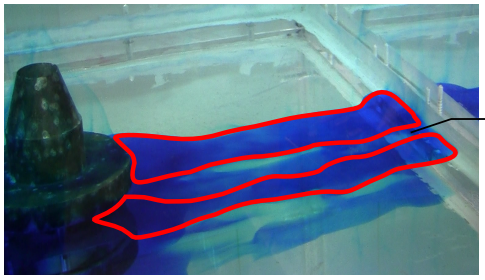
Figure 7.5 shows the movement of some new dye added to the tank, laid at the far edge (timing was restarted for this investigation). This new streak of dye was observed to move towards the centre of the tank, eventually merging with the pre-existing dye at the tank floor to form distinct patterns in each quadrant of the tank. The dye patterns achieved are very similar to those of the particle settlement pattern observed in Figure 7.1. Figure 7.6 shows the movement of dye laid at the near edge, from which a similar outcome is obtained. The new dye streak was observed to spread towards the centre of the tank, merging with pre-existing dye streaks in the process. The movement of the dye was organised such that a vacant area emerged, with the dye moving along some specific paths, a possibility brought about by the motion of particular fluid structures localised within each tank quadrant. The dye accumulated in the vicinity of the 0^{o} planes and a vacant path re-emerged in the dye streaks along these planes once a steady state was achieved (Figure 7.6d). These outcomes support the notion that tank geometry, constraining the fluid flow into quadrants, produces a large-scale flow pattern that contributes to the organised manner in which particles accumulate in specific regions of a flow.



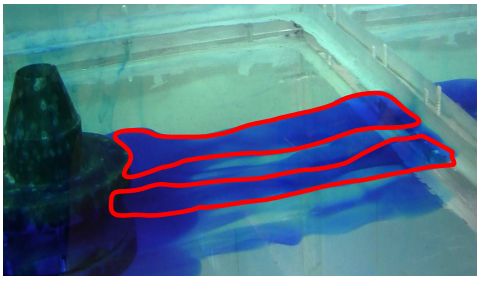
(a) t = 0s



(b) t = 20s



(c) t = 30s



(d) t = 60s

Figure 7.4: The movement of dye, outlined in red, initially placed along a 0° plane.

Figure 7.7 show a streak of dye laid out as a quarter-circle in one corner of the tank. This streak of dye was seen to spread towards the centre of the tank, moving towards the vicinity of the 0° plane. Some of the dye was drawn into the ZNMF jet and was observed to recirculate back into the quadrant it came from. These outcomes indicate that fluid mixing between quadrants does occur in a limited fashion at the ZNMF jet, but the geometrical constraints of the tank forces fluid to recirculate primarily within their respective quadrants.

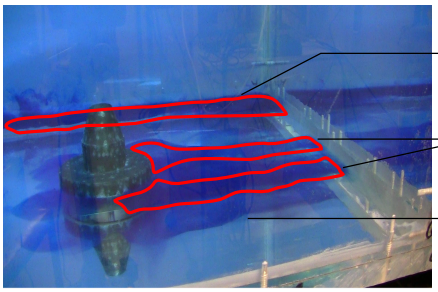
7.2.3 Conclusions of the Additional Experiments

The dye visualisation results confirm that the tank geometry places a constraint on the flow field generated within the tank as the piston system is operated. This geometrical constraint forces fluid to recirculate primarily within quadrants of the tank, resulting in the generation of a large-scale flow pattern that causes particles to accumulate in an organised manner.

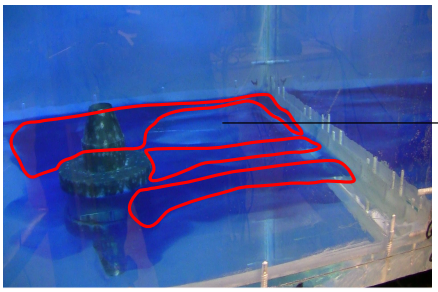
7.3 Summary

This chapter detailed an experimental study which aimed to examine the effects of fluid excitation frequency on the preferential concentration mechanism on a large-scale. Experiments examined the movement of particles within a water tank instead of focusing on particle movement within vortex structures previously investigated in Chapters 5 and 6. Within the existing experimental arrangement, particles are able to respond to fluid turbulence and move in a directed manner when the fluid excitation frequencies are within a certain range. It was also established that the Stokes number has an insignificant effect on the observed directed particle motion.

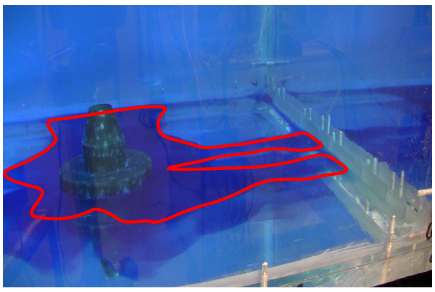
Further investigations confirmed that the tank geometry, forcing fluid to recirculate on a macro scale, plays a major role in how particles move and ultimately accumulate in the tank. Consequently, the results indicate that these directed particle motions are brought about by large-scale flow patterns within the tank, combined with relatively large settling velocities of the polystyrene particles. The directed particle motions observed and presented are therefore unlikely to be associated with the preferential concentration mechanism. Given that there is also insufficient evidence to support the occurrence of the preferential concentration mechanism, the effect of fluid excitation frequency on the preferential concentration mechanism remains unsubstantiated in the current research.



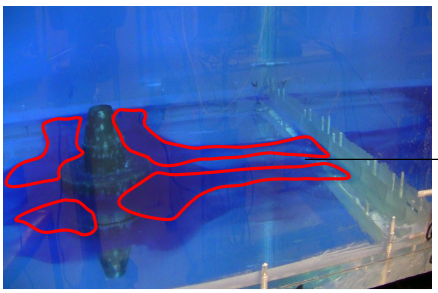
(a) t = 0s



(b) t = 20s

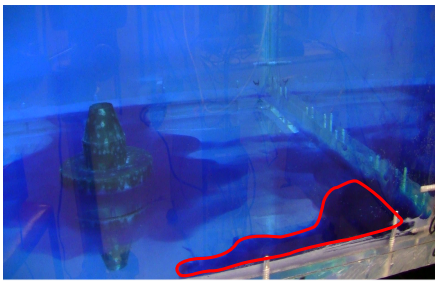


(c) t = 80s



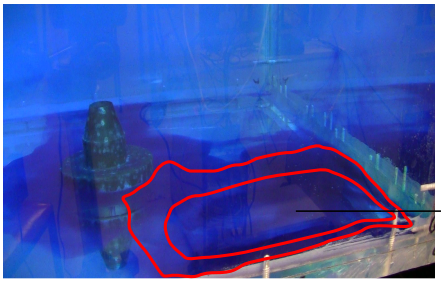
(d) t = 260s

Figure 7.5: Movement of dye when dye is initially laid at the edge of the tank.



New dye placement at front edge of tank

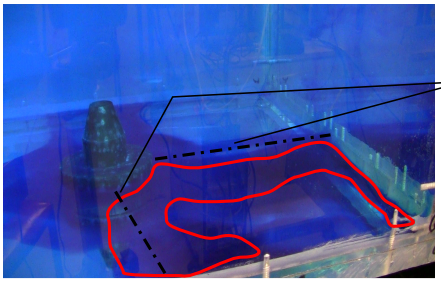
(a) t = 280s



New dye merges with old dye

Dye merging leaving vacant area

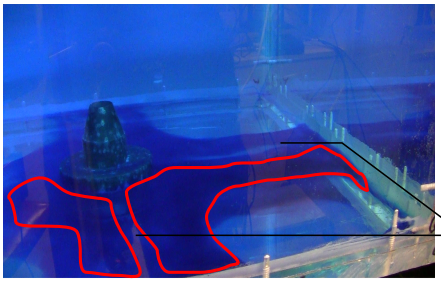
(b) t = 290s



Location of 0° planes

New dye continues moving towards 0° planes

(c) t = 300s

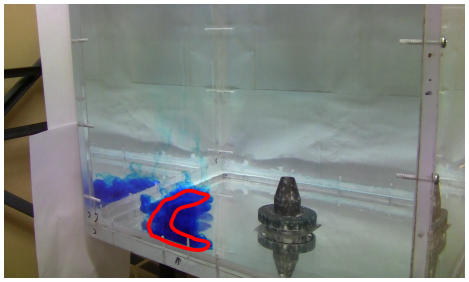


Distinct dye streaks orientated in tank quadrants

Vacant paths

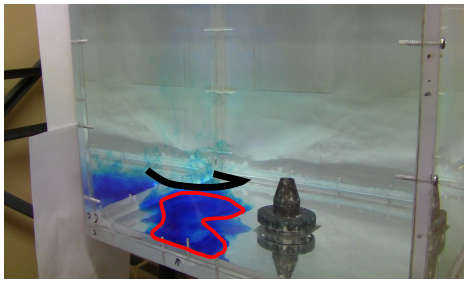
(d) t = 380s

Figure 7.6: The movement of dye, laid initially at the edge of the tank, directed towards the 0° planes.



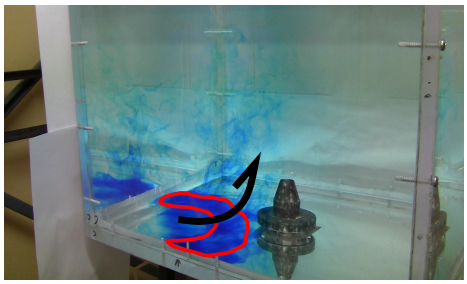
Dye placement in a quadrant of the tank

(a) t = 0s



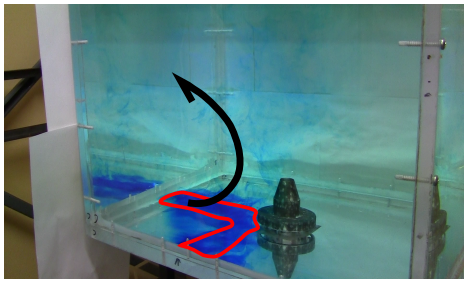
Dye moves towards tank centre

(b) t = 20s



Dye is drawn towards the ZNMF jet

(c) t = 60s



Dye indicates fluid recirculating in quadrant

(d) t = 110s

Figure 7.7: Dye movement indicates that ambient fluid recirculates within the tank quadrant.

8 Conclusions and Future Work

The study of particle-laden fluids and particle-fluid interactions is a complex and challenging task. The aim of the present research was to examine a novel approach of particle separation using fluid turbulence, through a mechanism known as preferential concentration. This mechanism works by inducing directed motion in particles to accumulate in specific regions of the fluid flow field. This chapter summarises the major conclusions, outcomes and achievements of the present research. Due to the complexities associated with particle-laden fluids and the preferential concentration mechanism, areas of significant future work have been identified and are discussed.

8.1 Conclusions

The focus of the present research was to examine the preferential concentration mechanism and to assess the feasibility of using this mechanism on particles in a fluid suspension for the purposes of selective particle un-mixing. In an effort to address the limited literature and fundamental knowledge available on particle-laden fluids, the initial work was to substantiate existing theories on forces driving the preferential concentration mechanism. Experiments commenced by examining the interaction between particles and fluid structures using neutrally-buoyant particles. By tracking these particles within a fluid flow field, the influence of particle inertia was effectively suppressed and the occurrence of directed particle motion examined. The outcomes of these experiments were then used to shed more light on the workings of

the preferential concentration mechanism, particularly to determine whether there are other factors besides particle mass and inertia driving the preferential concentration mechanism.

Preliminary experimental outcomes showed particle and fluid interactions that cannot be explained using conventional concepts of the preferential concentration mechanism, based solely on particle mass and inertia. Irregularities in the vorticity and circulation plots were noted and although the cause of such irregularities could not be definitively established, consideration was given to the possibility that the different ways in which fluid systems are seeded with particles affects the local effective viscosity within the vicinity of the vortex structures. Changes in local effective viscosity in turn could impact on the normal diffusive process of vorticity, which contributes to the experimental discrepancies noted. Consequently, the observed directed motion in particles may be due to a range of factors other than particle mass and inertia, which may or may not be associated with the preferential concentration mechanism.

It should be noted that the PIV work undertaken was opportunistic in nature, in that particle selection and equipment was optimised for PN measurements and the preferential concentration mechanism, and not the PIV measurements. As such, the application of the PIV technique was limited to focus on evaluation of the overall particle-fluid behaviour. The focus of the results analysis was on comparison of observed trends rather than the absolute numerical values. Optimisation of particle and fluid parameters for PIV measurements as well as validation of the technique's uncertainties for the given setup, should be considered for further research. However care would need to be taken to ensure that the optimisation for PIV measurement does not adversely affect the effective study of the preferential concentration mechanism. It is likely that these unavoidable conflicting constraints be difficult to resolve due to the nature of experimental work.

Benchmarking experiments were undertaken to establish the feasibility of particle-fluid surface interactions contributing to directed motion in particles and/or influencing the preferential concentration mechanism. The results suggest that particle interaction with vortex structures under certain flow conditions contributes to the accumulation of

particles within wake regions of a vortex ring as well as in braid regions between successive vortical structures. These experiments suggest that the local particle number density affects local viscosity and the rate of diffusion of vorticity within a vortex structure. In addition, the local particle number density also influences the particle volume fraction, which in turn affects local viscosity, diffusion and shear rates. Collectively, the outcomes indicate that it is very likely that particle-fluid surface interactions, through changes in local particle number density, have evident influences on particles and fluid behaviours which contribute to directed motion in particles. Although the accumulation of particles in vortex wake and braid regions can be associated with particle-fluid surface interactions, there was insufficient evidence to either confirm or disprove the occurrence of the preferential concentration mechanism. The physical limitations of experimental work resulted in further attempts to isolate and study the influences of individual factors on particle and fluid interaction a near impossible task at the time of experimentation with the available resources. Despite these limitations, the major implication of these results is that the observed directed particle motion, although due to factors other than particle mass and inertia, may not be associated with the preferential concentration mechanism.

Further experiments to investigate the effect of fluid excitation frequencies were undertaken in an attempt to examine the preferential concentration mechanism on a large-scale. The results show that when fluid excitation frequencies were within a certain range, the flow conditions were conducive for particles to respond to fluid turbulence in order to move in a directed manner. In addition, the results also suggest that the Stokes number has an insignificant effect on the observed directed particle motion. The combination of tank geometry, forcing fluid to recirculate on a macro scale, and particle settling velocities, was found to have caused the observations where particles settled in a structured manner at the base of the tank. These outcomes collectively indicate that the observed directed particle motion is unlikely to be due to the preferential concentration mechanism.

The research discussed in this thesis was undertaken with the intention of contributing to the field of particle-laden fluids and further understanding of the preferential concentration mechanism. Within the

construct of the current experimental arrangements, the results did not provide further evidence to support the findings of published results regarding the preferential concentration mechanism. However, these results also did not present sufficient evidence to disprove or contradict the published data. Instead, there is evidence to support the idea that particle-fluid surface interactions are able to influence particle and fluid behaviour, thus contributing to the directed motion in particles. Although the relationship between particle-fluid surface interactions and the preferential concentration was not substantiated in the present research, it is reasonable to suppose that there may be other factors driving the preferential concentration mechanism or that there may be alternative mechanisms driving the directed motion and accumulation of particles.

The results presented in this research provide additional material from which knowledge can be drawn, including the possibility of extending the scope of existing preferential concentration theories that are based solely on particle mass and inertia. It is anticipated that through future work, additional research will be able to shed more light into the various factors, contributing to particle-fluid dynamics causing directed particle motion and accumulation, with the aim to further the understanding of preferential concentration and other mechanisms that contribute to particles moving in a directed manner. Hence, the additional and valuable insights the present research have contributed to the field of two-phase flow indicate that the original intention of this work has been partially fulfilled.

Reflection on the experimental work undertaken for this research provided opportunities to consider possible improvements that may be implemented in future. The use of a larger water tank would enable vortex structures to be tracked for longer time periods, which would provide more recorded images and hence more data for analysis regarding the behaviour of particle-fluid interactions. The use of an alternative experimental setup that generates vortex structures at a lower frequency would also enable more images to recorded, with perhaps greater clarity in terms of particle tracking capabilities since the vortex would be propagating at a lower speed. Consideration should also be given to the use of different experimental techniques, such as the use of stereoscopic PIV to obtain 3D velocity and vorticity

measurements of the flow field. The data collected from this technique would provide valuable insights into particle-fluid interactions and negate data collection issues associated with particles moving out of the laser plane such as those encountered in this research. Such improvements may be explored in future work if access to the necessary resources is available.

8.2 Suggested Future Work

Although this research started with the aim of understanding and developing particle separation techniques based on the preferential concentration mechanism, the outcomes discussed represent the beginnings of an alternative approach to examining directed particle motion and the preferential concentration mechanism. The potential of the work extending from the conclusions of this research is significant.

Directed particle motion observed in neutrally buoyant particles and subsequent analysis suggests that particle-fluid surface interactions are a contributing factor. However, the association of particle-fluid surface interactions with the preferential concentration mechanism is still unknown. Future studies should aim to establish the occurrence of the preferential concentration in experiments, while concurrently examining the possibility of particle-fluid surface interactions contributing to the preferential concentration mechanism. New experiments that use different vortex generators or drivers that produce different fluid perturbations/structures for investigation would have to be designed in order to explore particle-fluid interactions from a different perspective. Should this approach prove successful, parametric studies should then be undertaken to investigate how both particle mass and inertia, and particle-fluid surface interactions affect the effectiveness and capabilities of the preferential concentration mechanism. Given the physical limitations associated with experimental data, alternative avenues of data collection such as those from analytical and/or numerical simulations should also be explored. Comparing data from experimental and computational work would provide valuable insights to the workings of particle-fluid interactions that contribute to the bigger picture of two-phase flow research. From these investigations, it is

anticipated that a fundamental understanding of the workings and flow dynamics of the preferential concentration mechanism can be extended, thereby allowing for more precise methods of controlling the preferential concentration mechanism to be identified. This would consequently provide the means of adopting and implementing the preferential concentration mechanism to un-mix particles in a fluid suspension, thus allowing for its application in the particle separation industry.

Alternatively, directed particle motion due to particle-fluid surface interactions may be highlighting a different mechanism by which particles move and accumulate within a working system. Studies to examine this possibility would help to further our understanding of particle and fluid behaviour and characteristics. However, designing an experiment that enables the examination of particle-fluid surface interactions will prove challenging, given the complex nature of experimental work involving two-phase flows. Particle behaviour and characteristics in a fluid suspension are determined by the coupling interaction with the fluid phase. Since different types of coupling would occur to varying degrees within a particle-laden fluid system, investigating the effects of particle-fluid surface interactions on particle behaviour will be difficult if not impossible. A more feasible approach may be to engage in numerical and/or simulation work. However, computational work would need to take into account the various coupling interactions sustained within a particle-laden fluid system. Overall, the understanding of how particles and fluid behaviour are affected by particle-fluid surface interactions will provide further insight into particle and fluid dynamics, which will continue to justify further research into this field.

References

Abu-Gharbieh, R, Persson, JL, Forsth, M, Rosen, A, Karlstrom, A & Gustavsson, T 2000, 'Compensation method for attenuated planar laser images of optically dense sprays', *Applied Optics*, vol. 39, pp. 1260-1267.

Achenbach, E 1974, 'Vortex shedding from spheres', *Journal of Fluid Mechanics*, vol. 62, pp. 209-221.

Adrian, RJ 1997, 'Dynamic ranges of velocity and spatial resolution of particle image velocimetry', *Measurement, Science and Technology*, vol. 8, pp. 1393-1398.

Adrian, RJ 2005, 'Twenty years of particle image velocimetry', *Experiments in Fluids*, vol. 39, pp. 159-169.

Akhmetov, DG 2001, 'Formation and basic parameters of vortex rings', *Journal of Applied Mechanics and Technical Physics*, vol. 42, no. 5, pp. 794-805.

Akhmetov, DG 2009, *Vortex rings*, Springer, Berlin-Heidelberg.

Aliseda, A, Cartellier, A, Hainaux, F & Lasheras, JC 2002, 'Effect of preferential concentration on the settling velocity of heavy particles in homogeneous isotropic turbulence', *Journal of Fluid Mechanics*, vol. 468, pp. 77-105.

Allen, JJ & Auvity, B 2002, 'Interaction of a vortex ring with a piston vortex', *Journal of Fluid Mechanics*, vol. 465, pp. 353-378.

Allen, JJ & Chong, MS 2000, 'Vortex formation in front of a piston moving through a cylinder', *Journal of Fluid Mechanics*, vol. 416, pp. 1-28.

Alletto, M & Breuer, M 2012, 'One-way, two-way and four-way coupled LES predictions of a particle-laden turbulent flow at high mass loading downstream of a confined bluff body', *International Journal of Multiphase Flow*, vol. 45, pp. 70-90.

Anderson, SL & Longmire, EK 1995, 'Particle motion in the stagnation zone of an impinging air jet', *Journal of Fluid Mechanics*, vol. 299, pp. 333-366.

Anlauf, H 2007, 'Recent developments in centrifuge technology', *Separation Purification Technology*, vol. 58, pp. 242-246.

Auerbach, D 1991, 'Stirring properties of vortex rings', *Physics of Fluids A: Fluid Dynamics*, vol. 3, pp. 1351-1355.

Barnes, HA, Hutton, JF & Walters, K, 1989, *An introduction to rheology*, Elsevier, Amsterdam, The Netherlands.

Bastiaans, RJM 2000, 'Cross-correlation PIV: Theory, implementation and accuracy', EUT Report 99-W-001, Department of Mechanical Engineering, Eindhoven University of Technology, The Netherlands.

Batchelor, GK 1977, 'The effect of Brownian motion on the bulk stress in a suspension of spherical particles', *Journal of Fluid Mechanics*, vol. 83, pp. 97-117.

Bec, J, Biferale, L, Boffetta, G, Celani, A, Cencini, M, Lanotte, A, Musacchio, S & Toschi, F 2006, 'Acceleration statistics of heavy particles in turbulence', *Journal of Fluid Mechanics*, vol. 550, pp. 349-358.

Becker, HA, Hottel, HC & Williams, GC 1967, 'On the light-scatter technique for the study of turbulence and mixing', *Journal of Fluid Mechanics*, vol. 30, part 2, pp. 259-284.

Becker, HA 1977, Mixing, concentration fluctuations, and marker nephelometry, in BE Launder (ed.), *Studies in convection vol. II, theory, measurement and applications*, Academic Press, New York, pp. 45-139.

Bellofram, n.d., *Bellofram Desgin Manual*, Available from: <www.bellofframdiaphragms.com>. [2 February 2015]

Berlemont, A, Desjonqueres, P & Gouesbet, G 1990, 'Particle Lagrangian simulation in turbulent flows', *International Journal of Multiphase Flow*, vol. 16, no. 1, pp. 19-34.

Berrocal, E, Kristensson, E, Richter, M, Linne, M & Alden, M 2008, 'Application of structured illumination for multiple scattering suppression in planar laser imaging of dense sprays', *Optics Express*, vol. 16, no. 22, pp. 17870-17881.

Best, JL 1998, 'The influence of particle rotation on wake stability at particle Reynolds numbers, $Re_p < 300$ - Implications for turbulence modulation in two-phase flows', *International Journal of Multiphase Flow*, vol. 24, pp. 693-720.

Birzer, CH, Kalt, PAM & Nathan, GJ 2009, 'The influences of jet precession on near field particle distributions', *International Journal of Multiphase Flow*, vol. 35, pp. 288-296.

Birzer, CH, Kalt, PAM & Nathan, GJ 2011, 'The influences of jet precession on large-scale instantaneous turbulence particle clusters', *International Journal of Multiphase Flow*, vol. 37, pp. 394-402.

Birzer, CH, Kalt, PAM & Nathan, GJ 2012, 'The influences of particle mass loading on mean and instantaneous particle distributions in precessing jet flows', *International Journal of Multiphase Flow*, vol. 41, pp. 13-22.

Blevin, WR & Brown, WJ 1961, 'Effect of particle separation on the reflectance of semi-infinite diffusers', *Journal of the Optical Society of America*, vol. 51, no. 2, pp. 129-134.

Boree, J, Ishima, T & Flour, I 2001, 'The effect of mass loading and inter-particle collision on the development of the polydispersed two-phase flow downstream of a confined bluff body', *Journal of Fluid Mechanics*, vol. 443. pp. 129-165.

Bosecker, K 1997, 'Bioleaching: Metal solubilization by microorganisms', *Microbiology Reviews*, vol. 20, pp. 591-604.

Bouhabila, EH, Aim, RB & Buisson, H 2001, 'Fouling characterisation in membrane bioreactors', *Separation and Purification Technology*, vol. 22-23, pp. 123-132.

Bowen, W & Jenner, F 1995, 'Theoretical descriptions of membrane filtration of colloids and fine particles: An assessment and review', *Advances in Colloid and Interface Science*, vol. 56, pp. 141-200.

Brown, GL & Roshko, A 1974, 'On density effects and large structure in turbulence mixing layers', *Journal of Fluid Mechanics*, vol. 64, part 4, pp. 775-816.

Brugman, ThM, Stoffels, GGM, Dam, N, Meerts, WL & ter Meulen, JJ 1997, 'Imaging and post-processing of laser-induced fluorescence from NO in a diesel engine', *Applied Physics B: Lasers and Optics*, vol. 64, pp. 717-724.

Bruun, HH 1995, *Hot-wire anemometry: Principles and signal analysis*, Oxford University Press, Oxford.

Cater, JE & Soria, J 2002, 'The evolution of round zero-net-mass-flux jets', *Journal of Fluid Mechanics*, vol. 472, pp. 167-200.

Cater, JE, Soria, J & Lim, TT 2004, 'The interaction of the piston vortex with a piston-generated vortex ring', *Journal of Fluid Mechanics*, vol. 499, pp. 327-343.

Chang I-S & Lee, C-H 1998, 'Membrane filtration characteristics in membrane-coupled activated sludge system - The effect of physiological states of activated sludge on membrane fouling', *Desalination*, vol. 120, pp. 221-233.

Chao, Y-C & Jeng, M-S 1992, 'Behaviour of the lifted jet flame under acoustic excitation', *Twenty-Fourth Symposium (International) on Combustion, The Combustion Institute*, vol. 24, pp. 333-340.

Chao, Y-C, Wu, C-Y, Yuan, T & Cheng T-S 2002, 'Stabilization process of a lifted flame tuned by acoustic excitation', *Combustion Science and Technology*, vol. 174, pp. 87-110.

Chein, R & Chung, JN 2004, 'Simulation of particle dispersion in a two-dimensional mixing layer', *American Institute of Chemical Engineering Journal*, vol. 34, pp. 946-954.

Chen, L, Goto, S & Vassilicos, JC 2006, 'Turbulent clustering of stagnation points and inertial particles', *Journal of Fluid Mechanics*, vol. 553, pp. 143-154.

Cheong, M, Birzer, C & Lau, T 2012a, *Single image corrections to facilitate planar imaging of particle concentration in particle-laden fluids*, 18th Australasian Fluid Mechanics Conference, Launceston, Australia.

Cheong, M, Birzer, C & Lau, T 2012b, *Single-image attenuation corrections to facilitate instantaneous planar imaging of densely seeded particle-laden flows*, 7th Australasian Congress on Applied Mechanics, Adelaide, Australia.

Chmielewski, A, Urbanski, T & Migdal, W 1997, 'Separation technologies for metals recovery from industrial wastes', *Hydrometallurgy*, vol. 45, pp. 333-344.

Chung, JN & Troutt, TR 1988, 'Simulation of particle dispersion in an axisymmetric jet', *Journal of Fluid Mechanics*, vol. 186, pp. 199-222.

Churchill, SW, Clark, GC & Sliepcevich, CM 1960, 'Light-scattering by very dense monodispersions of latex particles', *Discussions of the Faraday Society*, vol. 30, pp. 192-199.

Coleman, SW & Vassilicos, JC 2009, 'A unified sweep-stick mechanism to explain particle clustering in two- and three-dimensional homogeneous, isotropic turbulence', *Physics of Fluids*, vol. 21, pp. 113301.

Collins, LR & Keswani, A 2004, 'Reynolds number scaling of particle clustering in turbulent aerosols', *New Journal of Physics*, vol. 6, no. 119.

Concha, AF 2014, *Solid-liquid separation in the mining industry*, Spinger, Switzerland.

Crook, A, Crowther, WJ & Wood, NJ 2000, *A parametric study of a synthetic jet in a cross flow*, 22nd International Congress of Aeronautical Sciences, Harrogate, United Kingdom.

Crow, SC & Champagne, FH 1971, 'Orderly structure in jet turbulence', *Journal of Fluid Mechanics*, vol. 48, part 3, pp. 547-591.

Crowe, CT, Gore, RA & Troutt, TR 1985, 'Particle dispersion by coherent structures in free shear flows', *Particulate Science and Technology: An International Journal*, vol. 3, pp. 149-158.

Crowe, CT, Chung, JN & Troutt, TR 1988, 'Particle mixing in free shear flows', *Progress in Energy and Combustion Science*, vol. 14, pp. 171-194.

Crowe, CT, Troutt, TR & Chung, JN 1995, Particle interactions with vortices, in SI Green (ed.), *Fluid vortices*, Kluwer Academic Publishers, Netherlands, pp. 829-261.

Crowe, CT 2000, 'On models for turbulence modulation in fluid-particle', *International Journal of Multiphase Flow*, vol. 26, pp. 719-727.

Dabiri, JO & Gharib, M 2004,'Fluid entrainment by isolated vortex rings', *Journal of Fluid Mechanics*, vol. 511, pp. 311-331.

Dabiri, JO 2009, 'Optimal vortex formation as a unifying principle in biological propulsion', *Annual Review of Fluid Mechanics*, vol. 41, pp. 17-33.

Dahm, WJA & Dimotakis, PE 1987, 'Measurements of entrainment and mixing in turbulent jets', *AIAA Journal*, vol. 25, no. 9, pp. 1216-1223.

Dejoan, A & Monchaux, R 2013, 'Preferential concentration and settling of heavy particles in homogeneous turbulence', *Physics of Fluids* vol. 25, 013301.

DeSpirito, J & Wang, L-P 2001, 'Linear instability of two-way coupled particle-laden jet', *International Journal of Multiphase Flow*, vol. 27, pp. 1179-1198.

Didden, N 1979, 'On the formation of vortex rings: Rolling-up and production of circulation', *Journal of Applied Mathematics and Physics*, vol. 30, pp. 101-116.

Di Giacinto, M, Sabetta, F & Piva, R 1982, 'Two-way coupling effects in dilute gas-particle flows', *ASME Journal of Fluids Engineering*, vol. 104, pp. 304-311.

Durst, F, Melling, A & Whitelaw, JH 1976, *Principles and practice of laser-Doppler anemometry*, Academic Press, London.

Durst, F, Milojevic & D, Schonung, B 1984, 'Eulerian and Lagrangian predictions of particulate two-phase flows: A numerical study', *Applied Mathematical Modelling*, vol. 8, pp. 101-115.

Eaton, J & Fessler, J 1994, 'Preferential concentration of particles by turbulence', *International Journal of Multiphase Flow*, vol. 20, pp. 169-209.

Ehlers, GAC & Turner, SJ 2011, 'Evaluation of extracellular biopolymer and its impact on bioflocculation in activated sludge bioreactors', *Water Science and Technology*, vol. 63, pp. 689-694.

Elghobashi, S, Abou-Arab, T, Rizk, M & Mostafa, A 1984, 'Prediction of the particle-laden jet with a two-equation turbulence model', *International Journal of Multiphase Flow*, vol. 10, no. 6, pp. 697-710.

Elghobashi, S 1991, 'Particle-laden turbulent flows: Direct simulation and closure models', *Applied Scientific Research*, vol. 48, pp. 301-314.

Elghobashi, S & Truesdell, GC 1993, 'On the two-way interaction between homogeneous turbulence and dispersed solid particles, part I: Turbulence modification', *Physics Fluids A: Fluid Dynamics*, vol. 5, no. 7, pp. 1790-1801.

Elghobashi, S 1994, 'On predicting particle-laden turbulent flows', *Applied Scientific Research*, vol. 52, pp. 309-329.

Falkinhoff, F, Obligado, M, Bourgoin, M & Mininni, PD 2020, 'Preferential concentration of free-falling heavy particles in turbulence', *Physical Review Letters*, vol. 125, 064504.

Fan, J, Zhao, H & Cen, K 1996, 'Particle concentration and size measurements in two-phase turbulent coaxial jets', *Chemical Engineering Communications*, vol. 156, pp. 115-129.

Fessler, JR, Kulick, JD & Eaton, JK 1994, 'Preferential concentration of heavy particles in a turbulent channel flow', *Physics of Fluids*, vol. 6, no. 11, pp. 3742-3749.

Fiabane, L, Zimmermann, R, Volk, R, Pinton, J-F & Bourgoin, M 2012, 'On the clustering of finite-size particles in turbulence', *Physical Review E*, vol. 86, 035301.

Forster, C 1976, 'Bioflocculation in activated sludge process', *Water SA*, vol.2, no. 3, pp. 119-125.

Friedlander, SK 1977, *Smoke, dust and haze - Fundamentals of aerosol behavior*, John Wiley & Sons, USA.

Fukumoto, Y & Moffatt, HK 2000, 'Motion and expansion of a viscous vortex ring. Part 1. A higher-order asymptotic formula for the velocity', *Journal of Fluid Mechanics*, vol. 417, pp. 1-45.

Geiss, S, Dreizler, A, Stojanovic, Z, Chrigui, M, Sadiki, A & Janicka, J 2004, 'Investigation of turbulence modification in a non-reactive two-phase flow', *Experiments in Fluids*, vol. 36, pp. 344-354.

Geoffroy, N & Cardarelli, F 2005, 'A method for leaching or dissolving gold from ores or precious metal scrap', *Journal of the Minerals, Metals, and Materials Society*, vol. 57, no. 8, pp. 47-59.

Gharib, M, Rambod, E & Shariff, K 1998, 'A universal time scale for vortex ring formation', *Journal of Fluid Mechanics*, vol. 360, pp. 121-140.

Gharib, M & Daribi, D 2000, Digital particle image velocimetry, in AJ Smits and TT Lim (eds.) *Flow visualization: Techniques and examples*, Imperial College Press, London.

Glezer, A 1988, 'The formation of vortex rings', *Physics of Fluids*, vol. 31, pp. 3532-3542.

Glezer, A & Amitay, M 2002, 'Synthetic jets', *Annual Review of Fluid Mechanics*, vol. 34, pp. 503-529.

Glezer, A & Coles, D 1990, 'An experimental study of a turbulent vortex ring', *Journal of Fluid Mechanics*, vol. 211, pp. 243-283.

Goldschmidt, V, & Eskinazi, S 1966, 'Two-phase turbulence flow in a plane jet', *Journal of Applied Mechanics*, vol. 33, vol. 4, pp. 735-747.

Gordon, M, Cater, JE & Soria, J 2004, 'Investigation of the mean passive scalar field in zero-net-mass-flux jets in cross-flow using planar-laser-induced fluorescence', *Physics of Fluids*, vol. 16, no. 3, pp. 794-808.

Gore, RA & Crowe, CT 1989, 'Effect of particle size on modulating turbulent intensity', *International Journal of Multiphase Flow*, vol. 15, no. 2, pp. 279-285.

Goto, S & Vassilicos, JC 2006, 'Self-similar clustering of inertial particles and zero-acceleration points in fully developed two-dimensional turbulence', *Physics of Fluids*, vol. 18, pp. 115103.

Gouesbet, G 1994, 'Generalized Lorenz-Mie theory and applications', *Particle-Particle Systems Characterizations II*, pp. 22-34.

Grehan, G, Gouesbet, G, Naqwi, A & Durst F 1994, 'Trajectory ambiguities in phase Doppler systems: Study of a near forward and a near-backward geometry', *Particle-Particle Systems Characterizations II*, pp. 133-144.

Hadinoto, K, Jones, EN, Yurteri, C & Curtis, JS 2005, 'Reynolds number dependence of gas-phase turbulence in gas-particle flows', *International Journal of Multiphase Flow*, vol. 31, pp. 416-434.

Haidari, AH & Smith, CR 1994, 'The generation and regeneration of single hairpin vortices', *Journal of Fluid Mechanics*, vol. 277, pp. 135-162.

Han, K, Lee, H & Hwang, W 2020, 'Pseudo real-time continuous measurements of particle preferential concentration in homogeneous isotropic turbulence', *Experimental Thermal and Fluid Science*, vol. 112, 109968.

Herbet, PM, Gauthier, TA, Briens, CL & Bergougnou MA 1994, 'Application of fiber optic reflection probes to the measurement of local particle velocity and concentration in gas-solid flow', *Powder Technology*, vol. 80, pp. 243-252.

Hestroni, G & Sokolov, M 1971, 'Distribution of mass, velocity and intensity of turbulence in a two-phase turbulent jet', *Journal of Applied Mechanics*, vol. 38, no. 2, pp. 315-327.

Hestroni, G 1989, 'Particles-turbulence interaction', *International Journal of Multiphase Flow*, vol. 15, no. 5, pp. 735-746.

Hishida, K, Ando, A & Maeda, M 1992, 'Experiments on particle dispersion in a turbulence mixing layer', *International Journal of Multiphase Flow*, vol. 18, pp. 181-194.

Hogan, RC & Cuzzi, JN 2001, 'Stokes and Reynolds number dependence of preferential particle concentration in simulated three-dimensional turbulence', *Physics of Fluids*, vol. 13, no. 10, pp. 2938-2945.

Hwang, SD & Cho, HH 2003, 'Effects of acoustic excitation positions on heat transfer and flow in axisymmetric impinging jet: main jet excitation and shear layer excitation', *International Journal of Heat and Fluid Flow*, vol. 23, pp. 199-209.

Irdmusa, JZ & Garris, CA 1987, 'Influence of initial and boundary conditions on vortex ring development', *AIAA Journal*, vol. 25, no. 3, pp. 371-372.

Iritani, E & Katagiri, N 2016, 'Developments of blocking filtration model in membrane filtration', *KONA Powder and Particle Journal*, no. 33, pp. 179-202.

Jabbal, M, Wu, J & Zhong, S 2006, 'The performance of round synthetic jets in quiescent flow', *The Aeronautical Journal*, paper no. 3043, pp. 385-393.

James, RD, Jacobs, JW & Glezer, A 1996, 'A round turbulent jet produced by an oscillating diaphragm', *Physics of Fluids*, vol. 8, no. 9, pp. 2484-2495.

James, S & Madnia CK 1996, 'Direct numerical simulation of a laminar vortex ring', *Physics of Fluids*, vol. 8, no. 9, pp. 2400- 2414.

Kalt, PAM, Birzer, CH & Nathan, GJ 2007, 'Corrections to facilitate planar imaging of particle concentration in particle-laden flows using Mie scattering, part 1: Collimated laser sheets', *Applied Optics*, vol. 46, no. 23, pp. 5823-5834.

Kelso, RM & Smits AJ 1995, 'Horseshoe vortex systems resulting from the interaction between a laminar boundary layer and a transverse jet', *Physics of Fluids*, vol. 7, no. 1, pp. 153-158.

Kelso RM, Lim TT & Perry AE 1996, 'An experimental study of round jets in cross-flow', *Journal of Fluid Mechanics*, vol. 306, pp. 111-144.

Kiger, KT & Pan C 2000 'PIV technique for the simultaneous measurement of dilute two-phase flows', *Journal of Fluids Engineering*, vol. 122, pp. 811-818.

Kline, SJ, Reynolds, WC, Schraub, FA & Runstadler, PW 1967, 'The structure of turbulent boundary layers', *Journal of Fluid Mechanics*, vol. 30, part. 4, pp. 741-773.

Kobayashi, H, Masutani, SM, Azuhata, S & Morita, S 1992, 'Particle dispersion in a plane mixing layer with streamwise pressure gradient', *JSME International Journal*, vol. 35, no. 1 pp. 29-37.

Koh, H, Jeon, J, Kim, D, Yoon, Y & Koo, J-Y 2003, 'Analysis of signal attenuation for quantification of a planar imaging technique', *Measurement, Science and Technology*, vol. 14, pp. 1829-1838.

Krieger, IM 1972, 'Rheology of monodisperse lattices', *Advances in Colloid and Interface Science*, vol. 3, pp. 111-136.

Kristensson, E, Berrocal, E, Richter, M, Pettersson, S-G & Alden, M 2008, 'High-speed structured planar laser illumination for contrast improvement of two-phase flow images', *Optics Letters*, vol. 33, no. 23. pp. 2752-2754.

Kristensson, E, Araneo, L, Berrocal, E, Manin, J, Richter, M, Alden, M & Linne, M 2011, 'Analysis of multiple scattering suppression using structured laser illumination planar imaging in scattering and fluorescing media', *Optics Express*, vol. 19, no. 14, pp. 13647-13663.

Kulick, JD, Fessler, JR & Eaton, JK 1994, 'Particle response and turbulence modification in fully developed channel flow', *Journal of Fluid Mechanics*, vol. 277, pp. 109-134.

Labanda, J & Llorens, J 2008, 'Wool scouring waste treatment by a combination of coagulationflocculation process and membrane separation technology', *Chemical Engineering Processing*, vol. 47, pp. 1061-1068.

Lamb, H 1932, *Hydrodynamics*, Cambridge University Press, Cambridge.

Lain, S, Sommerfeld, M & Kussin, J 2002, 'Experimental studies and modelling of four-way coupling in particle-laden horizontal channel flow', *International Journal of Heat and Fluid Flow*, vol. 23, pp. 647-656.

Lapsirikul, W, Ho, G & Cord-Ruwisch, R 1994, 'Mechanisms in anaerobic bioflocculation of wool scouring effluent', *Water Research*, vol. 28, no. 8, pp. 1749-1754.

Lasheras, JC, Cho, JS & Maxworthy, T 1986, 'On the origin and evolution of streamwise vortical structures in a plane free shear-layer', *Journal of Fluid Mechanics*, vol. 172, pp. 231-258.

Lawn, CJ, Williams, TC & Schefer, RW 2005, 'The response of turbulent premixed flames to normal acoustic excitation', *Proceedings of the Combustion Institute*, vol. 30, pp. 1749-1756.

Lazaro, B & Lasheras, JC 1992, 'Particle dispersion in the developing free shear layer, part I: Unforced flow, part II: Forced flow', *Journal of Fluid Mechanics*, vol. 235, pp. 143-221.

Lee, C, Hong, G, Ha, QP & Mallinson, SG 2003, 'A piezoelectrically actuated micro synthetic jet for active flow control', *Sensors and Actuators A*, vol. 108, pp. 168-174.

Leighton, D & Acrivos, A 1987, 'The shear-induced migration of particles in concentrated suspensions', *Journal of Fluid Mechanics*, vol. 181, pp. 415-439.

Lim, TT & Nickels, TB 1992, 'Instability and reconnection in the head-on collision of two vortex rings', *Nature*, vol. 357, pp. 225- 227.

Lim, TT, Nickels TB 1995, Vortex rings, in SI Green (ed.), *Fluid vortices*, Kluwer Academic Publishers, Netherlands, pp. 95-153.

Lim, TT 1997, 'A note on the leapfrogging between two coaxial vortex rings at low Reynolds numbers', *Physics of Fluids*, vol. 9, no. 1, pp. 239-241.

Lim, TT 2000, Dye and smoke visualisation, in AJ Smits and TT Lim (eds.) *Flow visualization: Techniques and examples*, Imperial College Press, London.

Lim, TT, New, TH & Luo, SC 2001, 'On the development of large-scale structures of a jet normal to a cross flow', *Physics of Fluids*, vol. 13, no. 3, pp. 770-775.

Limbach, L, Bereiter, R, Muller, E, Krebs, R, Galli, R & Stark, W 2008, 'Removal of oxide nanoparticles in a model wastewater treatment plant: Influence of agglomeration and surfactants on clearing efficiency', *Environmental Science and Technology*, vol. 42, pp. 5828-5833.

Lischer, J & Louge, MY 1992, 'Optical fiber measurements of particle concentration in dense suspensions: Calibration and simulation', *Applied Optics*, vol. 31, no. 24, pp. 5106-5113.

Liu, H & Montaser, A 1994, 'Phase-Doppler diagnostic studies of primary and tertiary aerosols produced by a high-efficiency nebulizer', *Analytical Chemistry*, vol. 66, pp. 3233-3242.

Logan, B & Hunt, J 1988, 'Bioflocculation as a microbial response to substrate limitations', *Biotechnology and Bioengineering*, vol. 31, pp. 91-101.

Longmire, EK & Eaton, JK 1992, 'Structure of a particle-laden round jet', *Journal of Fluid Mechanics*, vol. 236, pp. 217-257.

Lopez-Maldonado, EA, Oropeza-Guzman, MT, Jurado-Baizaval, JL & Ochoa-Teran, A 2014, 'Coagulation-flocculation mechanisms in wastewater treatment plants through zeta potential measurements', *Journal of Hazardous Materials*, vol. 279. pp. 1-10.

Lu, LJ & Smith, CR 1985, 'Image processing of hydrogen bubble flow visualization for determination of turbulence statistics and bursting characteristics', *Experiments in Fluids*, vol. 3, pp. 349-356.

Luckham, PK & Ukeje, MA 1999, 'Effect of particle size distribution on the rheology of dispersed systems', *Journal of Colloid and Interface Science*, vol. 220, pp. 347-356.

Lugt, HJ 1983, *Vortex flow in nature and technology*, Wiley, New York.

Lun, CKK 2000, 'Numerical simulation of dilute turbulent gas-solid flows', *International Journal of Multiphase Flow*, vol. 26, pp. 1707-1736.

Maas, HG, Gruen, A & Papantoniou, D 1993, 'Particle tracking velocimetry in three-dimensional flows. Part 1 Photogrammetric determination of particle coordinates', *Experiments in Fluids*, vol. 15, pp.133-146.

Martin, JE & Meiburg, E 1991, 'Numerical investigation of three-dimensionally evolving jet subject to axisymmetric and azimuthal perturbations', *Journal of Fluid Mechanics*, vol. 230, pp. 271-318.

Maxey, MR & Corrsin, S 1986, 'Gravitational settling of aerosol particles in randomly oriented cellular flow fields', *Journal of the Atmospheric Sciences*, vol. 43, no. 11, pp. 1112-1134.

Maxey, MR 1987, 'The gravitational settling of aerosol particles in homogeneous turbulence and random flow fields', *Journal of Fluid Mechanics*, vol. 174, pp. 441-465.

Maxworthy, T 1972, 'The structure and stability of vortex rings', *Journal of Fluid Mechanics*, vol. 51, part 1, pp. 15-32.

McCormick, DC 2000, *Boundary layer separation control with directed synthetic jets*, 38th Aerospace Sciences Meeting & Exhibit, Reno, Nevada.

McDonell, VG, Lee, SW & Samuelsen, GS 1995, *Interpretation of spray behavior in complex aerodynamic flows using phase Doppler interferometry and planar-liquid-laser-induced fluorescence*, Proc. SPIE 2546, Optical Techniques in Fluid, Thermal, and Combustion Flow, San Diego, California.

Merkus, HG, 2016, 'Flotation' in Merkus, HG & Meesters, GMH (ed.) *Production, Handling and Characterization of Particulate Materials*, Springer, Switzerland.

Merzkirch, W 1987, *Flow visualization*, Academic Press Inc. (London) Ltd., London.

Miyazaki, K, Chen, G, Yamamoto, F, Ohta, J, Murai, Y & Horii, K 1999, 'PIV measurement of particle motion in spiral gas-solid two-phase flow', *Experimental Thermal and Fluid Science*, vol. 19, pp. 194-203.

Modarress, D, Tan, H & Elghobashi, S 1984, 'Two-component LDA measurement in a two-phase turbulent jet', *AIAA Journal*, vol. 22, no. 5, pp. 624-630.

Monchaux, R, Bourgoin, M & Cartellier, A 2010, 'Preferential concentration of heavy particles: A Voronoi analysis', *Physics of Fluids*, vol. 22, pp. 103304.

Monchaux, R, Bourgoin, M & Cartellier, A 2012, 'Analyzing preferential concentration and clustering of inertial particles in turbulence', *International Journal of Multiphase Flow*, vol. 40, pp. 1-18.

Morton, BR 1984, 'The generation and decay of vorticity', *Geophysical & Astrophysical Fluid Dynamics*, vol. 28, pp. 277-308.

Moses, L & Petersen, F 2000, 'Flotation as a separation technique in the coal gold agglomeration process', *Minerals Engineering*, vol. 13, pp. 255-264.

Mueller, S, Llewellin, EW & Mader, HM 2010, 'The rheology of suspensions of solid particles', *Proceedings of the Royal Society A: Mathematical, Physical & Engineering Sciences*, vol. 466, pp. 1201-1228.

Muller, MO, Bernal, LP, Miska, PK, Washabaugh, PD, Chou, TKA, Parviz, BA, Zhang, C & Najafi, K 2001, *Flow structure and*

performance of axisymmetric synthetic jets, 39th Aerospace Sciences Meeting & Exhibit, Reno, Nevada.

Murugananthan, M, Bhaskar Raju, G & Prabhakar S 2004, 'Separation of pollutants from tannery effluents by electro flotation', *Separation Purification Technology*, vol. 40, pp. 69-75.

Myers, D 1999, *Surfaces, interfaces, and colloids: Principles and applications*, John Wiley and Sons, New York, USA.

Nicodemo, L, Nicolais, L & Landel, RF 1974, 'Shear rate dependent viscosity of suspensions in Newtonian and non-Newtonian liquids', *Chemical Engineering Science*, vol. 29, pp. 729-735.

Obligado, M, Missaoui, M, Monchaux, R, Cartellier, A & Bourgoin, M 2011, 'Reynolds number influence on preferential concentration of heavy particles in turbulent flows', *Journal of Physics: Conference Series*, vol. 318, 052015.

Obligado, M, Teitelbaum, T, Cartellier, A, Mininni, PD & Bourgoin, M 2014, 'Preferential Concentration of Heavy Particles in Turbulence', *Journal of Turbulence*, vol. 15, no. 5, pp. 293310.

Ohmi, K & Li, H-Y 2000, 'Particle tracking velocimetry with new algorithms', *Measurement Science and Technology*, vol. 11, pp. 603-616.

Pant, D, Joshi, D, Upreti, M & Kotnala, RK 2012, 'Chemical and biological extraction of metals present in E waste: A hybrid technology', *Waste Management*, vol. 32, pp. 979-990.

Pearse, M 2003, 'Historical use and future development of chemicals for solidliquid separation in the mineral processing industry', *Minerals Engineering*, vol. 16, pp. 103-108.

Petersen, RA & Samet, MM 1988, 'On the preferred mode of jet instability', *Journal of Fluid Mechanics*, vol. 194, pp. 153-173.

Popper, J, Abuaf, N & Hetsroni, G 1974, 'Velocity measurements in a two-phase turbulent jet', *International Journal of Multiphase Flow*, vol. 1, pp. 715-726.

Pronk, W, Ding, A, Morgenroth, E, Derlon, N, Desmond, P, Burkhardt, M, Wu, B, & Fane, AG 2019, 'Gravity-driven membrane filtration for water and wastewater treatment: A review', *Water Research*, vol. 149, pp. 553-565.

Raffel, M, Willert, CE, & Kompenhans, J 1998, *Particle Image Velocimetry. A Practical Guide*, Springer, Switzerland.

Ratoarinoro, N, Wilhelm, AM, Berlan & Delmas, H 1992, 'Effects of ultrasound emitter type and power on a heterogeneous reaction', *The Chemical Engineering Journal*, vol. 50, pp. 27-31.

Rezakazemi, M, Khajeh, A & Mesbah, M 2018, 'Membrane filtration of wastewater from gas and oil production', *Environmental Chemistry Letters*, vol. 16, pp. 367-388.

Rosensweig, RE, Hottel, HC & Williams, GC 1961, 'Smoke-scattered light measurement of turbulent concentration fluctuations', *Chemical Engineering Science*, vol. 15, pp. 111-129.

Rubio, J, Souza, M & Smith, R 2002, 'Overview of flotation as a wastewater treatment technique', *Minerals Engineering*, vol. 15, pp. 139-155.

Rundqvist, R, Magnusson, A, van Wachem, BGM & Almstedt, AE 2003, 'Dual optical fibre measurements of the particle concentration in gas/solid flows', *Experiments in Fluids*, vol. 35, pp. 572-579.

Rushton, A, Ward, A & Holdeich, R 1996, *Solid-liquid filtration separation technology*, Wiley-VCH, Weinheim, Germany.

Saffman, PG 1956, 'On the motion of small spheroidal particles in a viscous liquid', *Journal of Fluid Mechanics*, vol. 1, no. 5, pp. 540-553.

Saffman, PG 1965, 'The lift on a small sphere in a slow shear flow', *Journal of Fluid Mechanics*, vol. 22, no. 2, pp. 385-400.

Saffman, PG 1970, 'The velocity of viscous vortex rings', *Studies in Applied Mathematics*, vol. 49, pp. 371-380.

Saffman, PG 1971, The velocity of viscous vortex rings, in JH Olsen, A Goldburg, M Rogers (ed.), *Aircraft wake turbulence and its detection*, Plenum, New York, pp. 9-10.

Saffman, PG 1992, *Vortex dynamics*, Cambridge University Press, New York.

Salehi, F, Cleary, MJ, Masri, AR & Kronenburg, A 2019, 'PDF-PBE modelling of polydisperse inertial particles in a turbulent recirculating flow', *International Journal of Multiphase Flow*, vol. 117, pp. 42-52.

Sanin, D & Vesilind P 2000, 'Bioflocculation of activated sludge: The role of calcium ions and extracellular polymers', *Environmental Technology*, vol. 21, pp. 1405-1412.

Scott, SJ, Karnik, AU & Shrimpton, JS 2009, 'On the quantification of preferential accumulation', *International Journal of Heat and Fluid Flow*, vol. 30, pp. 789-795.

Serafini, JS 1954, 'Impingement of water droplets on wedges and double-wedge airfoils at supersonic speeds', NACA Technical Report 1159.

Sheen, SH, Lawrence, WP & Raptis AC 1989, 'Cavitation-controlled ultrasonic agitator', *Proceedings of the IEEE Ultrasonics Symposium*, vol. 1, pp. 653-656.

Sheen, HJ, Jou, BH & Lee, YT 1994, 'Effect of particle size on a two-phase turbulent jet', *Experimental Thermal and Fluid Science*, vol. 8, pp. 315-327.

Sick, V & Stojkovic, B 2001, 'Attenuation effects on imaging diagnostics of hollow-cone sprays', *Applied Optics*, vol. 40, no. 15, pp. 2435-2442.

Song, L 1998, 'Flux decline in crossflow microfiltration and ultrafiltration: Mechanisms and modelling of membrane fouling', *Journal of Membrane Science*, vol. 139, pp. 183-200.

Smith, BL & Glezer, A 1998, 'The formation and evolution of synthetic jets', *Physics of Fluids*, vol. 10, no. 9, pp. 2281-2297.

Smith, BL & Glezer, A 2002, 'Jet vectoring using synthetic jets', *Journal of Fluid Mechanics*, vol. 458, pp. 1-34.

Smith, CR, Seal, CV, Praisner, TJ, Sabatino, DR 2000, Hydrogen bubble visualisation, in AJ Smits and TT Lim (eds.) *Flow visualization: Techniques and examples*, Imperial College Press, London.

Sommerfeld, M & Qiu, HH 1995, 'Particle concentration measurements by phase-Doppler anemometry in complex dispersed two-phase flows', *Experiments in Fluids*, vol. 18, pp. 187-198.

Squires, KD & Eaton, JK 1990, 'Particle response and turbulence modification in isotropic turbulence', *Physics of Fluids A: Fluid Dynamics*, vol. 2, no. 7, pp. 1191-1203.

Squires, KD & Eaton, JK 1991, 'Preferential concentration of particles by turbulence', *Physics of Fluids A: Fluid Dynamics*, vol. 3, no. 5, pp. 1169-1178.

Stickel, JJ & Powell, RL 2005, 'Fluid mechanics and rheology of dense suspensions', *Annual Review of Fluid Mechanics*, vol. 37, pp. 129-149.

Stumm, W 1977, 'Coagulation and filtration in water and wastewater treatment become more efficient by modifying the chemical variables to improve the efficiency of collisions between particles and particles and filter grains', *Environmental Science and Technology*, vol. 11, pp. 1066-1070.

Sumbekova, S, Cartellier, A, Aliseda, A & Bourgoin, M 2016, 'Preferential concentration of inertial sub-Kolmogorov particles: The roles of mass loading of particles, Stokes numbers, and Reynolds numbers', *Physical Review Fluids*, vol. 2, 024302.

Syed, AH & Sung, HJ 2009a, 'Propagation of orifice- and nozzle-generated vortex rings in air', *Journal of Visualization*, vol. 12, no. 2, pp. 139-156.

Syed, AH & Sung, HJ 2009b, 'Effect of an exit-wedge angle on pinch-off and mass entrainment of vortex rings in air', *Flow, Turbulence and Combustion*, vol. 82, pp. 391-406.

Talley, DG, Verdieck JF, Lee, SW, McDonell, VG & Samuelsen, GS 1996, *Accounting for laser sheet extinction in applying PLLIF to sprays*, AIAA 34th Aerospace Sciences Meeting and Exhibit, Reno, Nevada.

Tang, L, Wen, F, Yang, Y, Crowe CT, Chung JN & Troutt, TR 1992, 'Self-organizing particle dispersion mechanism in a plane wake', *Physics of Fluids*, vol. 4, no. 10, pp. 2244-2251.

Tarleton, S & Wakeman, R 2016, 'Particle separations by filtration and sedimentation' in Merkus, HG & Meesters, GMH (ed.) *Production, Handling and Characterization of Particulate Materials*, Springer, Switzerland.

Uhlmann, M & Chouippe 2017, 'Clustering and preferential concentration of finite-size particles in forced homogeneous-isotropic turbulence', *Journal of Fluid Mehanics*, vol. 812, pp. 991-1023.

Urbain, V, Block, J & Manem, J 1993, 'Bioflocculation in activated sludge: An analytic approach', *Water Research*, vol. 27, no. 5, pp. 829-838.

Valentine, HR 1959, *Applied hydrodynamics*, Butterworths Scientific Publications, London.

van de Hulst, HC 1957, *Light scattering by small particles*, John Wiley & Sons, Inc., New York.

Van Dierdonck, J, Van den Broeck, R, Vervoort, E, Dhaeninck, P, Springael, D, Van Impe, J & Smets, I 2012, 'Does a change in reactor loading rate affect activated sludge bioflocculation?', *Process Biochemistry*, vol. 43, pp. 2227-2233.

Versluis, M, Georgiev, N, Martinsson, L, Alden, M & Kroll, S 1997, '2-D absolute OH concentration profiles in atmospheric flames using

planar LIF in a bi-directional laser beam configuration', *Applied Physics B: Lasers and Optics*, vol. 65, pp. 411-417.

Verbiezen, K, Klein-Douwel, RJH, Van Vliet, AP, Donkerbroek, AJ, Meerts, WL, Dam, NJ & ter Meulen, JJ 2006, 'Attenuation corrections for in-cylinder NO LIF measurements in a heavy-duty Diesel engine', *Applied Physics B: Lasers and Optics*, vol. 83, pp. 155-166.

Vladimirov, VA 1977, 'Vortical momentum of flows of an incompressible liquid', *Journal of Applied Mechanics and Technical Physics*, vol. 18, no. 6, pp. 791-794.

Vladimirov, VA 1979, 'Vortical momentum of bounded ideal incompressible fluid flows', *Journal of Applied Mechanics and Technical Physics*, vol. 20, no. 2, pp. 157-163.

Vreman, B, Geurts, BJ, Deen, NG, Kuipers, JAM & Kuerten, JGM 2009, 'Two- and four-way coupled Euler-Lagrangian large-eddy simulation of turbulent particle-laden channel flow', *Flow, Turbulence and Combustion*, vol. 82, pp. 47-71.

Wakeman, R & Tarleton, S 2005, *Solid/liquid separation: principles of industrial filtration*, Elsevier, Oxford.

Walker, JDA, Smith, CR, Cerra, AW & Doligalski, TL 1987, 'The impact of a vortex ring on a wall', *Journal of Fluid Mechanics*, vol. 181, pp. 99-140.

Wang, L-P & Maxey, MR 1993, 'Settling velocity and concentration distribution of heavy particles in homogeneous isotropic turbulence', *Journal of Fluid Mechanics*, vol. 256, pp. 27-68.

Wang, A, Song, Q & Yao, Q 2016, 'Study on inertial capture of particles by droplet in a wide Reynolds number range', *Journal of Aerosol Science*, vol. 93, pp. 1-15.

Wark, C, Eickmann, K & Richards, C 2000, 'The structure of an acoustically forced, reacting two-phase jet', *Combustion and Flame*, vol. 120, pp. 539-548.

Weigand, A & Gharib, M 1997, 'On the evolution of laminar vortex rings', *Experiments in Fluids*, vol. 22, pp. 447-457.

Wellander, R, Berrocal, E, Kristensson, E, Richter, M & Alden, M 2011, 'Three-dimensional measurement of the local extinction coefficient in a dense spray', *Measurement, Science and Technology*, vol. 22, pp. 125303.

Wen, F, Kamalu, N, Chung, JN, Crowe, CT & Troutt TR 1992, 'Particle dispersion by vortex structures in plane mixing layers', *ASME Journal of Fluids Engineering*, vol. 114, pp. 657-666.

Wildemuth, CR & Williams, MC 1984, 'Viscosity of suspensions modelled with a shear-dependent maximum packing fraction', *Rheologica Acta*, vol. 23, pp. 627-635.

Wittemeier, T & Shrimpton, JS 2018, 'Explanation of differences in experimental and computational results for the preferential concentration of inertial particles', *Computers and Fluids*, vol. 173, pp. 37-41.

Wood, AM, Hwang, W & Eaton, JK 2005, 'Preferential concentration of particles in homogeneous and isotropic turbulence', *International Journal of Multiphase Flow*, vol. 31, pp. 1220-1230.

Wicker, RB & Eaton, JK 2001, 'Structure of a swirling, recirculating coaxial free jet and its effect on particle motion', *International Journal of Multiphase Flow*, vol. 27, pp. 949-970.

Xue, Y, Arjomandi, M & Kelso, R 2011, 'Visualisation of the flow structure in a vortex tube', *Experimental Thermal and Fluid Science*, vol. 35, no. 8, pp. 1514-1521.

Yang, Y, Crowe, CT, Chung, JN & Troutt, TR 2000, 'Experiments on particle dispersion in a plane wake', *International Journal of Multiphase Flow*, vol. 26, pp. 1583-1607.

Yang, Y, Jones, DL & Liu, C 2010, 'Recovery of rectified signals from hot-wire/film anemometers due to reversal in oscillating flows', *Review of Scientific Instruments*, vol. 81, pp. 015104.

Yokomizo, T 1994, 'Ultrafiltration membrane technology for regeneration of building wastewater for reuse', *Desalination*, vol. 98, pp. 319-326.

Zhang, H-Q, Fey, U & Noack, BR 1995, 'On the transition of the cylinder wake', *Journal of Physics*, vol. 7, no. 4, pp. 779-794.

Zouboulis, A & Katsoyiannis, I 2002, 'Removal of arsenates from contaminated water by coagulation-direct filtration', *Separation Science and Technology*, vol. 37, no. 12, pp. 2859-2873.